From Tag to Target:
Development of Strategies to avoid Selection of His-tag-binding Aptamers using the Example of N-terminally His-tagged Carbapenemases KPC-2 and NDM-1 for the Implementation of Carbapenemase-specific Aptamers in Lateral Flow Devices

Inaugural-Dissertation
to obtain the academic degree
Doctor rerum naturalium (Dr. rer. nat.)

submitted to the Department of Biology, Chemistry, Pharmacy
of Freie Universität Berlin

by

Wiebke Sabrowski

2023

This work was prepared from February 2019 - January 2023 under the supervision of Dr. Eva Ehrentreich-Förster at the Fraunhofer Institute for Cell Therapy and Immunology, Branch Bioanalytics and Bioprocesses (IZI-BB) in Potsdam.

1st reviewer: Dr. Eva Ehrentreich-Förster
Fraunhofer Institute for Cell Therapy and Immunology,
Branch Bioanalytics and Bioprocesses IZI-BB
Am Mühlenberg 13
14476 Potsdam

2nd reviewer: Prof., Ph.D. Markus Wahl
Freie Universität Berlin
Institute of Chemistry and Biochemistry - Biochemistry
Takustr. 6
14195 Berlin

Date of defense: 05.04.2023

Preface

Parts of this work have been published in the following publication:

Wiebke Sabrowski, Nico Dreymann, Anja Möller, Denise Czepluch, Patricia P. Albani, Dimitrios Theodoridis & Marcus M. Menger. *The use of high-affinity polyhistidine binders as masking probes for the selection of an NDM-1 specific aptamer.* Sci Rep 12, 7936 (2022).

The lateral flow device shown in this work was developed by nal von minden GmbH (Göttingen, Germany).

Acknowledgments

First, I would like to express my gratitude to Dr. Marcus Menger for giving me the opportunity to conduct my doctoral thesis in his laboratory. Thank you for the freedom in the design of my research and for your confidence in me. I would like to thank Dr. Eva Ehrentreich-Förster and Prof. Dr. Markus Wahl for reviewing my thesis. Many thanks to Nico Dreymann for numerous discussions about experimental designs, for proofreading papers, emails, and everything else that included the written language. And last but not least for keeping my head up at any time. I would like to thank Simon Krebs for endless discussions about selection strategies. Even though they were sometimes challenging, they were even more valuable. I am dearly grateful to Anja Möller and Denise Czepluch for introducing me to almost all the methods used in this work, for the performance of SPR and NGS experiments and for always helping me out with scientific questions. I would like to thank all my current and former colleagues, with special regards to Felix Pfisterer and Tobias Gerling, for lighting up every working day. Furthermore, I want to thank Arno Leenen and Lisa Adam for their support during their internships. I want to thank Katarina Fedorov, Dr. Patricia Albani and Dr. Dimitrios Theodoridis from nal von minden GmbH for the development of the aptamer-based lateral flow device and for the permission to use the data in my thesis. Thank you to my friends and family for all the emotional support you always give unconditionally. I am very lucky to have you in my life. And of course, thank you Tobias for freeing my mind from science every now and then. To even more surfs and travels.

Selbstständigkeitserklärung

Hierdurch versichere ich, dass ich meine Dissertation selbstständig verfasst und keine anderen als die von mir angegeben Quellen und Hilfsmittel verwendet habe. Geistiges Eigentum anderer Autoren wurde entsprechend gekennzeichnet. Ebenso versichere ich, dass ich an keiner anderen Stelle ein Prüfungsverfahren beantragt bzw. die Dissertation in dieser oder anderer Form an keiner anderen Fakultät als Dissertation vorgelegt habe.

Wiebke Sabrowski

Table of Contents

1. Summary

The rapid increase in occurrence of carbapenemase-producing multi-drug resistant *Entero-bacteriaceae* represents a world-wide health risk. Carbapenem antibiotics have long been used as a treatment of last resort for infections with multi resistant bacteria. Now that bacteria develop enzymes that render these agents useless, treatment options are limited, and the health care system is left with a fast-growing challenge. Easy to use and cost-effective detection of carbapenem resistance and discrimination between different carbapenemases are important to prevent spread and to facilitate appropriate treatment. The development of reliable detection systems strongly depends on the availability of highly affine and specific molecular recognition molecules. Aptamers are promising molecular recognition molecules. They are small and chemically synthesized, single stranded (ss) DNA or RNA molecules that bind to their targets with high affinity and specificity. Aptamers are selected by an *in vitro* selection process that can be tailored to suit the desired application. Chemical synthesis of aptamers minimizes batch-to-batch variations and facilitates easy and cost-effective modifications. Yet, an effective aptamer selection process is often hampered by non-specific binding to side targets. Thus, negative selections against potential side targets are recommended. In this work, selections were carried out against N-terminally polyhistidine (His)-tagged New Delhi metallo-beta-lactamase 1 (His-NDM-1) and *Klebsiella pneumoniae* carbapenemase-2 (His-KPC-2). Eleven selection rounds (SRs), partially conducted with negative selections against His-tagged carbapenemases did not result in the identification of aptamers. Three consecutive SRs without negative selections against His-tagged proteins resulted in the identification of high-affinity His-tag aptamers, only one His-KPC-2 and no His-NDM-1 aptamer. To facilitate carbapenemase binding while preventing His-tag binding, the selection against His-KPC-2 was restarted from SR eleven and three different selection strategies were designed. The strategies included masking of the His-tag and competitive elution of His-tag-binding sequences using a truncated version of the previously selected His-tag aptamer as well as immobilization of the protein via its His-tag. After three SRs, sequencing data was analyzed for the enrichment of a motif that is likely involved in His-tag binding. Based on this analysis, the masking approach was identified as the most promising strategy. Binding to His-KPC-2 was demonstrated for several aptamers. Two of these aptamers were further characterized for binding properties. Both very likely did not bind to the His-tag. Consequently, an aptamer-based lateral flow assay was developed for His-KPC-2. The masking approach was also applied to selection against His-NDM-1. Here, an aptamer with a binding affinity in the high nanomolar to low micromolar range, without cross reactivity to another His-tagged carbapenemase and a synthetic hexa-His peptide was identified. This aptamer may serve as a valuable tool for the detection of the very prevalent and harmful carbapenemase NDM-1.

2. Zusammenfassung

Die zunehmende Verbreitung von carbapenemase-produzierenden, multiresistenten *Enterobacteriaceae* stellt ein weltweites Gesundheitsrisiko dar. Carbapenem-Antibiotika (Carbapeneme) wurden lange Zeit als letztes Mittel zur Behandlung von Infektionen mit multiresistenten Bakterien eingesetzt. Jetzt, da Bakterien in der Lage sind Enzyme zu entwickeln, die Carbapeneme unwirksam machen, sind die Behandlungsmöglichkeiten begrenzt und die Gesundheitssysteme stehen vor einer schnell wachsenden Herausforderung. Ein einfach zu handhabender und kosteneffizienter Nachweis der Carbapenem-Resistenz, sowie die Unterscheidung zwischen verschiedenen Carbapenemasen, sind wichtig, um die Ausbreitung von carbapenem-resistenten Bakterien zu verringern und eine angemessene Behandlung zu ermöglichen. Voraussetzung für die Entwicklung eines verlässlichen Carbapenemase-Nachweissystems ist der Einsatz von hoch-affinen und spezifischen Erkennungs-molekülen. Vielversprechende Erkennungsmoleküle sind zum Beispiel Aptamere. Bei Aptameren handelt sich um kleine, chemisch hergestellte, einzelsträngige DNA- oder RNA-Moleküle, die mit hoher Affinität und Spezifität an Zielmoleküle binden können. Sie werden in einem *in-vitro*-Selektionsverfahren generiert, das spezifisch an die geplante Art der Nutzung angepasst werden kann. Die chemische Synthese der Aptamere minimiert Qualitäts-schwankungen zwischen verschiedenen Chargen und ermöglicht kostengünstige Modifizierungen. Ein effektiver Aptamer-Selektionsprozess wird jedoch häufig durch unspezifische Bindungen an Nebenepitope behindert. Daher wird eine Negativselektion gegen potenzielle Nebenepitope empfohlen.

In dieser Arbeit wurden Selektionen gegen N-terminal Polyhistidin (His)-markierte Carbapenemasen Neu-Delhi-Metallo-beta-Laktamase 1 (His-NDM-1) und *Klebsiella pneumoniae* Carbapenemase-2 (His-KPC-2) durchgeführt. Elf Selektionsrunden, die teilweise mit Negativselektionen gegen andere His-markierte Carbapenemasen durchgeführt wurden, führten nicht zur Identifizierung von Aptameren. Drei darauffolgende Selektionsrunden ohne Negativselektionen gegen His-markierte Proteine führten zur Identifizierung von Aptameren mit hoher Affinität zur His-Markierung, nur einem His-KPC-2 Aptamer und keinen His-NDM-1 Aptamer. Um die Carbapenemasebindung zu ermöglich, gleichzeitig aber die Bindung der His-Markierung zu verhindern, wurde die Selektion gegen His-KPC-2 ab der elften Selektionsrunde wiederholt und es wurden drei unterschiedliche Selektionsstrategien entwickelt. Diese beinhalteten die Maskierung der His-Markierung und die kompetitive Elution His-Markierungsbindender Sequenzen mit einer verkürzten Version des zuvor selektierten His-Markierungs-Aptamers, sowie die Immobilisierung des Proteins über die His-Markierung. Nach drei Selektionsrunden wurden die Sequenzierungsdaten hinsichtlich der Anreicherung eines Sequenzmotivs untersucht, dass wahrscheinlich an der Bindung der His-Markierung beteiligt ist.

Anhand dessen konnte die Maskierungsstrategie als die Vielversprechendste ausgewählt werden. Nach der Analyse des angereicherten Nukleinsäurepools und dem Screening von potenziellen Aptamerkandidaten konnte für mehrere Aptamere eine Bindung an His-KPC-2 gezeigt werden. Für zwei weiterführend charakterisierte Aptamere konnte gezeigt werden, dass sie wahrscheinlich nicht an die His-Markierung binden. Aufgrund dessen wurde im Folgenden ein aptamer-basierter Schnelltest zur Detektion von His-KPC-2 entwickelt. Der Maskierungsansatz wurde auch bei der Selektion gegen His-NDM-1 angewendet. Es wurde ein Aptamer mit einer hoch nanomolaren bis niedrig mikromolaren Bindungsaffinität, ohne Kreuzreaktivität zu einer anderen His-markierten Carbapenemase sowie zu einem synthetischen hexa-His Peptid, identifiziert. Dieses Aptamer kann als wertvolles Erkennungsmolekül für den Nachweis der sehr verbreiteten und gesundheitsgefährdenden Carbapenemase NDM-1 dienen.

3. Introduction

3.1. β-Lactam Antibiotics

Since their discovery, antibiotics have become an essential part of modern medicine as they facilitate the treatment of previously life-threatening bacterial infections. The most relevant and commonly used family of anti-bacterial drugs are beta-lactam antibiotics [1]. Members of this family contain a cyclic amide (lactam), with the nitrogen atom attached to the β-carbon atom relative to the carbonyl (β-lactam) (**Figure 1**) and act as inhibitors of bacterial cell wall synthesis [2].

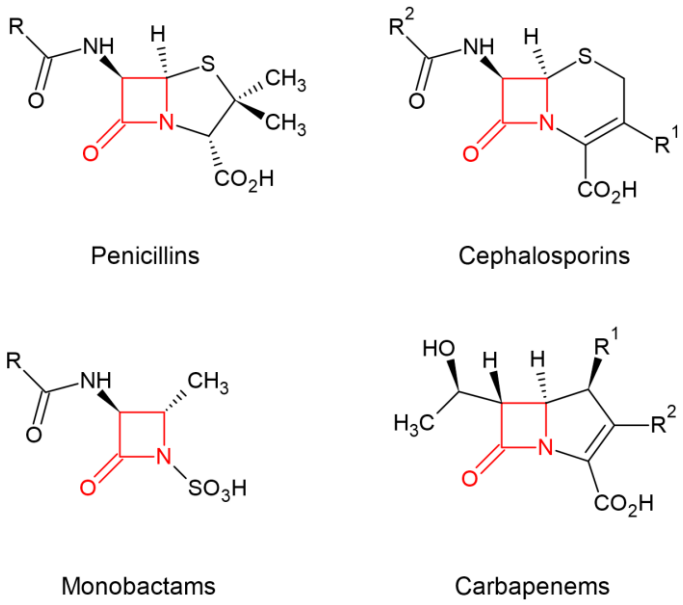

Figure 1: The basic structure of different classes of β-lactam antibiotics. The β-lactam ring is highlighted in red. Drawing based on Palacios *et al.* (2020) [3].

Bacterial cell walls cover the cytoplasmic membrane. They mainly consist of a rigid network of cross-linked hetero polymers called peptidoglycans (PGN). Gram-positive bacteria have a thick (20 - 80 nm) cell wall which represents the outer shell of the cell. In Gram-negative bacteria, the cell wall is thinner (< 10 nm) and covered by an additional cell membrane [4]. For both Gram-negative and Gram-positive bacteria, cell walls are pivotal to maintain their shape and to withstand intracellular pressure. For many bacteria, mutations affecting PGN synthesis are inter alia associated with defects in cell shape [5].

PGN biosynthesis can be divided into three main stages:

1. Production of uridine diphosphate (UDP)-acetylmuramyl-pentapeptide in the cytoplasm
2. Hetero polymer formation (UDP-acetylmuramyl-pentapeptide and UDP acetylglucosamine), linkage to phospholipids in the cytoplasmic membrane, movement through the cytoplasmic membrane and orientation through the periplasm
3. Cleavage from the cytoplasmic membrane and crosslinking completion catalyzed by transpeptidases

The last step of cell wall synthesis, the transpeptidation reaction, is targeted by β-lactam antibiotics. They bind to the transpeptidases and inhibit their action, resulting in a weak cross-linking of the PGN network. Weakly cross-linked cell walls make bacterial growth highly susceptible for cell lysis due to osmotic rupture [6]. Inhibition of bacteria-specific enzymes required for cell wall synthesis, ensures selective toxicity, and makes its use in humans and animals safe [7]. β-lactam antibiotics can be roughly classified as penicillins, cephalosporins, monobactams and carbapenems (**Figure 1**).

3.1.1. Penicillins

Benzylpenicillin (also called Penicillin G) was discovered in 1928 by Alexander Fleming [8] and became commercially available in 1942. It is active against Gram-positive bacteria and strongly decreased the prevalence of streptococci as nosocomial pathogens. However, the first penicillin resistant *Staphylococcus aureus* isolates were found as early as 1942, which were resistant due to the expression of a penicillinase [9]. In subsequent years, penicillins were chemically improved to increase their stability to penicillinases and to broaden their spectrum so that they were also effective against Gram-negative pathogens. Improved stability to penicillinases was achieved by replacement of the benzene ring with an isoxazol ring resulting in isoxazolylpenicillins like methicillin and oxacillin which are primarily used for the treatment of staphylococcal infections [10]. Activity against Gram-negative bacteria was achieved by the addition of an amin group in α-position of a benzyl-penicillin (aminopenicillin), e.g., ampicillin and amoxicillin. Even though penicillins were continuously improved to increase or maintain efficacy, bacteria adapted quickly through acquisition of genes encoding new β-lactam hydrolyzing enzymes (β-lactamases) [7]. Thus, the search for new agents with antibiotic activity continued.

3.1.2. Cephalosporins

The original member of the cephalosporin subfamily, Cephalosporin C was characterized in 1961. It contains a side chain derived from D-α-aminoadipic acid condensed with a dihydrothiazine β-lactam ring system making it resistant to staphylococcal penicillinase [11]. Cephalosporins can be divided into five generations. First generation cephalosporins were introduced in the mid-1960s and are resistant to β-lactamases known at that time. They further permeate the outer membrane of Gram-negative bacteria more readily than penicillins. However, the emergence of bacterial isolates with lower cell wall permeability and the hyperproduction of cephalosporinases decreased treatment success in patients. Later generations of cephalosporins are characterized by higher stability against β-lactamases and increased activity against Gram-negative bacteria. Yet, mutations in β-lactamase genes resulted in new β-lactamase mediated resistance. In 1983 the discovery of isolates, resistant to oxyiminocephalosporins mediated by extended-spectrum β-lactamases (ESBL) heralded a new era of resistance [12].

3.1.3. Monobactams

In contrast to bicyclic β-lactam antibiotics, monobactams have a single β-lactam ring (see also **Figure 1**). The ring itself has weak antibiotic activity and requires molecular substituents. Monobactams are resistant to a broad range of β-lactamases, yet labile to class A chromosomal β-lactamase of *Klebsiella oxytoca*, class C β-lactamases, and ESBLs. The only clinically used monobactam is aztreonam with primary activity against Gram-negative bacteria [12,13].

3.1.4. Carbapenems

The emergence and widespread expression of β-lactamases necessitated the search for new classes of β-lactam antibiotics. In the late 1970s two examples of a so far unknown β-lactam antibiotic class were discovered in Gram-positive bacteria [14,15]. Olivanic acid from *Streptomyces olivaceus* and thienamycin from *Streptomyces cattleya* share special features in their two cyclic β-lactam rings. Here, the sulfur in the β-lactam ring structure is replaced by a methylene group, and the C2-C3 bond is unsaturated (double bond). Thienamycin further stands out due to its side chain at C6 of the β-lactam ring which is in trans configuration. Up to this point, classical β-lactam antibiotics all shared C6 side chains in the cis configuration [16]. While olivanic acid displays poor antimicrobial activity, it functions as a potent β-lactamase inhibitor in both Gram-positive and Gram-negative bacteria. Thienamycin shows antibacterial activity as well as β-lactamase inhibition and became the precursor of carbapenem antibiotics.

Therapeutical use of thienamycin was prohibited by its instability in concentrated solutions. Nevertheless, therapeutically used carbapenem antibiotics are structural analogues of thienamycin. Carbapenems have the broadest spectrum of activity of all β-lactamase antibiotics and great stability against a wide range of β-lactamases which has been attributed to the trans configuration of the C6 side chains [17]. Hence, up to this day, carbapenem antibiotics are considered as drugs of last resort for patients infected with multi-drug resistant bacteria [18].

3.2. β-Lactamases

When Penicillin was discovered in the early 20th century, the battle against bacterial infection seemed to be won. However, it quickly turned out that bacteria were able to develop resistance mechanisms against this kind of medication. Increasing use of antibiotics in humans and animals as well as inappropriate prescriptions have exacerbated the resistance problem [19]. To date, bacterial resistance remains a global threat to human health [20].

Bacterial resistance can be divided into natural resistance or acquired resistance. Natural resistance occurs universally in bacterial species and is not dependent on previous exposure to antibiotics or horizontal gene transfer. Acquired resistance is either mediated by horizontal gene transfer or mutations in the chromosomal DNA [21]. Mechanisms of bacterial resistance can be divided into four categories which are: Limitation of drug uptake, modification of the drug target, drug inactivation, and active drug efflux. Limitation of drug uptake is part of natural resistance while modification of the drug target is usually acquired. Drug inactivation and drug efflux can be part of both – natural and acquired resistance. Excessive exposure to antibiotics can be a cause for the acquisition of resistances as it functions as a selective pressure that favors genetic mutations. Natural resistance is an ancient phenomenon and an expected result of the interaction of microorganisms and the environment they live in. In the clinical setting, the bigger concern is the increasing emergence of acquired resistance in bacterial populations that used to be susceptible to a certain kind of antimicrobial drug [21]. One of the most worrisome developments is the increasing resistance to an extended spectrum of β-lactams in Gram-negative bacteria, especially in *Enterobacteriaceae*. While β-lactam antibiotics are the most frequently used class of antibiotics, *Enterobacteriaceae* are among the most common human pathogens and are also inhabitants of the intestinal flora. While colonialization with *Enterobacteriaceae* is part of a healthy intestinal flora, infections with certain strains can cause digestive disorders, severe diarrhea, or urinary tract infections [22]. *Enterobacteriaceae* spread easily from person to person, e.g., through hand contact, contaminated water, or food, and are capable of rapid horizontal gene transfer [23].

In general, resistance to β-lactams is mediated through three mechanisms. The first mechanism is characterized by the alteration of existing or the acquisition of new transpeptidases, enzymes required for PGN synthesis that no longer interact with the drug. The second and third mechanisms are based on the expression of either efflux pumps or β-lactam hydrolyzing enzymes: β-lactamases. The production of β-lactamases is the most important resistance mechanism against β-lactam antibiotics and most commonly used by Gram-negative bacteria [24]. β-lactamases are commonly classified by the Ambler classification (class A-D) which is based on amino acid homology. Members of classes A, C and D are serine-β-lactamases while members of class B are metallo-β-lactamases that require Zn^{2+} for their activity. Members of class A are inter alia penicillinases and ESBL, class C contains cephalosporinases, class D oxacillinases and class B certain carbapenemases like New Delhi metallo-β-lactamase 1 (NDM-1).

3.3. Carbapenemases

The development of ever newer, improved β-lactam antibiotics has been accompanied by the acquisition of ever newer β-lactamase-encoding genes in bacteria. However, the discovery of carbapenem antibiotics brought along hope. The extensive stability against β-lactamases and their broad spectrum of activity made them potent agents of last resort. Yet, the first β-lactamase with the ability to hydrolyze carbapenems in *Enterobacteriaceae* was already identified in 1993 [25]. To date, resistance to carbapenems is increasingly detected in both nosocomial and community-acquired infections. Carbapenem-resistant *Enterobacteriaceae* (CRE) are associated with longer hospital admissions, higher health care costs and increased mortality than susceptible *Enterobacteriaceae* [26]. In general, there are three particularly relevant mechanisms by which *Enterobacteriaceae* can become carbapenem-resistant, which are enzyme (carbapenemase) production, expression of efflux pumps and porin mutation [27]. The latter two mechanisms are not transferable via horizontal gene transfer and may be accompanied by a significant fitness loss. Carbapenemase production is considerably more important from a human health perspective as carbapenemase producing CRE are associated with higher minimum inhibitory concentrations (MICs) of carbapenems and mortality than non-carbapenemase producing-CRE [20].

Carbapenemases are mostly β-lactamases from classes A, B and D that hydrolyze most β-lactams including carbapenems. Clinically important types of carbapenemases are, for example, the *Klebsiella pneumoniae* carbapenemase (KPC) type. KPCs are a group of class A β-lactamases that were first reported in the early 2000s [28,29]. Only a few years later, KPC type carbapenemases were also reported in other bacterial species such as *Salmonella enterica* [30] and *Klebsiella oxytoca* [31]. KPC type carbapenemases hydrolyze all β-lactams but can be

inhibited by boronic acid, and partially by clavulanic acid and tazobactam. Class B carbapenemases in *Enterobacteriaceae* are inter alia Verona Integron-encoded metallo-β-lactamases (the VIM type), the NDM type and carbapenemases classified by their activity against impenem (the IMP type). They have the highest carbapenemase activity and a broad spectrum of activity, hydrolyzing almost all β-lactams except for the monobactam aztreonam. Class B carbapenemases are not inhibited by common β-lactamases inhibitors. However, as they require a divalent zinc ion for activity, chelators like ethylenediaminetetraacetic acid (EDTA) can inhibit their activity. Class D carbapenemases are of the oxacillinase (OXA) type. They weakly hydrolyze carbapenems and broad spectrum cephalosporins and are neither inhibited by clavulanic acid nor by EDTA [32].

3.4. Carbapenemase Detection

The identification of carbapenemase producing CRE colonized patients is pivotal for adequate treatment and the prevention of further spread. Discrimination between different types of carbapenemases is further relevant as certain new antibacterial drugs, like ceftazidime-avibactam show activity against some carbapenemases (like the KPC type) but not against others (like the NDM type) [33]. To date, detection of carbapenemases can be performed by molecular testing to identify carbapenemase encoding genes, by phenotypic activity tests that detect carbapenemase activity or by immunoassays which detect carbapenemases on the protein level. Molecular tests such as polymerase chain reaction (PCR) provide accurate results and high sensitivity. However, gene mutations may impede detections and well-trained personnel, as well as costly equipment, are required. Furthermore, for genomic analysis, no information about carbapenemase expression on the protein level is available [34]. Phenotypic activity tests, like the modified Hodge test, the carbapenemase inactivation method or Carba NP test, are inexpensive and easy to handle [35]. Yet, they mostly fail to distinguish between different types of carbapenemases. Additionally, false positive results may occur in some cases when bacteria produce the cephalosporinase AmpC in combination with porin mutations [34]. Lateral flow devices (LFD) utilizing antibodies as recognition elements (lateral flow immunoassay, LFIA) facilitate detection of carbapenemases on the protein level. Discrimination between different carbapenemase types is possible by using specific antibodies. Furthermore, LFIAs are usually cost and time efficient and can be operated by non-specialized users. Over the last decade, several LFIAs have been developed allowing simultaneous detection of up to five different carbapenemase types (NDM, KCP, IMP, VIM and OXA in case of NG-Test® CARBA 5 from NG Biotech) with high sensitivity and specificity [36-38]. Hence, LFIAs are valuable tools for the detection of carbapenemases.

3.5. Lateral Flow Devices

An LFD test strip is comprised of several, overlapping membranes which are fixed on a backing card. The pretreated sample is applied to the sample pad which is coated with suitable buffer components. Through capillary forces, the sample migrates to the conjugate pad which contains recognition molecules that are conjugated to reporter molecules such as gold nanoparticles (Au-NPs). From here, the sample migrates toward the detection zone along with a complex of the reporter molecule and the analyte in the sample. The detection zone is a membrane with two different lines. One is the test line, the other the control line [39]. The test line indicates the presence of a specific analyte in a sample, while the control line indicates the correct fluid flow and activity of the test reagents. The composition of the test line as well as its readout differ depending on the LFD format. The classical LFD format is the sandwich assay format (**Figure 2**).

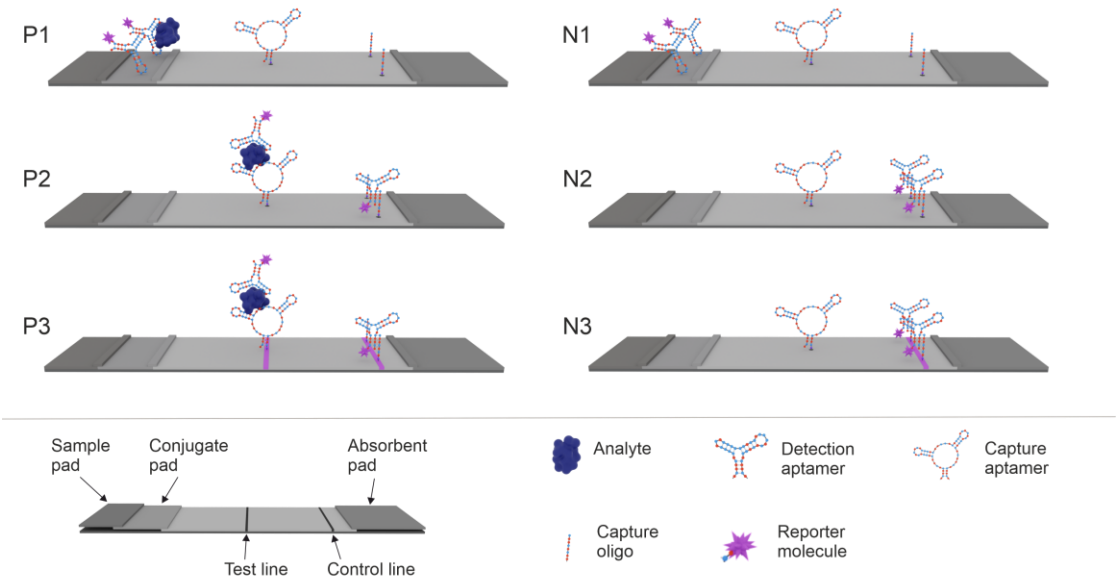

Figure 2: Principle of an aptamer-based LFD in the sandwich assay format. P1-P3 with the analyte present in the sample and N1-N3 without the analyte. The tested sample is applied to the sample pad and migrates to the conjugate pad coated with analyte-specific aptamers conjugated to reporter molecules (P1, N1). The analyte is bound by the aptamer-reporter conjugate (P1) and migrates to the detection zone. Here, the test line is coated with another type of analyte-specific aptamers (P2, N2), capturing the analyte-aptamer-reporter molecule complex (P2). Remained, unbound reporter-aptamer conjugates further migrate to the control line, coated with aptamer binding molecules (capture oligo) (P3, N3). A positive result is indicated by two signals derived from the test and the control line (P3). A negative result is indicated by only one signal derived from the control line (N3). Figure design in collaboration with Sebastian Wieser.

Here, a second analyte detection molecule (capture molecule) is applied to the membrane, which captures the complex of analyte, detection molecule, and reporter molecule, resulting in a visible line and indicating a positive test result. Sandwich assay formats are commonly used for analytes with higher molecular weight that offer different binding epitopes for the capture and detection molecules. The detection of smaller molecules is often limited to competitive LFD formats (**Figure 3**).

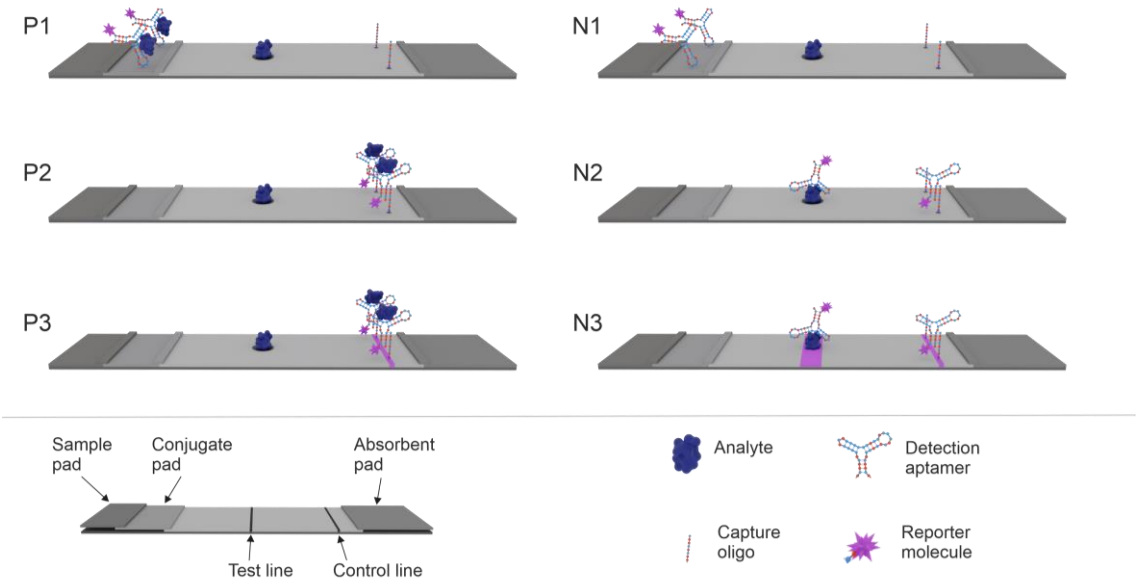

Figure 3: Principle of an aptamer-based LFD in the competitive assay format. P1-P3 with the analyte present in the sample and N1-N3 without the analyte. The tested sample is applied to the sample pad and migrates to the conjugate pad coated with analyte-specific aptamers conjugated to reporter molecules (P1, N1). The analyte is bound by the aptamer-reporter conjugate (P1) and migrates to the detection zone. Here, the test line is coated with the analyte. Unbound reporter-aptamer conjugates bind to the analyte molecules immobilized on the test line and to the aptamer binding molecules (capture oligo) immobilized on the control line (N2). Analyte-aptamer-reporter molecule complexes do not bind to the target molecules immobilized on the test line but migrate to the control line where they bind to the capture oligos immobilized on the control line (P2). A positive result is indicated by only one signal derived from the control line (P3). A negative result is indicated by two signals derived from the test and the control line (N3). Figure design in collaboration with Sebastian Wieser.

In the case of a competitive LFD format, the test line consists of the analyte molecule itself. When the analyte is present in the sample, the complex of analyte, detection molecule, and reporter molecule is formed. Thus, the detection molecule can no longer bind to the analyte on the test line and therefore moves on to the control line. Here, no signal from the test line indicates a positive test result. In case the analyte is not present in the sample, the detection molecule - reporter molecule conjugate binds to the analyte on the test line and a visible line appears which indicates a negative test result [40]. In both LFD formats, the control line is

impregnated with capture molecules that recognize the detection molecule independently of the analyte, ensuring the validity of the results obtained. After passing the control line, the excess liquid is absorbed by an absorption pad and prevented from flowing back into the detection zone.

3.6. Aptamers

Key components of LFD are recognition molecules, responsible for capture and detection of the analyte in a sample. Their binding properties are decisive for the sensitivity and selectivity of the assay. Traditionally, antibodies have been the molecules of choice. They often exhibit high affinity and specificity to their target molecules as well as high serum stability [41]. Furthermore, handling of antibodies for LFD development has been tried and tested for decades. Yet, there is another very promising class of recognition molecules, so-called aptamers, that offers certain advantages over antibodies and bears high potential for the development of robust, highly affine, and specific LFDs. Aptamers are single-stranded (ss) DNA or RNA molecules that bind to their target molecules with high affinity and specificity via their three-dimensional structure. Three-dimensional aptamer structures are influenced by the aptamer sequence and the properties of the used solvent. The chemical nature of aptamer synthesis allows easy and cost-efficient modification and is almost free of batch-to-batch variations [42]. Aptamers have been selected against a wide range of target molecules, including metal ions [43], small molecules [44], proteins [45] viruses [46], bacteria [47] and other whole cells [48]. Dissociation constants for aptamers often reach up to the low nanomolar or high picomolar range which is comparable to many monoclonal antibodies. An *in vitro* aptamer selection process allows convenient adaptation to desired assay conditions and is not limited to immunogenic or non-toxic targets. Aptamers can refold after denaturation and are small, allowing repeated use, for example as recognition elements in assay platforms, and high-density sensor loading. The numerous desirable features of aptamers make them ideal candidates for several application fields, including food and environmental safety, bioimaging, therapeutics and diagnostics [49]. Especially the implementation of aptamers in biosensors (aptasensors), like electrochemical aptasensors [50-52], optical aptasensors (including LFDs) [53-56] and mass sensitive aptasensors [57,58] resulted in the development of numerous, sensitive detection systems [59].

3.6.1. Selection of Aptamers by SELEX

Aptamers are predominantly generated in an *in vitro* selection process called systematic evolution of ligands by exponential enrichment (SELEX), first described in 1990 [60,61]. SELEX consists of iterative cycles of incubation of ssDNA or RNA with the target molecule, removal of non-binding sequences, and an elution and amplification of bound sequences which are then used as the nucleic acid pool for the next round of selection. An exemplary SELEX procedure with a ssDNA library and target immobilization on magnetic beads to facilitate the separation of bound and unbound sequences used for a semi-automated SELEX [62] is represented in **Figure 4**.

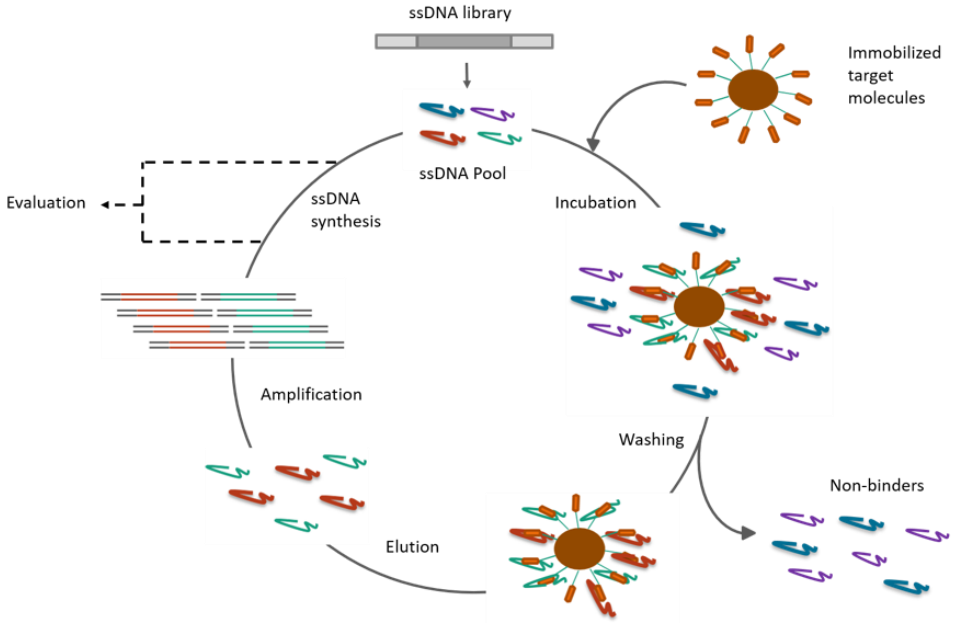

Figure 4: SELEX process with an ssDNA library. The iterative SELEX process starts with a highly diverse ssDNA library that usually consists of a randomized stretch (dark grey), flanked by two defined stretches (light gray) serving as primer binding sites. The ssDNA is incubated with a target molecule that can be immobilized on magnetic beads which are washed to remove non-binders and collected using a magnet. Bound ssDNA molecules are eluted and amplified via PCR. Subsequently, ssDNA is regenerated for use in the next selection round. After every round of selection enrichment and binding properties of the nucleic acid pool can be evaluated. Graphical representation based on Wochner *et al.* (2007) [62].

Selection starts with a highly diverse oligonucleotide library with a variety of approximately 10^{14} - 10^{15} different sequences [63] (for more detailed information see 3.6.2). Usually, the library consists of two constant primer binding sites flanking a randomized region of mostly 20 - 60 nucleotides (nt). If the selection of ssDNA aptamers is desired, the library can be used without pretreatment. If RNA is used, the ssDNA library or DNA pool needs to be transcribed prior to each round of selection. The library is then incubated with the target molecule. Incubation times

and buffer conditions can be conveniently tailored regarding the desired application. The following step, a key step in SELEX, the separation of bound and unbound sequences, is often facilitated by immobilization of the target molecule on a solid matrix like magnetic beads (see also **Figure 4**). Here, unbound sequences are removed by extensive washing. Bound sequences are then eluted either nonspecifically or specifically. Nonspecific elution can be performed using heat and substances like urea, sodium dodecyl sulfate (SDS) or EDTA to denature and thereby elute all remaining sequences [64-66]. Specific elution of target bound sequences can be facilitated by competition using either the target molecule or competitive binders in excess [67,68]. Moreover, immobilization of the target molecules via, e.g, photo or redox-based cleavable linkers or on affinity resins allows specific elution of the aptamer-target complexes [67,69,70]. Amplification of eluted sequences is performed by PCR using the constant regions of the nucleic acid library as primer binding sites. Double-stranded (ds)DNA is either transcribed into RNA or converted into ssDNA, for example, by asymmetric PCR [71], alkaline denaturation [62], size separation on denaturing poly acryl amide gels [72] or exonuclease digestion of the antisense strand [73]. The progress of the SELEX procedure can be monitored, e.g., by (real-time) PCR, next generation sequencing (NGS), radio- or fluorescent labeling of the nucleic acid pool or melting curve analysis [63]. Thereby, bound sequences can be quantified and / or the decrease in nucleic acid pool diversity (referred to as enrichment) can be analyzed. Furthermore, affinity to the target, can be monitored by various methods like surface plasmon resonance spectroscopy (SPR), electromobility shift assay (EMSA), fluorescent dye-linked aptamer assay (FLAA) or isothermal titration calorimetry (ITC) [62,74].

3.6.2. Design of a SELEX Library

Prior to starting a selection, the design of a suitable nucleic acid library is pivotal for successful aptamer selection. Many advantages of aptamers, such as high binding affinity and ease of chemical synthesis, strongly depend on the nature of the nucleic acid library. Critical factors of library design are the choice of the chemical nature of the nucleic acid, the inclusion of modifications and the length of the random region.

In the early years of aptamer development, RNA libraries were primarily used because it was assumed that only RNA had the ability to fold into functional structures. However, Ellington and Szostak showed early on that ssDNA is also capable of adopting functional structures [75]. Although the structural complexity of RNA oligonucleotides can be higher than that of their ssDNA counterparts [76], DNA offers the advantage of higher chemical and biological stability as well as a simpler and less expensive manufacturing process [77]. In addition, differences in the affinity of DNA and RNA molecules for their targets are not striking [78]. Hence, the choice of the nature of the nucleic acid library is mainly influenced by the planned application. The

application is also crucial for the decision whether a modified library should be used. If the intended use includes the need for aptamer functionality in physiological samples like serum, nuclease susceptibility of both RNA and DNA can be detrimental. Here, libraries containing modified nucleic acids with improved nuclease stability can be beneficial. Generally, nucleic acids can be introduced at the sugar moieties, e.g., 2′-O-methyl and 2′-fluoro ribose, the nucleobases, e.g., 5-ethynyl-2′-deoxyuridine or the backbone, e.g., phosphorothioate modifications [79,80]. Modified libraries have the advantage that modifications are introduced prior to selection as all post-SELEX modifications may alter the aptamers binding properties [78]. However, the synthesis of modified libraries as well as the potential need for mutated polymerases for amplification throughout SELEX increases selection costs strongly.

Another critical factor for SELEX library design is the length of the randomized region as it largely accounts for its diversity. It is generally believed that a diversity of 10^{15} nt is sufficient for successful aptamer selection [81]. This corresponds to a nucleic acid library consisting of 25 nt ($4^{25} = 1.1 * 10^{15}$). Due to limitations in the amount of the library used for selection, larger libraries may not be fully represented. However, libraries with larger randomized regions offer a higher diversity of three-dimensional structures. Furthermore, library length has an impact on experimental procedures throughout SELEX and on post-SELEX processes. Longer DNA templates are more prone to byproduct formation and polymerase chain reaction (PCR) is less efficient for templates longer than 100 nt [82]. They are also less efficiently transcribed in the case of an RNA library. Chemical synthesis of selected aptamers decreases in efficiency and increases in cost with increasing length. Thus, the optimal length of the randomized regions should provide enough diversity for the formation of a variety of three-dimensional structures but should not encumber the synthesis and the selection process. Mostly, randomized regions are designed to consist of 20 - 60 nt [81].

3.6.3. SELEX Strategies

A step of high relevance throughout the selection process is the partitioning of target-bound from unbound sequences. A variety of SELEX methods facilitate this crucial step in different ways. Some depend strongly on the type of target molecule such as cell-SELEX for cells [59] or capture-SELEX for small molecules [83,84]. For protein targets, early SELEX studies used nitrocellulose filter binding for the partitioning of bound and unbound sequences. While unbound sequences pass the filter, protein-bound sequences are retained. An advantage of this method is the equilibrium binding of aptamer and target in solution. Yet, the efficiency of protein capture varies for different proteins and experimental conditions. Furthermore, cellulose binding aptamers have been identified that share a tendency for G-richness [85,86]. Thus, binding of G-rich sequences to the filter may hamper selection success. The

immobilization of the target molecule on column material is another frequently used technique. However, large amounts of the target molecule have long been required [87]. To date, micro-columns may present a suitable alternative. Bead-based SELEX can circumvent some of the limitations described above. A variety of coupling chemistries and affinity resins replace non-specific adsorption, allowing e.g., covalent, or site-directed immobilization. Incubation with the nucleic acid library or nucleic acid pools after a selection round (SR) can be done with pre-immobilized target or in solution prior to immobilization. Both methods bear certain pitfalls. Pre-immobilization can lead to artifactual cooperative binding if immobilization is performed at high density. Capturing of targets bound to aptamers after incubation in solution requires a larger amount of beads that can attract matrix-binding aptamers [88]. Nevertheless, convenient fine-tuning of selection stringency is possible and very little specialized equipment as well as small amounts of the target protein are required. SELEX methods that omit the requirement for target immobilization include EMSA-SELEX and capillary electrophoresis SELEX. Both methods facilitate in-solution binding, however, are limited to target molecules that induce an electrophoretic shift. More advanced methods like microfluidic, microarray- or SPR-based SELEX have been proposed and offer advantages like parallel selection in microfluidic systems or the need for very limited selection rounds. Yet, they often require specialized equipment and are thus not available for many users [88]. The choice of a SELEX strategy is also influenced by the target molecule and the planned application field. Selection strategies employing libraries with modified nucleic acids like click-SELEX [89] or Spiegelmer-SELEX [90] can offer advantages like an expanded chemical diversity of the nucleobases or higher stability in complex media [69] (see also 3.6.2).

3.6.4. Post-SELEX Processes

After a certain amount of SELEX cycles, usually between 6 and 20, the pool's affinity to the target molecule does not improve further. Nucleic acid pools can be either cloned and sequenced or prepared for next generation sequencing (NGS). While for cloning and Sanger sequencing, sequencing data coverage mostly does not exceed a few hundred clones [62,91,92], NGS allows parallel sequencing of tens of thousands to billions of DNA samples [93]. NGS approaches that first entered the market are short-read techniques facilitating massive, parallel sequencing of DNA fragments of 250 - 800 base pairs (bp). They are either based on sequencing by synthesis employing polymerases, like pyrosequencing (e.g., Roche platforms) or reversible dye termination (e.g., Illumina platforms), or on sequencing by ligation (e.g., Life Technologies platforms) [94]. Newer techniques focus on sequencing single molecules. Thereby they allow read lengths exceeding 10 kilo bases and prevent amplification bias. Sequencing data is generated by detection of incorporation of fluorescently labeled nucleotides (used in

Pacific Biosciences platforms) or changes of the electrical conductance during translocation of single DNA strands through nanopores (used in Oxford Nanopore Technologies platforms) [93,95]. Using NGS, the entire nucleic acid pool is sequenced, and not just a few selected clones. Furthermore, nucleic acid pools from various selection rounds can be sequenced in parallel, providing even more information about the SELEX process [96]. Sequencing data is analyzed bioinformatically, and prominent sequences can be chemically synthesized and characterized regarding their affinity and specificity.

Aptamer characterization aims to verify whether selected sequences bind to the target molecule. Qualitative results can be obtained, for example by radioactivity-. fluorescence- or electrophoresis-based assays like radioactive binding assay, FLAA or EMSA [45,97]. Beyond this, quantitative methods are used to test binding properties of the selected aptamers. Methods of choice are MicroScale Thermophoresis (MST), ITC or SPR [98].

Finally, characterized sequences can be optimized. Truncated versions of aptamers are generally lower in production costs and may even exhibit more desirable binding parameters. Research by Cowperthwaite and Ellington suggests that aptamer function is mostly independent of the primer binding regions [99]. Hence, removal of these regions appears rational. Further truncations may be based on secondary structure predictions, comparison with similar sequences obtained from sequencing of the nucleic acid pool or from structure analysis like NMR or X-ray crystallography. Nuclease resistance can be increased by chemical modifications of the sugar rings, bases, or phosphodiester linkage [100]. Base modification can also improve binding affinity of aptamers. Clickmers and SOMAmers, e.g., reach desirable binding parameters by increasing the limited chemical diversity of the four nucleic acid bases [69,101]. Another approach to increase the affinity of a selected aptamer is the conduction of a doped SELEX. The aptamer sequence is partially randomized which creates a new, doped library. NGS data can be used to identify motifs which may be important for binding. Such motifs can be excluded from randomization to maintain affinity for the target molecule. The doped library can be employed for a limited number of SELEX cycles in order to select for sequences with binding properties that are superior to those of the initially selected aptamer [102].

3.6.5. Possible Pitfalls throughout SELEX

Aptamers are promising molecules for a wide range of applications. Over the last three decades various methods were developed for the optimization of the selection, pre- and post-SELEX processes to obtain highly affine and specific binders. Yet, some pitfalls remain that impede efficient aptamer selection. One of the major pitfalls of SELEX is the selection of non-target binders. Commonly used SELEX-methods rely on immobilization of the target

molecule on a solid support. Here, the immobilization matrix may serve as an undesired side target against which aptamers may be selected [103]. Another critical aspect with high impact on the outcome of selection is the sourcing and quality of the target molecule. In case of a protein target, recombinant proteins are often expressed including purification tags to facilitate isolation from cell lysates. Highly pure target molecules are desirable for SELEX to ensure the selected aptamers are selectively directed against the target of choice. Common purification tags include small-size tags like His-, FLAG-, Strep II- or calmodulin-binding-tag, as well as large size tags like maltose-binding protein or glutathione S-transferase-tag. While large tags can improve protein solubility, they can also affect the folding and biological activity of the protein and need to be removed after purification. Smaller tags usually have minimal impact on structure and function and are therefore not frequently removed. The most commonly used tag is the His-tag because it is small, contains no charge, and has very low toxicity and immunogenicity [104]. The His-tag does not interfere with a variety of downstream applications and many commercially available proteins include N- or C-terminal His-tags. However, when performing SELEX, purification tags may also serve as additional, potentially binding epitopes.

The abundance of matrix- or tag-binding sequences within the nucleic acid pool can be decreased by the implementation of negative selection steps. Incubation of the nucleic acid pool with the immobilization matrix or other proteins carrying the same purification tag prior to incubation with the immobilized target molecule can aid to deplete the nucleic acid pool of matrix- or tag-binding sequences. Negative selections can also be performed against structurally related molecules to increase the specificity of selected aptamers [77]. Still, negative selections exert additional selective pressure on the nucleic acid pool and increase stringency [105]. This may be beneficial in some cases but can also result in a loss of binding sequences. Especially when selecting against a suboptimal target molecule, e.g., with overall negative charge, fine tuning of stringency is pivotal. Introduction of negative selections may increase selection stringency strongly and thereby hamper enrichment of the already low number of potential binders. Furthermore, negative selections may not always be sufficient to completely deplete the nucleic acid pool from sequences that bind to other epitopes than the target molecule itself. Yet, this phenomenon has been reported mainly for cell-SELEX in which a broad variety of potential binding epitopes are presented [81]. Nevertheless, the design of selection strategies that overcome the common hurdles in aptamer selection should be well tailored regarding the used immobilization matrix and the target molecule with consideration of the envisaged application.

4. Aim of the Work

In this work, different strategies for the selection of carbapenemase-specific aptamers are evaluated. The goal was to select highly affine and specific aptamers targeting different carbapenemases. The aptamers were selected with respect to implementation in LFDs for rapid, simple, and inexpensive detection of carbapenemase producing CRE. First selections against N-terminally His-tagged carbapenemases His-KPC-2 and His-NDM-1 with negative selections against other His-tagged carbapenemases did not result in the identification of carbapenemase aptamers. Discontinuation of negative selections against related proteins for consecutive selection rounds resulted in the identification of highly affine His-tag aptamers. Based on this, it became a goal to develop selection strategies that prevent His-tag binding while facilitating carbapenemase binding. Three selection strategies were developed, two of which utilized the previously selected high-affinity His-tag aptamer. The strategies were tested using His-KPC-2 as a model target, since high-affinity aptamers had been selected in the meantime [106]. The goal was firstly to select for further KPC-2 specific aptamers and secondly to transfer the most successful strategy to selection against His-NDM-1. For His-NDM-1, no highly affine ssDNA aptamer was found in the scientific literature. Thus, the most successful selection strategy was applied to selection against His-NDM-1 with the aim of selecting highly affine, specific, and well characterized aptamers for the implementation into an LFD.

5. Results

This work describes the development of selection strategies for the selection of aptamers against carbapenemases. Due to their high abundance and clinical relevance, KPC-2 and NDM-1 were chosen as first targets for selection. In order to generate aptamers against these targets, an ssDNA library was designed (section 5.1). Recombinantly expressed N-terminally His-tagged carbapenemases His-NDM-1 and His-KPC-2 were purchased and immobilization on magnetic beads was tested to facilitate separation of bound and unbound sequences. To ensure functional folding, enzymatic activity was tested before and after immobilization (section 5.2). Eleven selection rounds were performed with negative selections against other His-tagged carbapenemases but did not result in the identification of aptamers (section 5.3). Consecutive selection rounds without negative selections against other carbapenemases resulted in the identification of highly affine His-tag-binding aptamers (also referred to as His-tag aptamers, section 5.4). Three selection strategies, two of which employed the previously selected His-tag aptamers, were developed to prevent His-tag binding (section 5.5) and tested using His-KPC-2 as a model target (section 5.6). As His-KPC-2 specific aptamers were identified, a sandwich assay-based LFD for the detection of His-KPC-2 was developed (section 5.7). The most promising approach to prevent His-tag binding was chosen and applied to selection against His-NDM-1 (section 5.8). An NDM-1 specific aptamer with high nanomolar to low micromolar affinity was identified. As an approach to increase aptamer affinity, a doped library with a partially randomized library, based on the NDM-1 aptamer was performed (section 5.9).

5.1. Design and Testing of the SELEX Library

The first step was the design of an ssDNA library composed of a continuous, fully randomized region flanked by two primer regions. The length of the randomized region was set to 44 nt and the length of the primer was set to 18 nt. Here, sufficient structural diversity, but also the need for good PCR performance and synthesis costs were considered. For the design of the primer regions, random sequences were generated using the Maduro Labs Random DNA Sequence Generator software. Resulting sequences were analyzed using IDT Oligo-Analyzer™ software (see also 8.1.5). The maximum Gibbs free energy change (maximum Δ*G*) of homodimer and hairpin formation of a single sequence and heterodimer formation with the other potential primer binding site were compared with the maximum Δ*G* of the desired primer binding reaction. The 5’ forward primer site was designed as GTA TCT GGT GGT CTA TGG and exhibited Δ*G* values of > −1.47 kcal/mol for homodimer formation and > 0.84 kcal/mol for hairpin formation while maximum Δ*G* of the desired primer binding reaction was −30.31 kcal/mol. The 3’ reverse primer binding site was designed as GTT CTT CGT CGT CTA

TGC and exhibited Δ*G* values of > −3.61 kcal/mol for homodimer formation and > 1.19 kcal/mol for hairpin formation while maximum Δ*G* of the primer binding its complement was −32.16 kcal/mol. Hetero dimer formation was calculated at a maximum Δ*G* of > −1.47 kcal/mol. Hairpin formation was not energetically favored, and dimer formation was considerably less favorable than the desired primer binding reaction. The resulting forward primer GTA TCT GGT GGT CTA TGG, termed F44 and the reverse primer GTT CTT CGT CGT CTA TGC, termed R44 were synthesized.

Subsequently, primers were tested for nonspecific amplification either without template or with an already established ssDNA library (AGG TAG AGG AGC AAG CCA TC - N(42) - GAT GCG TGA TCG AAC CTA CC, termed Library 42) containing different primer binding regions and a randomized region of 42 nt (see also 8.3.1). Melting temperatures for the primers were calculated by the IDT OligoAnalyzer™ software as 59 °C for F44 and 61.1°C for R44. Amplification was tested with annealing temperatures of 56 °C, 61 °C and 66 °C for 10, 20, 30 and 40 PCR cycles. After ten, twenty and thirty cycles no PCR product was detectable. After 40 cycles, nonspecific PCR products were detected for reactions with annealing temperatures of 56°C and 61°C and 300 ng Library 42 as template DNA. No nonspecific product was detected for the primers only reactions (**Figure 5**).

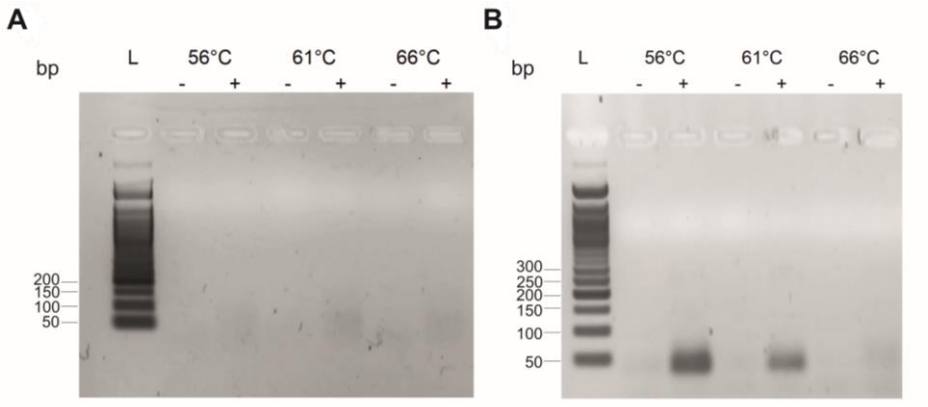

Figure 5: Test for non-specific DNA amplification with primers F44 and R44. PCR products after (A) 30 and (B) 40 PCR cycles with different annealing temperatures (56 °C, 61 °C and 66 °C) are visualized on a 2% agarose gel. Primers were used for PCR either without template DNA (-) or with 300 ng of Library 42 (+) to test for non-specific amplification. After 30 PCR cycles no PCR products were detected, while after 40 PCR cycles PCR products were only detected for non-specific amplification of library 42. L = 50 bp DNA Ladder.

Thus, the library was synthesized as 5'- GTA TCT GGT GGT CTA TGG - N(44) - GCA TAG ACG ACG AAG AAC - 3'. To control the quality of the newly established library, next generation sequencing (NGS) – Illumina Dye Sequencing (see also 8.8) was performed. Bioinformatic evaluation of the results using the AptaAnalyzer™-SELEX software showed that the library was composed of 99.8% of unique sequences. 92.5% of sequences contained a randomized region of 44 nt, 5.2% contained 43 nt, 0.7% contained 42 nt and 0.4% 45 nt. Sequences with random regions < 42 nt or > 45 nt summed up to less than 0.3%. As the library was highly diverse and mostly correct in length, it was chosen for selection. Amplification was tested with annealing temperatures of 55 °C, 60 °C and 65 °C. Amplification of 300 ng template DNA was successful for all three annealing temperatures. After 20 PCR cycles, concentrations were measured. Amplification with annealing temperatures of 55 °C, 60 °C and 65 °C resulted in 2.65, 2.17 and 1.6 µg dsDNA per 100 µl PCR reaction. As the highest yield was reached at a temperature of 55 °C, the annealing temperature was set to 55 °C.

5.2. Target Preparation

KPC-2 and NDM-1 were chosen as first targets for SELEX as their abundance among carbapenemases as well as their clinical relevance are high. Hence, rapid detection of these carbapenemases is desirable. Both targets as well as a third carbapenemase OXA-23 were obtained including an N-terminal hexa-His-tag. To ensure that the recombinantly expressed targets were functionally folded, and thus suitable targets for SELEX, enzymatic activity of His-NDM-1 and His-KPC-2 was tested using RAPIDEC® CARBA NP test from bioMérieux (see also 8.1.1). His-OXA-23 was chosen as a negative selection target and was thus tested for activity alongside the two target proteins. 1 µg of all three carbapenemases were used for activity assessment. A positive result was visible for all three carbapenemases (**Figure 6**). For the negative selection target His-OXA-23, the color change was much weaker than for His-KPC-2 and His-NDM-1, consistent with the low carbapenemase activity of the oxacillinases (see also 3.3).

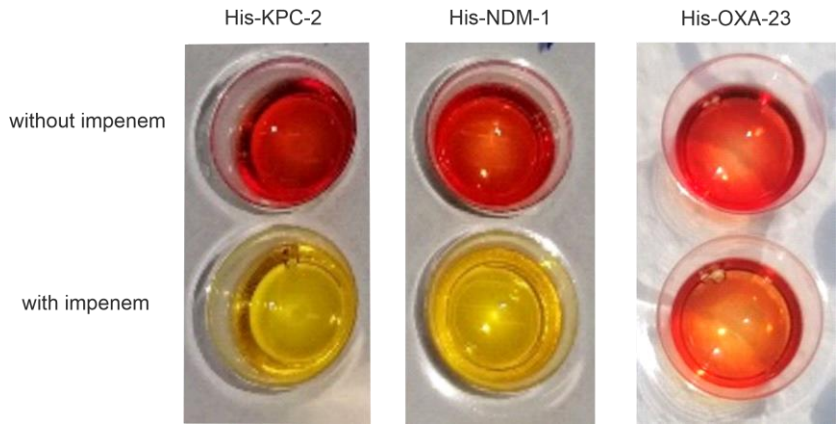

Figure 6: Activity assessment of His-KPC-2, His-NDM-1, and His-OXA-23. RAPIDEC® CARBA NP test from bioMérieux was used to visualize the pH shift upon impenem hydrolysis caused by carbapenemases His-KPC-2, His-NDM-1, and His-OXA-23. For His-KPC-2 and His-NDM-1 a strong color change was detected in the presence of impenem while for His-OXA-23 the color change was considerably weaker.

For SELEX, His-KPC-2, His-NDM-1 and His-OXA-23 were covalently coupled to Dynabeads™ M-280 Tosylactivated (see also 8.1.2). Coupling efficiencies varied between the targets as well as when coupling was repeated throughout the selection process. An overview of coupling efficiencies and the concentration of coupled carbapenemase and unrelated proteins used for negative selections per µl beads are shown in the appendix (**Appendix Table 1-5**). After the first immobilization of His-KPC-2 and His-NDM-1, coupling success was also evaluated by detection of the His-tags, by ELISA (**Figure 7A**, see also 8.1.4).

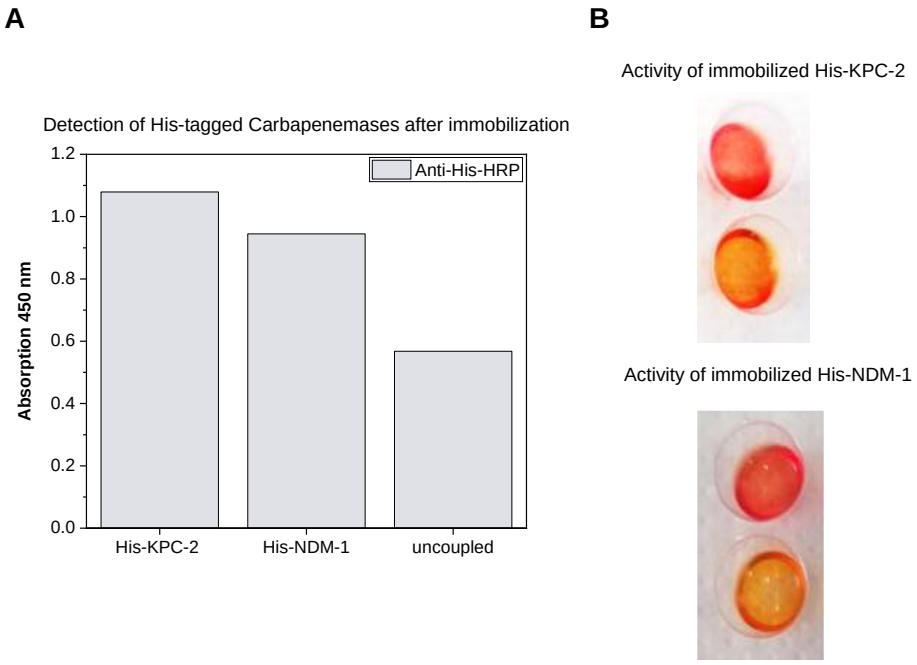

Figure 7: Detection and activity assessment of immobilized His-KPC-2 and His-NDM-1. (A) Detection of His-tagged carbapenemases 1 coupled to Dynabeads™ M-280 Tosylactivated by ELISA was performed with a HRP-labeled anti-penta-His-antibody. Signals of beads coated with His-KPC-2 and His-NDM-1 exceeded the signal derived from the uncoupled beads control. Absorption measurement at 450 nm was performed using Mithras² LB 943. (B) Carbapenemase activity of His-KPC-2 and His-NDM-1 coupled to Dynabeads™ M-280 Tosylactivated was assessed using RAPIDEC® CARBA NP test from bioMérieux. Weak enzymatic activity of immobilized carbapenemases was detectable.

Background binding of the anti-penta-His antibody was high. Nevertheless, beads carrying either 89 pmol His-KPC-2 or 31 pmol His-NDM-1 showed absoprtion values exceeding that of the negative control by factors 1.9 and 1.7, respectively. Thus, ELISA providided an indication that immobilization of the His-tagged carbapenemases was succesful. To further substantiate coupling success and to assess whether functional folding was retained, activity of the coupled carbapenemases was tested using RAPIDEC® CARBA NP test from bioMérieux (see also 8.1.1). As coupling efficiencies had varied, 0.6 µg of immobilized His-NDM-1 and 0.9 µg of immobilized His-KPC-2 were added to the test. A color change was detected for both immobilized carbapenemases Here, the colour change was considerably weaker than for uncoupled His-KPC-2 and His-NDM-1 (**Figure 7B**). Nevertheless, a positive test result was obtained for both carbapenemases accounting for a successful immobilization and allowing the assumption that at least a portion of the active centers were still available. Hence, carbapenemase-coupled beads were used for selection.

5.3. First Selection Rounds against His-KPC-2 and His-NDM-1

First aptamer selections against His-KPC-2 and His-NDM-1 were carried out with both targets immobilized on Dynabeads™ M-280 Tosylactivated. Selections against His-NDM-1 and His-KPC-2 failed after SR1.1 and SR2.1, respectively as no PCR product was obtained after these rounds. Thus, selection was restarted as SR1.2. From SR1.2 on, the number and duration of washing steps as well as the number of negative selections carried out against beads only were increased while the amount of ssDNA was decreased. To obtain specific binders, from SR5.1 - 11.1 negative selections were performed against the respective other target molecule (His-NDM-1 for His-KPC-2 and vice versa). From SR8.1 on, additional negative selections against a third carbapenemase – His-OXA-23 – were performed. From SR3.1 (His-NDM-1 selection) or SR4.1 (His-KPC-2 selection) on, control selections were introduced against beads only (see also 8.2.1, 8.2.2, **Table 19** and **Table 20**). The selection progress was monitored by PCR analysis (see also 8.3.2), the diversity assay for nucleic acids (DANA, see also 8.7) and finally by FLAA (see also 8.9).

5.3.1. PCR Analysis

After each selection step, ssDNA amplification of different fractions was analyzed. An endpoint analysis of amplified DNA from the last washing step, the eluted ssDNA that was bound to the beads, and the remaining ssDNA on the beads to test whether elution was successful, was evaluated by gel electrophoresis. Control selections with uncoupled beads as the target were carried out for various rounds of selection (see also **Table 1**). Here the PCR products of fractions derived from uncoupled beads were compared to PCR products from fractions with carbapenemase-coupled beads. Sequences eluted from negative selection beads, coupled with other His-tagged carbapenemases, were also amplified and loaded onto a gel. However, signals derived from negative selections were not directly comparable to signals derived from target selection. For negative selections, elution was conducted without additional washing steps after target incubation, while for target selections, increasing numbers of washing steps were performed. **Figure 8** shows two exemplary PCR analyses (for SR5.1 and 11.1) of the last washing step, the elution step, and the remaining ssDNA on the beads for each target molecule.

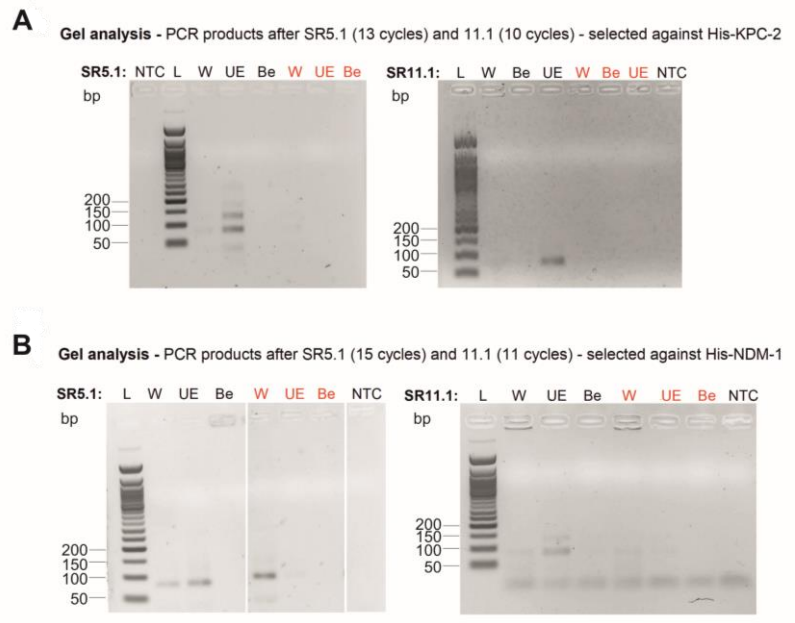

Figure 8: Gel analysis after SRs 5.1 and 11.1. (A) Gel analysis is shown for selection against His-KPC-2 after SR5.1 with 13 PCR cycles and SR11.1 with 10 PCR cycles. (B) Gel analysis is shown for selection against His-NDM-1 after SR5.1 with 15 PCR cycles and SR11.1 with 11 PCR cycles. Fractions last washing step (W), urea elution (UE) and beads (Be) were compared between target selection (black) and control selection (red) as well as between SRs. NTC = no template control, L = 50 bp DNA ladder.

For both SRs, control selections were conducted and compared to selections against the target molecules His-KPC-2 and His-NDM-1. For selection against His-KPC-2, after SR5.1 a highly intense signal for the eluted ssDNA as well as a faint signal for the last washing step was detected after 13 PCR cycles. No PCR product was obtained for the control selection (**Figure 8A**). Here, 20 PCR cycles were necessary to obtain signals for the elution and washing fractions (data not shown). Signals for ssDNA remaining on the beads after elution were not obtained. After SR11.1, a highly intense signal for the eluted ssDNA was detected after 10 PCR cycles (**Figure 8A**). After 13 PCR cycles, a clear signal from ssDNA in the last washing step of the target selection as well as faint signals for the washing and elution fraction from the control selection were detected (data not shown). Thus, as early as SR5.1, target selection resulted in an elution fraction signal after fewer PCR cycles than control selection, indicating the presence of target-binding sequences in higher copy number than matrix binders. In addition, a reduction in the number of PCR cycles required to obtain an elution fraction signal from SR5.1 to SR11.1, from 13 to 10 (see also **Table 1**), suggests enrichment of target-binding sequences in the ssDNA pool. For selection against His-NDM-1, after SR5.1 signals for the elution and washing step as well as the washing step of the control selection were detected after 15 PCR cycles (**Figure 8B**). A signal for the elution fraction of the control selection was detected after 20 PCR cycles (data not shown). Hence, a signal for the elution fraction derived

from the target selection was detected after fewer PCR cycles than that of the elution fraction derived from the control selection (see also **Table 1**). After SR11.1, a clear signal for the elution fraction as well as a faint signal for the washing fraction were detected after 11 PCR cycles (**Figure 8B**). For the control selection, a faint signal for the elution fraction and a clear signal for the washing fraction were detected after 14 PCR cycles. Signals for remaining ssDNA on the beads after elution were not detected (data not shown). For selection against His-NDM-1, the same trend was visible as for selection against His-KPC-2. PCR cycles decreased from SR5.1 - SR11.1 from 15 to 11 even though washing steps were increased and the initial amount of ssDNA was decreased. Furthermore, more PCR cycles were necessary to obtain signals from the control selection than from the target selection (see also **Table 1**), indicating enrichment of target-binding sequences. PCR analysis indicated a successful progression of selection. Still, selection was hampered by byproduct formation. For both targets, byproduct formation of both higher and lower molecular weight was detected frequently after PCR and had to be removed by polyacrylamide gel electrophoresis (PAGE) purification (see also 8.4.2). An exemplary gel of PCR2a (see also 8.3.3) after SR8.1, selected against His-NDM-1 is shown in **Appendix Figure 1**. Here, a byproduct of approximately 130 bp, displaying an intensity comparable to the PCR product at the expected length of 80 bp, is detectable. Another byproduct below 50 bp exhibits a lower intensity than the PCR product at the expected length.

Table 1: PCR cycles required to obtain a signal from the elution fractions for SR1.1 - SR11.1 for selections against His-KPC-2 and His-NDM-1.

SR His-KPC-2	PCR cycles	SR His-NDM-1	PCR cycles
1.1	15	1.1	15
2.1	np	1.2	11
1.2	15	2.1	13
2.2	15	3.1	15
3.1	14	3.1_Control	18
4.1	10	4.1	15
4.1_Control	15	5.1	15
5.1	13	5.1_Control	20
5.1_Control	20	6.1	15
6.1	14	6.1_Control	15
7.1	11	7.1	16
7.1_Control	14	6.2	15
8.1	10	6.2_Control	18
9.1	9	7.2	10
9.1_Control	12	7.2_Control	12
10.1	9	8.1	10
11.1	10	8.1_Control	13
11.1_Control	13	9.1	9
		10.1	10
		10.1_Control	12
		11.1	11
		11.1_Control	18

**np = no product detected*

5.3.2. Enrichment and Affinity Analysis

Over the course of selection, enrichment was monitored by DANA (see also 8.7). Band intensities of gel electrophoresis obtained from reactions with S1 nuclease were compared to signals derived from reactions without S1 nuclease. Double stranded DNA from a highly diverse library served as a negative control and dsDNA from a single DNA sequence, e.g., an aptamer, served as a positive control. For selection against His-KPC-2, faint signals, exceeding that of the negative control, were obtained that slightly increased from SR7.1 - SR10.1. All signals derived from reactions with S1 nuclease were substantially lower than that derived from reactions without S1 nuclease except for the positive control. For selection against His-NDM-1, signals were more intense and clearly exceeded that of the negative control. Signal intensity also increased from SR7.1 - 10.1 (**Figure 9A**). As an increasing enrichment was indicated for both targets, one more SR was conducted after which affinity was tested by FLAA (see also 8.9). His-KPC-2 and His-NDM-1 were immobilized non-directionally and incubated with either the initial library or ssDNA pools of SR11.1 from selections against His-KPC-2 or His-NDM-1, respectively. For both immobilized carbapene-mases the respective ssDNA pool showed slightly higher fluorescence signals than the initial

library (**Figure 9B**). Yet, signal fluctuations were high for the ssDNA pool selected against His-KPC-2 when incubated with immobilized His-KPC-2 and for the initial library, when incubated with immobilized His-NDM-1. Nevertheless, affinity of the selected pools to the targets was indicated.

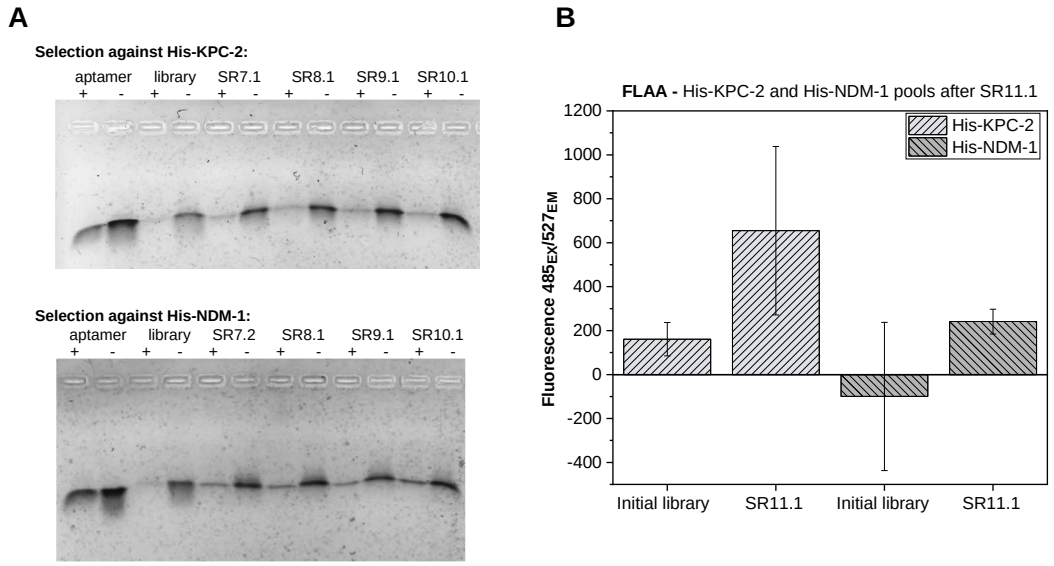

Figure 9: Enrichment and affinity analysis of DNA pools after SR11.1. (A) Enrichment was analyzed for selection against His-KPC-2 for SRs 7.1 - 10.1 (above) and against His-NDM-1 for SRs 7.2 - 10.1 (below), respectively. Signals obtained from reactions incubated with S1 nuclease (+) were compared to signals derived from reactions without S1 nuclease (-). Slight enrichment was detected for selection against His-KPC-2 and stronger enrichment that was increasing from SR7.2 - 10.1 for selection against His-NDM-1. (B) Affinity was tested after SR11.1 for selections against both targets by FLAA. Fluorescence units measured with excitation at 485 nm and emission at 527 nm using Mithras² LB 943 are shown. Signals derived from the ssDNA pools exceeded those derived from the initial library indicating affinity to the target. Fluorescence values of two target-coated and two negative control wells were averaged, and negative control values were subtracted. Error bars represent the square root of the sum of the variances of two target-coated wells and two negative control wells.

5.3.3. Next Generation Sequencing and Aptamer Candidate Analysis

As slight enrichment and affinity to the respective target molecule were detected for both selections, ssDNA pools from multiple selection rounds were sequenced. For selection against His-KPC-2, ssDNA pools from SR11.1 as well as 11.1_Control, 10.1 and 9.1 and for selection against His-NDM-1, ssDNA pools from SR11.1, 11.1_Control and 10.1 were prepared for NGS (see also 8.3.4) and sequenced (see also 8.8). The overall enrichment of the DNA pools was analyzed using the AptaAnalyzer™-SELEX software. For ssDNA pools selected against His-KPC-2 the percentage of unique sequences varied between 63.3%, 62.6% and 67.2% for SR9.1, SR10.1, and SR11.1 and 67.5% for SR11.1_Control. For ssDNA pools selected against

His-NDM-1, unique sequences accounted for 71.4% after SR10.1, 65.3% after SR11.1 and 75.6% after SR11.1_Control. Thus, diversity of the DNA pools decreased. Yet, the enrichment of single sequences was low. After SR11.1, the most enriched sequences accounted for 0.66% and 1.43% of total sequences for His-NDM-1 and His-KPC-2, respectively. The randomized regions of the 50 most enriched sequences were analyzed for repeatedly occurring motifs. The threshold for reoccurrence was set to at least three sequences bearing the motif. The threshold for nucleotides forming the motif to at least 5, based on the usual length of DNA motifs in genomic analysis [107]. For both selections, only one motif was identified that occurred in five sequences for selection against His-NDM-1 and four sequences for selection against His-KPC-2 (**Appendix Table 6**). Striking homology was not detected. Still, seven sequences from selection against His-KPC-2 and nine single sequences from selection against His-NDM-1 were synthesized as aptamer candidates (see also **Table 14**). Sequences were selected according to their overall enrichment after SR11.1 and on the condition that the percentage of total sequences was higher for SR11.1 than for SR11.1_Control.

Selected sequences were further tested for binding to their respective target (see also 8.9). FLAA was conducted separately with immobilized His-KPC-2 and potential His-KPC-2-binding sequences and immobilized His-NDM-1 and potential NDM-1-binding sequences. Binding signals of aptamer candidates were compared to binding of the initial library. For His-KPC-2, all aptamer candidates, except for KPC2-H11-12 showed slightly higher signals than the initial library. However, the range of signals was too high to conclude binding (**Figure 10A**). No binding for any single aptamer candidate was detected for His-NDM-1 (**Figure 10B**). To further analyze binding of the aptamer candidates, His-NDM-1 and His-KPC-2 were immobilized on different channels of an SPR sensor chip and all aptamer candidates were injected sequentially (see also 8.11). Unrelated, C-terminally His-tagged mouse programmed cell death protein 1 (mPD1-His) was immobilized on the reference channels. A third, His-tagged carbapenemase – His-OXA-23 – was immobilized on the fourth channel to test for cross reactivity with a carbapenemase from another Ambler class. Response units of the reference channel were subtracted. No binding of any aptamer candidate was detectable for both targets and for control target His-OXA-23. Signals derived from the His-KPC-2 channel are exemplarily shown in **Figure 10C**. Signals derived from the His-NDM-1 and His-OXA-23 channel can be found in **Appendix Figure 2A - B**. Aptamer candidates did not show binding to the reference channel as well (**Appendix Figure 2C**).

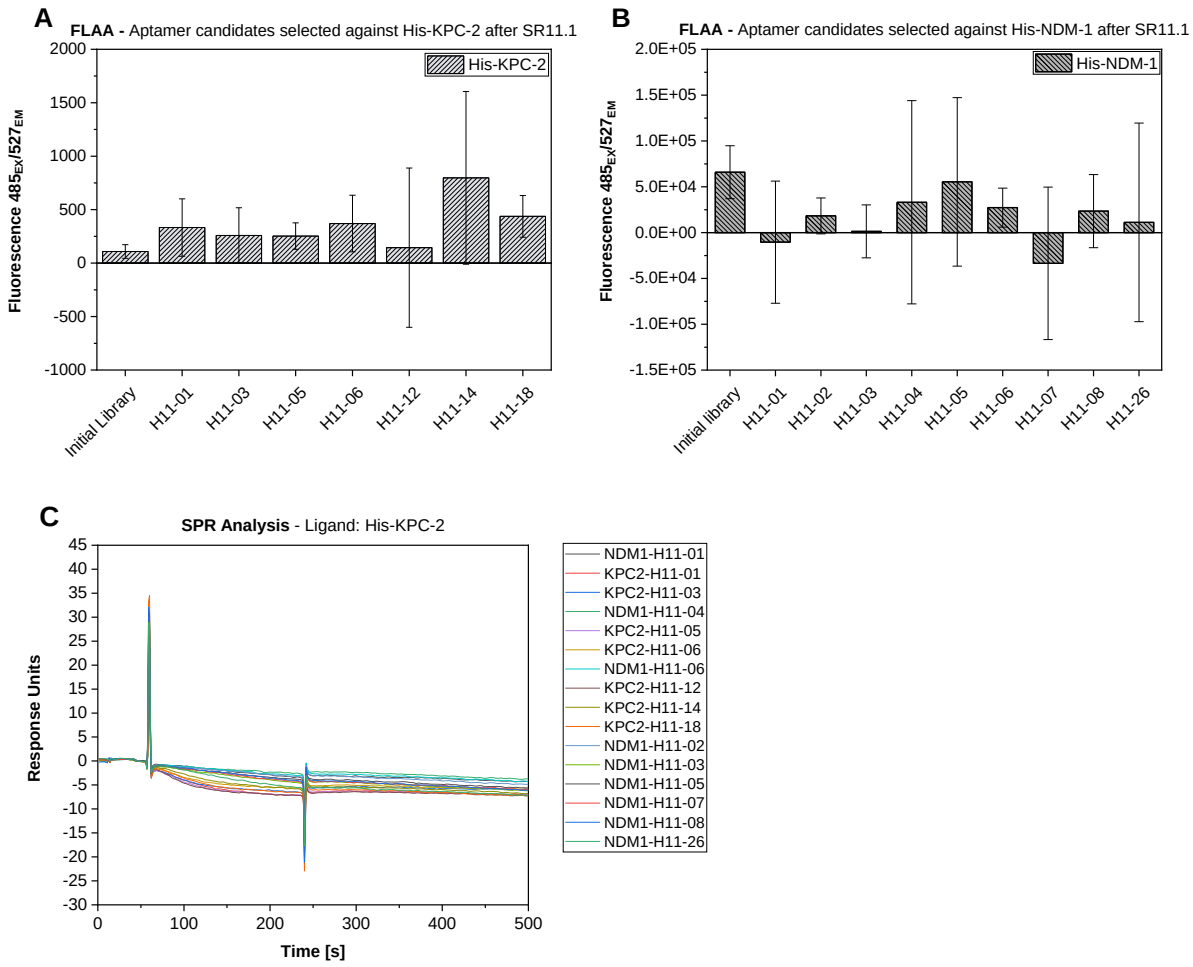

Figure 10: Characterization of aptamer candidates after SR11.1. (A) Aptamer candidates selected against His-KPC-2 were characterized by FLAA. Fluorescence units measured with excitation at 485 nm and emission at 527 nm using Mithras² LB 943 are shown. (B) Aptamer candidates selected against His-NDM-1 were also characterized by FLAA. Fluorescence units measured with excitation at 485 nm and emission at 527 nm using EnVision® 2105 are shown. Fluorescence values of two target-coated and two negative control wells were averaged, and negative control values were subtracted. Error bars represent the square root of the sum of the variances of two target-coated wells and two negative control wells. (C) All aptamer candidates after SR11.1 were characterized for binding to His-KPC-2 by SPR. Response units over the course of 500 seconds are shown. Signals derived from the reference channel were subtracted. Binding was also characterized to His-NDM-1 and His-OXA-23 **Appendix Figure 2A-B**). No binding was detected.

5.4. Selection Rounds without Negative Selections against Carbapenemases

From SR5.1 on, negative selections had been conducted against other His-tagged carbapenemases. Negative selections against related molecules can exhibit strong selective pressure on the ssDNA pool and may result in suppression of target-binding sequences. Hence, selection was continued for three consecutive SR (SR12.1 - 14.1) with negative

selections only against the selection matrix – Dynabeads™ M-280 Tosylactivated (see also 8.2.2, **Table 19** and **Table 20**).

5.4.1. PCR Analysis

Selection progress was monitored by analytical PCR1 (see also 8.3.2). For selection against both targets, selection pressure was kept constant throughout SR12.1 - 14.1 with equal washing steps, negative selections as well as equal ssDNA and target amounts. Still, PCR cycles required to detect a signal on an agarose gel for the elution fraction derived from target selection decreased. For both selections, elution fraction from the control selections all required more PCR cycles than those of the target selections (**Table 2**). Thus, comparison of PCR signals indicated enrichment of target-binding sequences rather than matrix binders. The number of PCR cycles required to detect a signal derived from the washing fractions varied between 10 and 20 PCR cycles (data not shown). Here, no trend was observed.

Table 2: PCR cycles required to obtain a signal from the elution fractions for SR12.1 - SR14.1 for selections against His-KPC-2 and His-NDM-1.

SR His-KPC-2	PCR cycles	SR His-NDM-1	PCR cycles
12.1	12	12.1	15
12.1_Control	19	12.1_Control	20
13.1	10	13.1	15
14.1	10	13.2	14
14.1_Control	16	13.2_Control	16
		14.1	10
		14.1_Control	18

5.4.2. Enrichment and Affinity Analysis

After two consecutive rounds of selection, DANA was performed to monitor enrichment of the DNA pools (see also 8.7). Double-stranded DNA from SR11.1, 12.1 and 13.1 derived from selection against His-KPC-2 and from SR10.1, 11.1, 12.1 and 13.2 derived from selection against His-NDM-1 was used for DANA. For selection against His-KPC-2, after gel electrophoresis, signals with high intensity derived from reactions with S1 nuclease were already detected for SR11.1 (selected with negative selections against other His-tagged carbapenemases) and 12.1. Even more intense signals were obtained from dsDNA from SR13.1. For selection against His-NDM-1, signals derived from reactions with S1 nuclease showed lower intensity than for selection against His-KPC-2. Nevertheless, a slight signal was obtained for dsDNA from SR11.1 (selected with negative selections against other His-tagged

carbapenemases) and signals for dsDNA after SR12.1 and 13.2 were of increasing intensity (**Figure 11A**). One more SR was performed, and target affinity was tested by FLAA (see also 8.9). This time, the overall signal intensity was considerably higher than for ssDNA from SR11.1 for both targets (see also **Figure 9B**). Here, fluorescence signals derived from ssDNA pools after SR14.1 exceeded those derived from the negative control by factors 26.3 for selection against His-KPC-2 and 155.9 for His-NDM-1 (**Figure 11B**). Thus, high affinity towards the respective target molecules was observed.

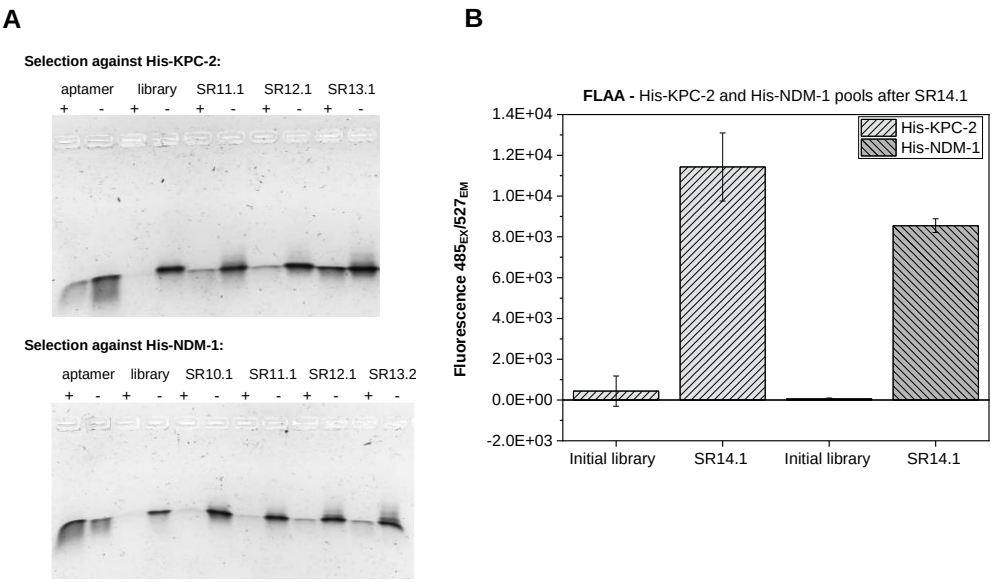

Figure 11: Enrichment and affinity analysis of DNA pools after SR14.1. (A) Enrichment was analyzed for selection against His-KPC-2 for SRs 11.1 - 13.1 (above) and against His-NDM-1 for SRs 10.1 - 13.2 (below), respectively. Signals obtained from reactions incubated with S1 nuclease (+) were compared to signals derived from reactions without S1 nuclease (-). Strong enrichment was detected for selection against His-KPC-2 after SR13.1 and slight enrichment for selection against His-NDM-1 after SR13.2. (B) Affinity was tested after SR14.1 for selections against both targets by FLAA. Fluorescence units measured with excitation at 485 nm and emission at 527 nm using Mithras² LB 943 are shown. Signals derived from the ssDNA pools exceeded those derived from the initial library considerably more than after SR11.1. Fluorescence values of two target-coated and two negative control wells were averaged, and negative control values were subtracted. Error bars represent the square root of the sum of the variances of two target-coated wells and two negative control wells.

5.4.3. Next Generation Sequencing and Characterization of Aptamer Candidates

As enrichment and affinity were detected, ssDNA pools from SR13.1, 14.1 and 14.1_Control (His-KPC-2) and SR13.2, 14.1 and 14.1_Control (His-NDM-1) were sequenced (see also 8.8). The percentage of unique sequences fluctuated strongly for His-KPC-2 with 31.5% for SR13.1, 58.0% for SR14.1 and 43.5% for SR14.1_Control. For His-NDM-1, the percentage of unique sequences was still rather high for target selections with 75.3% for SR13.2, 64.8% for SR14.1

and strongly decreased for control selection with 38.8% for SR14.1_Control. Yet, the most enriched sequences for both targets now accounted for 6.8% (SR14.1, His-KPC-2) and 4.7% (SR14.1, His-NDM-1) as expected for a successful aptamer selection. The randomized regions of the 50 most enriched sequences were analyzed for repeatedly occurring motifs (> 5nt) that were identifiable in more than three sequences. For selection against His-KPC-2, six repeatedly occurring motifs and for selection against His-NDM-1 four repeatedly occurring motifs were identified (**Appendix Table 6**). Sequences bearing the identified motifs were grouped as a sequence family. 20 sequences (see also **Table 14**), including members of the sequence families were synthesized on the condition that the percentage of total sequences was higher for SR14.1 than for SR14.1_Control. During the evaluation of the 50 most enriched sequences for selections against His-KPC-2 and His-NDM-1, it was noticed that most sequences also appeared in the NGS data from selection against the respective other target. Of 20 synthesized sequences, six were unique for selection against His-KPC-2 within the 50 most enriched sequences and three were unique for selection against His-NDM-1. Hence, more than half of the selected sequences were among the 50 most enriched sequences for both His-KPC-2 and His-NDM-1 selections. The most enriched sequence only differed by one nucleotide between the two selections and was synthesized as selected against His-KPC-2. As many sequences derived from selections against both targets aptamer candidates were named as follows:

1. The target for which the sequence was ranked higher (i.e., occurred more often)
2. H14 indicating urea elution and the SR
3. Rank of the sequence in the selection against the target for which the sequence was ranked higher
4. Rank of the sequence for the target for which the sequences was ranked lower in brackets

NDM1-H14-02(04) is an example for a sequence that was derived from urea elution and SR14, that was ranked second when selected against His-NDM-1 and fourth when selected against His-KPC-2. The most enriched sequence was named KPC2-H14-01(01) but also referred to as NDM1-H14-01 elsewhere [108]. Aptamer candidates were tested for their affinity to their respective target using FLAA (**Figure 12**), see also 8.9). For His-KPC-2, two aptamer candidates showed strikingly high signals, namely KPC2-H14-01(01) (80 nt) and KPC2-H14-08 (121 nt). For His-NDM-1, KPC2-H14-01(01) exhibited by far the highest signal.

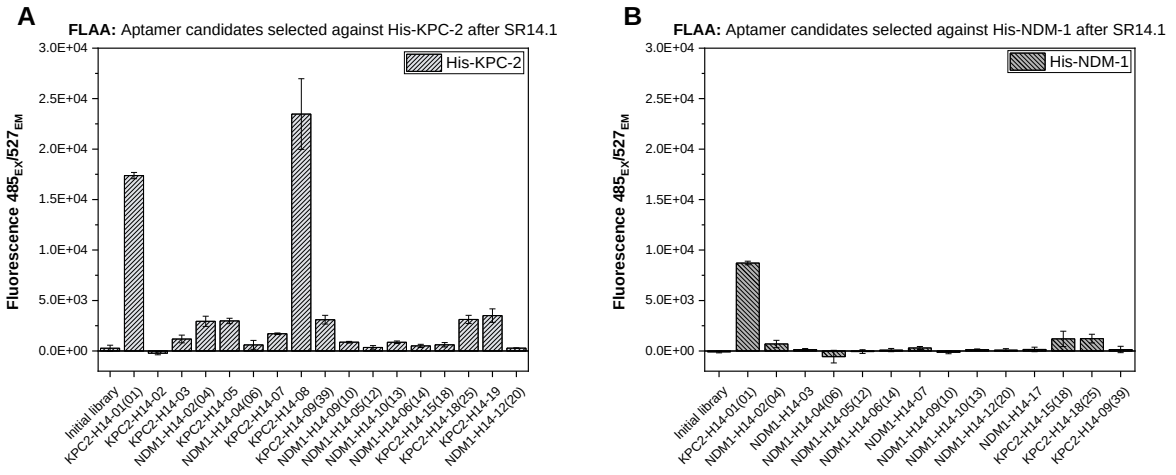

Figure 12: Characterization of aptamer candidates after SR14.1 by FLAA. FLAA was performed on aptamer candidates selected against (A) His-KPC-2 and (B) His-NDM-1. Fluorescence units measured with excitation at 485 nm and emission at 527 nm using Mithras² LB 943 are shown. High signals were obtained for aptamer candidates KPC2-H14-01(01) derived from selections against both targets and KPC2-H14-08 derived from selection against His-KPC-2. Fluorescence values of two target-coated and two negative control wells were averaged, and negative control values were subtracted. Error bars represent the square root of the sum of the variances of two target-coated wells and two negative control wells.

As high fluorescence signals were obtained by FLAA, truncated versions of these aptamers were synthesized to address whether those retained binding. KPC2-H14-01(01) (80 nt) was shortened by either the forward (KPC2-H14-01(01)**-F**, 62 nt) or reverse (KPC2-H14-01(01)**-R**, 62 nt) primer binding region or both (KPC2-H14-01(01)**-FR**, 44 nt). KPC2-H14-08 (121 nt) was only shortened by both primer binding regions (KPC2-H14-08-FR, 85 nt) because of its length. Longer aptamer sequences are more expensive and difficult to synthesize, and thus full truncation was necessary to obtain a reasonable aptamer length. For a more in-depth analysis of binding and cross reactivity, SPR analysis was conducted with the full-length as well as the truncated aptamers (see also 8.11). As for SR11.1, unrelated His-tagged protein mPD1-His was immobilized on the reference channel. The target proteins His-KPC-2 and His-NDM-1 were immobilized on channels two and three while a third, His-tagged carbapenemase – His-OXA-23 – was immobilized on the fourth channel. Response units of the reference channel were subtracted. Contrary to expectations, binding signals were strongest for the reference channel, resulting in negative response units (RU) for all three carbapenemases, when the reference signal was subtracted (see **Appendix Figure 3**). Thus, data was reevaluated without subtraction of the reference channel, showing strong binding signals for all aptamer candidates and all proteins on the flow channels. For all three His-tagged carbapenemases, binding signals were strongest for KPC2-H14-01(01)-R, followed by KPC2-H14-08. Only for mPD1-His, RU were higher for KPC2-H14-08 than for KPC2-H14-01(01)-R. For all four

His-tagged proteins, KPC2-H14-08-FR showed the lowest RU (**Figure 13**). As all four proteins contained a His-tag and binding was detected to all of them, His-tag binding was suspected.

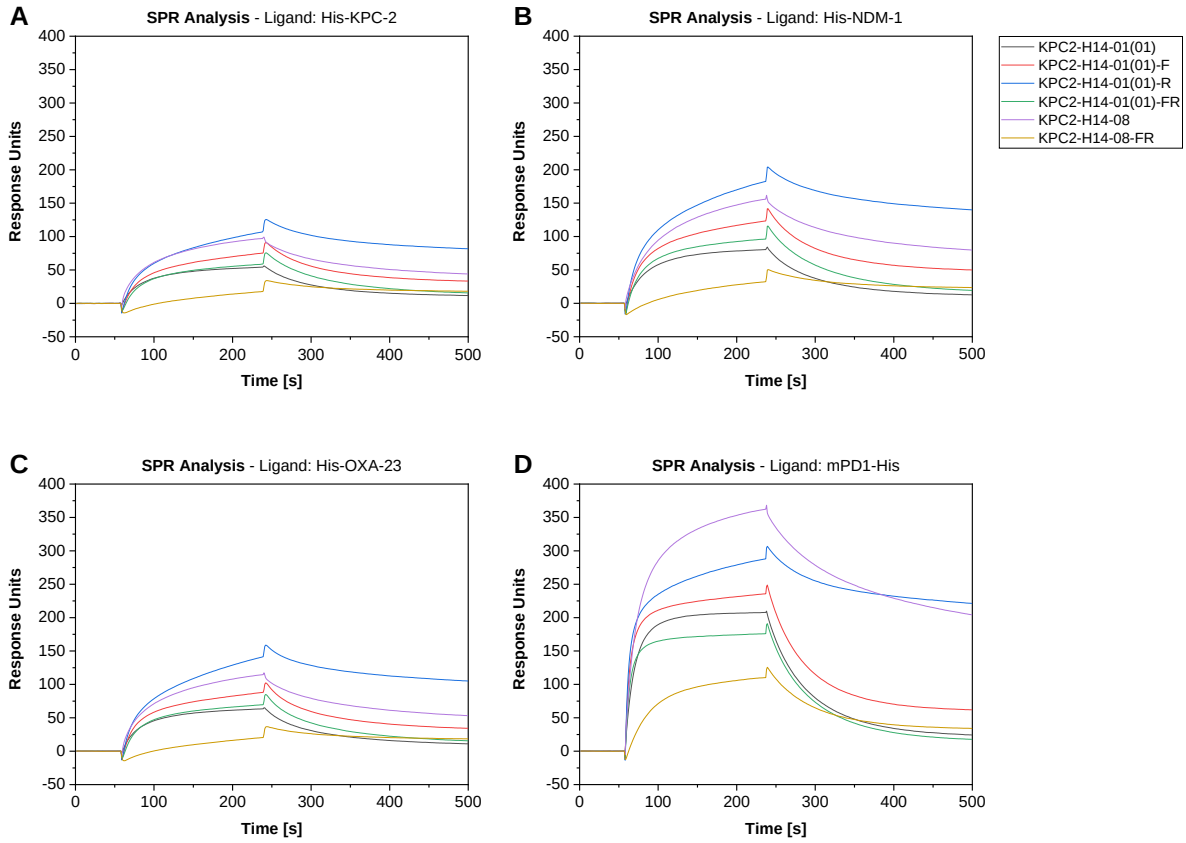

Figure 13: SPR analysis of His-KPC-2-binding aptamers. His-tagged carbapenemases (A) His-KPC-2, (B) His-NDM-1, (C) His-OXA-23 and (D) unrelated, His-tagged protein mPD1-His were immobilized on a SPR sensor chip with mPD1-His on the reference channel. Aptamers KPC2-H14-01(01), KPC2-H14-01(01)-R, KPC2-H14-01(01)-F and KPC2-H14-01(01)-FR as well as KPC2-H14-08 and KPC2-H14-08-FR were injected and screened for binding to the immobilized proteins. Response units over the course of 500 s are shown. Here, signals derived from the reference channel were not subtracted. Binding to all four proteins was detected, indicating His-tag binding.

5.4.4. Validation and Kinetic Characterization of Potential His-tag-binding Aptamers

As SPR experiments showed binding to four His-tagged proteins His-tag binding was suspected. Thus, His-tag binding was further tested by FLAA (see also 8.9). Immobilized, His-tagged carbapenemases His-KPC2 and His-NDM1 as well as another unrelated, C-terminally His-tagged protein human complement factor H-related 1 (CFHR1-His) and non-His-tagged phosphoprotein membrane anchor with glycosphingolipid microdomains (PAG) were incubated with KPC2-H14-01(01) and truncations thereof. KPC2-H14-08 was

excluded from further analysis due to its length and the fact that the truncated version had shown the RU in SPR. For KPC2-H14-01(01) and its derivates, high fluorescence signals were detected for all His-tagged proteins compared to the initial library but not for non-His-tagged protein PAG (**Figure 14A**). These findings further substantiated the suspected His-tag binding.

A final proof of His-tag binding was provided for KPC2-H14-01(01) by MST (**Figure 14B**, see also 8.10). 5'-Cyanine 5 (Cy5) labelled full-length aptamer KPC2-H14-01(01) and unrelated control aptamer Con1 were incubated with increasing concentrations of a synthetic hexa-His peptide. For KPC2-H14-01, a binding curve was obtained with a dissociation constant (K_D) of 2.81 ± 0.39 * 10^{-8} M (see also **Table 3** at the end of this section). Unrelated control aptamer Con1 did not show binding to the hexa-His peptide. Thus, sequence dependent His-tag binding could be confirmed.

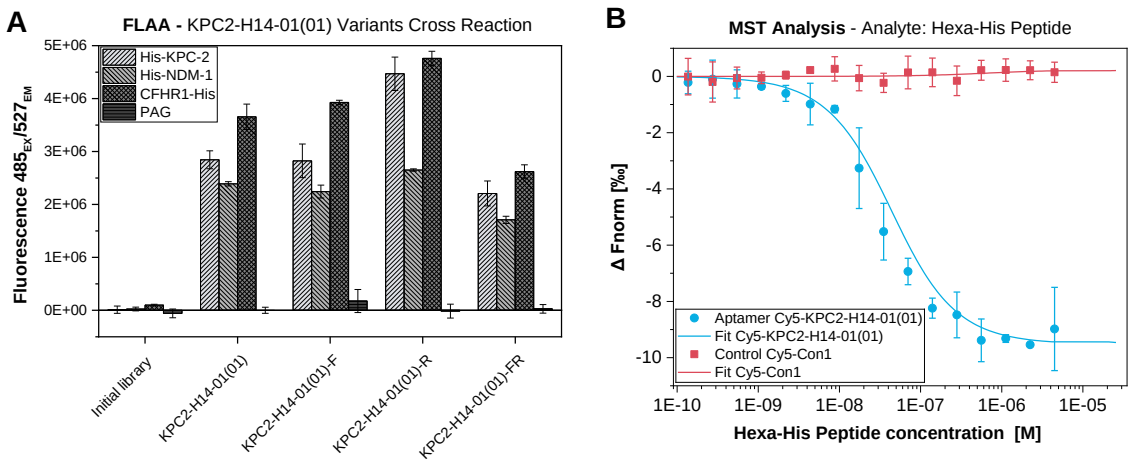

Figure 14: Cross reactivity assessment of KPC2-H14-01(01) and truncations thereof. (A) Cross reactivity of KPC2-H14-01(01) and truncations thereof was tested to three different His-tagged proteins (His-KPC-2, His-NDM-1 and CFHR1-His) and one non-His-tagged protein (PAG) by FLAA. Binding was detected to all three His-tagged proteins by all truncated versions of KPC2-H14-01(01) but not the initial library. None of the aptamers tested showed binding to non-His-tagged protein PAG. Fluorescence values of two target-coated and two negative control wells were averaged, and negative control values were subtracted. Error bars represent the square root of the sum of the variances of two target-coated wells and two negative control wells. (B) In MST, 5'-Cy5 labeled KPC2-H14-01(01) showed binding to a synthetic hexa-His peptide, while unrelated control aptamer Cy5-Con1 did not. Thus, His-tag binding was confirmed. Error bars reflect the standard deviation from three different, independent experiments.

Full-length aptamer KPC2-H14-01(01) and truncations -R and -FR were chosen for further kinetic characterization by SPR (see also 8.11). Aptamers were synthesized 5'-biotin-triethlyenglyokol modified (referred to as 5'-biotinylated or bio-) and immobilized on an SPR sensor chip. Varying concentrations of proteins His-NDM-1, mPD1-His and CFHR1-His were

injected and K_D-values were in the range of 2.86 * 10^{-11} (Bio-KPC2-H14-01(01)-FR binding to CFHR1-His) - 1.06 * 10^{-8} (Bio-KPC2-H14-01(01)-R binding to His-NDM-1), indicating strong binding to the His-tags of different proteins. Exemplary binding curves for all three aptamers binding to mPD1-His are shown in **Figure 15**. Comprehensive kinetic data can be found in **Table 3**.

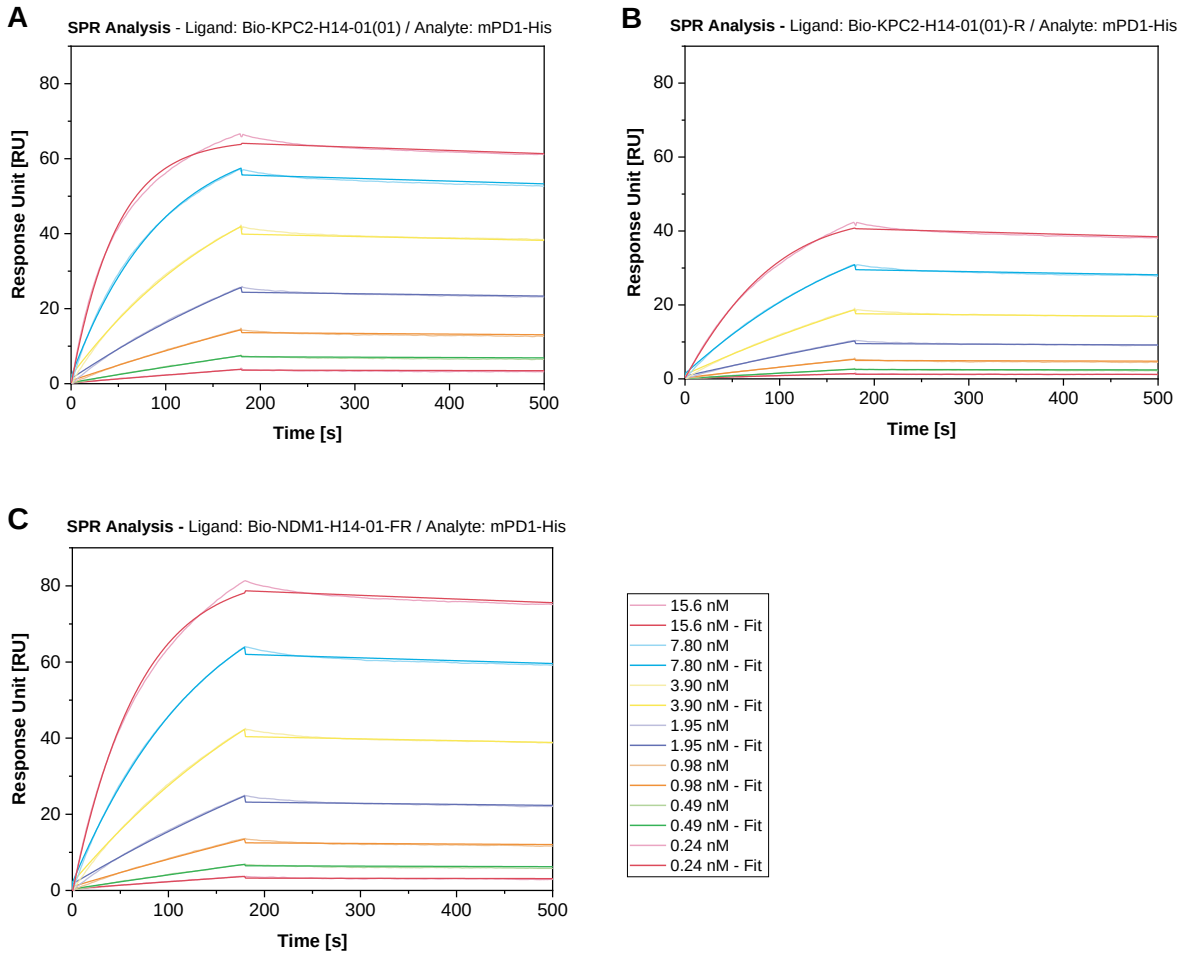

Figure 15: Kinetic characterization of potential His-tag-binding aptamers by SPR. 5'-biotinylated aptamers (A) KPC2-H14-01(01), (B) KPC2-H14-01(01)-R, (C) KPC2-H14-01(01)-FR were immobilized on a SPR sensor chip as ligands and injected with increasing amounts of different His-tagged proteins as analytes. The reference channel was blocked with biotin. Response units over the course of 500 s are shown for mPD1-His concentrations ranging from 0.24 - 15.6 nM. Signals derived from the reference channel were subtracted. Kinetic parameters for binding to mPD1-His, CFHR1-His and His-NDM-1 are listed in **Table 3**. Binding curves for binding to mPD1-His are exemplarily shown.

Table 3: Kinetic data and K_D-values of His-tag binding. Kinetic data of His-tag aptamers were assessed by SPR. K_D-values of full-length aptamer KPC-2-H14-01(01) and unrelated control aptamer Con1 were assessed by MST. Kinetic values: k_a = association constant, k_d = dissociation constant.

Method: SPR					
Ligand	**Analyte**	**k_a (1/Ms)**	**k_d (1/s)**	**K_D (M)**	**Chi² (RU²)**
Bio-KPC2-H14-01(01)	His-NDM-1	$1.30*10^6$	$5.62*10^{-3}$	$4.34*10^{-9}$	6.47
	mPD1-His	$1.40*10^6$	$1.38*10^{-4}$	$9.86*10^{-11}$	0.20
	CFHR1-His	$2.79*10^6$	$1.25*10^{-4}$	$4.49*10^{-11}$	6.97
Bio-KPC2-H14-01(01)-R	His-NDM-1	$6.26*10^5$	$6.65*10^{-3}$	$1.06*10^{-8}$	4.82
	mPD1-His	$1.10*10^6$	$1.86*10^{-4}$	$1.70*10^{-10}$	0.07
	CFHR1-His	$1.79*10^6$	$2.50*10^{-4}$	$1.40*10^{-10}$	14.7
Bio-KPC2-H14-01(01)-FR	His-NDM-1	$1.20*10^6$	$7.11*10^{-3}$	$5.91*10^{-9}$	9.68
	mPD1-His	$1.02*10^6$	$1.28*10^{-4}$	$1.25*10^{-10}$	0.20
	CFHR1-His	$4.28*10^6$	$1.22*10^{-4}$	$2.86*10^{-11}$	9.22

Method: MST			
Ligand	**Analyte**	**K_D (M)**	**K_D confidence (M)**
Cy5-KPC2-H14-01(01)	Hexa-His peptide	$2.81*10^{-8}$	$3.90*10^{-9}$
Cy5-Con1		-	

5.4.5. Characterization of Aptamer Candidates with Lower Signal Intensity in FLAA

Both aptamers that showed the highest signals in FLAA and SPR were identified as His-tag binders. Thus, aptamer candidates, for which weaker binding signals were detected in FLAA, were chosen for further characterization. As all aptamer candidates had shown binding signals when incubated with His-KPC-2, FLAA (see also 8.9) was repeated with His-KPC-2 for binding verification and with mPD1-His as an unrelated His-tag control protein. Here, for all aptamer candidates, fluorescence signals exceeded that of the initial library for incubation with His-KPC-2. For aptamer candidates NDM1-H14-02(04) (80 nt), KPC2-H14-15(18) (81 nt), KPC2-H14-18(25) (79 nt), and KPC2-H14-09(39) (84 nt) fluorescence signals exceeded that of the initial library for incubation with mPD1-His as well. Moreover, binding signals were higher for mPD1-His than for His-KPC-2. Hence, it is likely that these aptamer candidates were His-tag binders as well. Thus, no further characterization was conducted. Yet, KPC2-H14-05 (77 nt) and KPC2-H14-07 (80 nt) showed binding signals exceeding those of the initial library only for His-KPC-2 but not for mPD1-His (**Figure 16A**). Both aptamer candidates shared a

sequence motif (see also **Appendix Table 6**) – GGC GGG GGG-6-20(N)-GGG GGG ATG G – and KPC2-H14-05 had shown a slightly higher fluorescence signal in FLAA (**Figure 16A**). Thus, only KPC-2-H14-05 was chosen for further characterization by SPR.

5‘-biotinylated KPC2-H14-05 was synthesized and immobilized on an SPR sensor chip. Two different concentrations of His-KPC-2 (100 nM and 500 nM) were injected (see also 8.11). Upon injection of both concentrations a rather low, almost linear increase in RU was detected (**Figure 16B**). Here, binding may be indicated, yet the signal was not shaped as a regular binding curve. Thus, binding was not undoubtedly confirmed. Furthermore, upon injection of 500 nM His-KPC-2, a strong increase in signal was detected which is very likely to not be derived from binding to the aptamer but rather from incompatibility of the target buffer. His-KPC-2 was purchased dissolved in 100 mM NaH_2PO_4, 0.3 M NaCl and 4 M urea. The aptamer binding buffer in which His-KPC-2 was dissolved did not contain these agents. Thus, the steep increase in signal prior to binding may be attributed to these agents. High concentrations in a kinetic analysis resulted in higher signal increases but not in binding curves (data not shown). Thus, kinetic evaluation was not possible, which may be inter alia attributed to buffer incompatibility. Unfortunately, a buffer exchange failed as His-KPC-2 precipitated upon dialysis against aptamer binding buffer. Thus, kinetic measurements were not assessed. To still substantiate His-KPC-2 specific binding of KPC2-H14-05, a micro titer plate (MTP)-based sandwich assay was designed with 5‘-biotinylated KPC2-H14-05 immobilized on a streptavidin-coated micro titer plate (SA-MTP) as a capture molecule and a HRP-labelled anti-penta-His antibody as the detection molecule (see also 8.12.1). The signal derived from wells coated with 5’-biotinylated KPC2-H14-05 exceeded that of the wells without aptamer-coating by a factor of 5.6 (**Figure 16C**). Hence, detection of 80 pmol His-KPC-2 was facilitated.

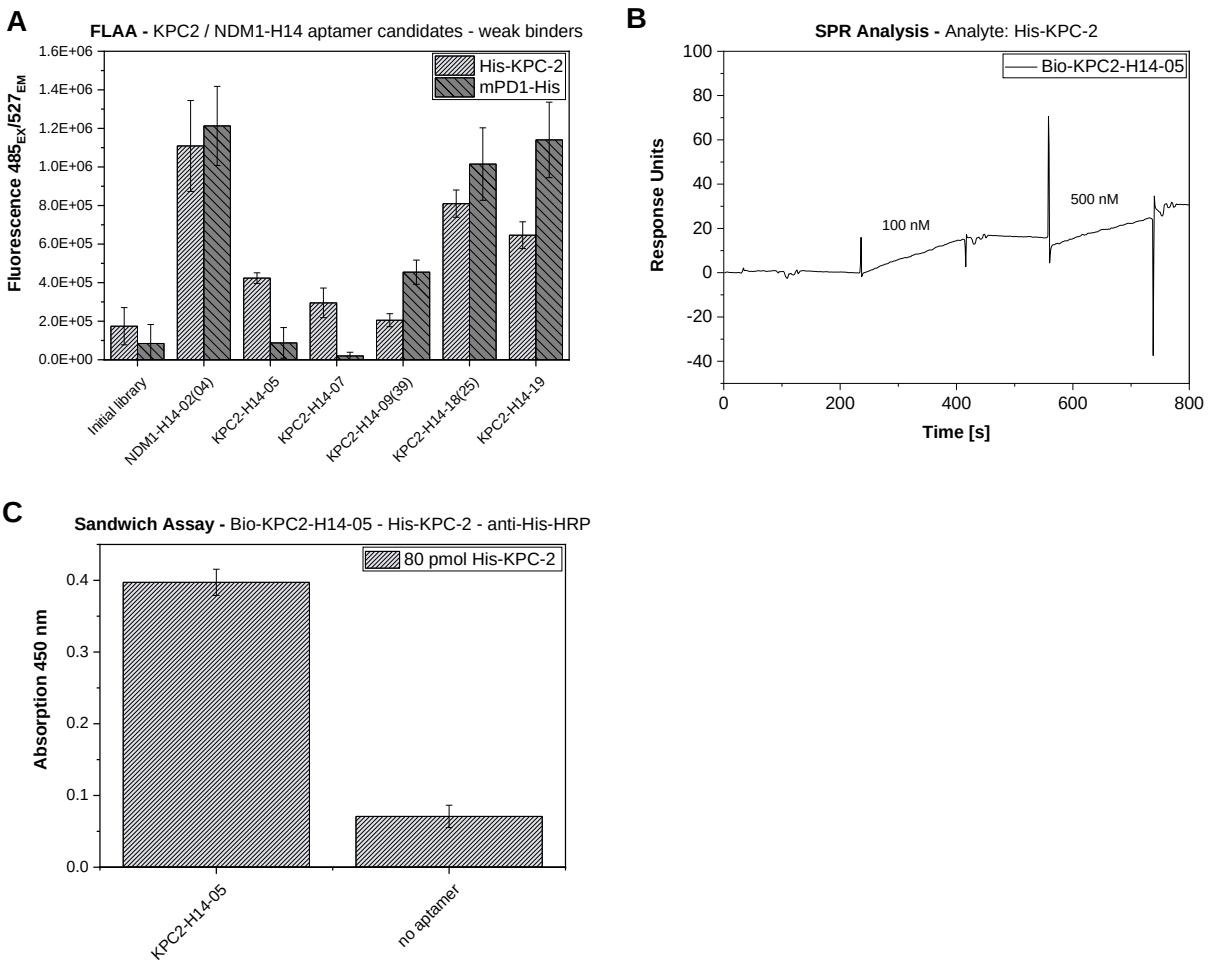

Figure 16: Characterization of further aptamer candidates after SR14.1. (A) Aptamer candidates that had shown lower fluorescence signals in FLAA than KPC2-H14-01(01) and KPC2-H14-08 were tested for cross reactivity with mPD1-His by FLAA. Fluorescence units measured with excitation at 485 nm and emission at 527 nm using EnVision® 2105 are shown. Only KPC2-H14-05 and KPC2-H14-07 showed higher signals for His-KPC-2 than for mPD1-His. Fluorescence values of two target-coated and two negative control wells were averaged, and negative control values were subtracted. Error bars represent the square root of the sum of the variances of two target-coated wells and two negative control wells. (B) 5'-biotinylated KPC2-H14-05, immobilized on an SPR sensor chip, was evaluated by SPR with single injections of 100 and 500 nM His-KPC-2. Response units over the course of 800 s are shown. Binding was not confirmed. (C) Immobilization of 5'-biotinylated KPC2-H14-05 on a SA-MTP facilitated capture of 80 pmol His-KPC-2 and detection by a HRP-labelled anti-penta-His antibody. Absorption values measured at 450 nm using EnVision® 2105 are shown. Absorption values of three aptamer-coated and three negative control wells were averaged, and negative control values were subtracted. Error bars represent the square root of the sum of the variances of three target-coated wells and three negative control wells.

So far, selection against N-terminally His-tagged carbapenemases His-NDM-1 and His-KPC-2 with negative selections against the respective other target as well as another His-tagged carbapenemase did not result in the selection of target-binding aptamers. Three consecutive selection rounds with negative selections only against the immobilization matrix resulted in

strong enrichment of two highly affine His-tag-binding sequences. Six further aptamer candidates were identified that showed low binding signals either for His-NDM-1 and His-KPC-2 or His-KPC-2 only. Four out of the six aptamer candidates also showed binding to mPD1-His, which indicates His-tag binding as well. Two aptamers exclusively bound to His-KPC-2 in FLAA. One aptamer was chosen for further characterization. Here, binding to His-KPC-2 could not be validated by SPR but by an MTP-based sandwich assay. However, signal intensities in FLAA and the MTP-based sandwich assay were low and no binders exclusively binding to His-NDM-1 were found. Thus, to facilitate target binding while preventing the selection of His-tag binders, three different selection strategies were designed. His-KPC-2 was chosen as a model target, as KPC-2 aptamers had been published in the meantime, proving a successful selection [106]. The most successful strategy was later to be applied to His-NDM-1, as no successful DNA aptamer development against NDM-1 was found in the scientific literature.

5.5. Design of strategies to prevent and reverse His-tag binding

Three strategies for restarting the selection against His-KPC-2 were developed. As NGS data showed that His-tag-binding sequences were strongly enriched after SRs 13.1 and 14.1 but not after SR11.1, it was decided to use the ssDNA pools from SR11.1 and conduct consecutive SRs with three different strategies. For all strategies, negative selections against uncoupled Dynabeads™ M-280 Tosylactivated, as well as with unrelated His-tagged protein mPD1-His were conducted. Negative selections against unrelated proteins were used to reduce His-tag binding while still allowing target binding.

The first two approaches were designed to make use of an already existing His-tag aptamer. The first approach was designed to mask the targets His-tag by preincubation with a 10-fold excess of the His-tag aptamer. The second approach was designed to use a 10-fold excess of the His-tag aptamer for competitive elution of sequences bound to the His-tag after target incubation. The third approach was to reduce His-tag accessibility through immobilization of the target via its N-terminal His-tag. A prerequisite for the first two strategies – epitope masking and competitive elution – is high affinity of the masking / elution aptamer. KPC2-H14-01(01) and its derivates had shown strong binding to various His-tagged proteins (see also **Table 3**). Thus, one of the derivates was supposed to be used for selection. Here, using an aptamer with the same primer binding sites as the ssDNA pools used for selection bears the risk of strong amplification of the masking / elution aptamer and suppression of other target binding sequences. Hence, the fully truncated version, lacking both primer binding sites (KPC2-H14-01(01)-FR) was chosen as the masking and competitive elution aptamer because the aptamer is not amplified throughout the PCRs after each selection round (see also 8.3.2

and 8.3.3). For the third approach, immobilization of His-KPC-2 was conducted on Co^{2+}-Nitrilotriacetic acid (NTA)-coated magnetic beads (Dynabeads™ His-Tag Isolation and Pulldown). To facilitate discrimination between the different strategies, selection rounds were termed SRxy_Mask, SRxy_Comp and SRxy_Co^{2+}-NTA, with xy representing the number of the selection round described.

5.6. Selection against His-KPC-2 with Different Strategies to Prevent His-tag binding

5.6.1. PCR Analysis

All three new strategies were started with ssDNA from SR11.1. The number of selection rounds that were supposed to be performed was set to three to facilitate comparison to SR13.1 and SR14.1. After the first round of selection, no signal was obtained for the elution fraction of the masking approach when performing analytical PCR (see also 8.3.2). Both other strategies resulted in sufficient PCR products. Hence, strategies competitive elution and immobilization of His-KPC-2 on Dynabeads™ His-Tag Isolation and Pulldown were continued while the masking approach was restarted with ssDNA from SR10.1. For the two strategies, competitive elution, and immobilization on Dynabeads™ His-Tag Isolation and Pulldown, stringency of selection was kept constant throughout the three selection rounds. PCR cycles required to obtain a signal for the elution fraction can be found in **Table 4**. For the competitive elution approach a control selection, SR14.2_Comp_Control was conducted. Here, PCR cycles required to obtain a signal derived from the elution fraction were higher than for the target selection. For the masking approach, PCR cycles required to obtain a signal derived from the elution fraction were constant from SR11.2_Mask - 13.3_Mask (see also **Table 4**). Here, stringency was increased in SR13.3_Mask with higher amounts of mPD1-His for the negative selection. Furthermore, a control selection was performed as SR13.3_Mask_Control. Here, 15 PCR cycles were required to obtain a signal derived from the elution fraction. As both control selections required more PCR cycles and for the target selections PCR cycles either decreased or remained constant even though stringency was increased, PCR analysis indicated enrichment of target-binding sequences. Thus, ssDNA pools from SRs 14.2_Comp, H14.2_Co^{2+}-NTA and 13.3_Mask as well as 13.3_Mask_Control were sequenced using NGS (see also 8.8). Unique sequences accounted for 57.6%, 52.6%, and 50.0% for SRs 14.2_Comp, H14.2_Co^{2+}-NTA and 13.3_Mask as well as 32.5% for 13.3_Mask_Control. Enrichment of the target selection was comparable to or higher than for SR14.1.

Table 4: PCR cycles required to obtain a signal from the elution fractions for selections against His-KPC-2 employing different strategies to avoid His-tag binding.

SR	PCR cycles	SR	PCR cycles	SR	PCR cycles
12.2_Mask	20	12.2_Comp	15	12.2_Co^{2+}-NTA	15
13.2_Mask	np	13.2_Comp	11	13.2_ Co^{2+}-NTA	11
11.2_Mask	10	14.2_Comp	10	14.2_ Co^{2+}-NTA	10
12.3_Mask	10	14.2_Comp_Control	15		
13.3_Mask	10				
13.3_Mask_Control	15				

**np = no product*

5.6.2. Analysis of Enrichment of His-tag-binding Sequences

Analysis of the pools was inter alia aimed at the detection of enrichment of His-tag-binding sequences. Thus, a motif, likely involved in His-tag binding was searched. Another selection that was conducted simultaneously had resulted in the identification of an aptamer with high affinity to the C-terminal His-tag of the target protein. Interestingly, even though a different library was used for selection, sequences within the randomized regions of both His-tag aptamers were partially similar. 26 nt out of the 44 or 42 nt of the randomized regions were homologous. As both aptamers showed strong affinity to His-tags, the overlapping motif – GGG GGA CTG CTC GGG ATT GCG GA – may likely be involved in His-tag binding. In fact, for selection against His-KPC-2, the motif was present among the 100 most enriched sequences after SRs 13.1 and 14.1 but not after SRs 10.1 and 11.1. Therefore, NGS data from selections against His-KPC-2 exploiting the three strategies to prevent and reverse His-tag binding was scanned for this motif. The 100 most enriched sequences after SRs 14.2_Comp, 14.2_Co^{2+}-NTA and 13.3_Mask were analyzed and the percentage of sequences including this motif were calculated as follows:

$$\frac{Sum\ of\ sequence\ counts\ that\ include\ the\ motive^{\#}}{Sum\ of\ all\ sequence\ counts^{\#}} * 100 \qquad (1)$$

[#] among the 100 most enriched sequences

For the 100 most enriched sequences after SR14.2_Comp, sequence counts which include the motif accounted for 21.6%, after SR14.2_Co^{2+}-NTA for 2.7% and after SR13.3_Mask for 0.7%. For comparison, after SRs 13.1 and 14.1 conducted without strategies to avoid His-tag binding, sequences including the motif accounted for 47.3% and 24% respectively. Hence, strong improvement was detected for two strategies – the masking approach and immobilization of His-KPC-2 on Dynabeads™ His-Tag Isolation and Pulldown, with the masking approach resulting in even lower enrichment of His-tag-binding motif.

5.6.3. Characterization of Aptamer Candidates Selected by the Masking Approach

Consequently, sequences derived from the masking approach were analyzed and compared to the other strategies and the control selection. Here, sequences including the identified His-tag-binding motif as well as identified non-binders from SRs 11.1 and 14.1 were excluded. Sequence analysis was extended to the 300 most enriched sequences for a more in-depth analysis of the NGS data. Most enriched sequences from the masking approach were also present in the NGS data from the other two strategies. Among randomized regions of the 300 most enriched sequences, eleven sequence motifs were found (**Appendix Table 6**). Sequences were grouped according to the motifs as sequence families. 19 aptamer candidates (see also **Table 14**), including members of the sequence families and the most enriched sequences, were synthesized on the condition that the percentage of total sequences exceeded that of the control selection. Furthermore, sequences including the His-tag-binding motif as well as non-binders from other selections or selection rounds were excluded. Aptamer candidates were screened for binding to His-KPC-2 and mPD1-His by FLAA (see also 8.9). In contrast to SR14.1, fluorescence signals were rather low. Nevertheless, some aptamer candidates showed fluorescence signals that were higher for His-KPC-2 than for mPD1-His and exceeded the fluorescence signal of the initial library (**Figure 17A-B**). Lower fluorescence signals with high standard deviations for mPD1-His may be derived from unspecific adsorption of the aptamers to the protein while higher fluorescence values with lower standard deviations for His-KPC-2 may indicated specific binding. Yet, further analysis is necessary to exclude His-tag binding. Firstly, for promising aptamer candidates, FLAA was repeated. Aptamer candidates repeatedly showing signals that were higher than the signals derived from the initial library and higher for His-KPC-2 than for mPD1-His were KPC2-H13.3_Mask-41 (80 nt), KPC2-H13.3_Mask-65 (84 nt), KPC2-H13.3_Mask-126 (80 nt), KPC2-H13.3_Mask-151 (83 nt), KPC2-H13.3_Mask-163 (85 nt), and KPC2-H13.3_Mask-294 (86 nt), with KPC2-H14_13.3_Mask-65 showing strong signal fluctuations (**Figure 17C**).

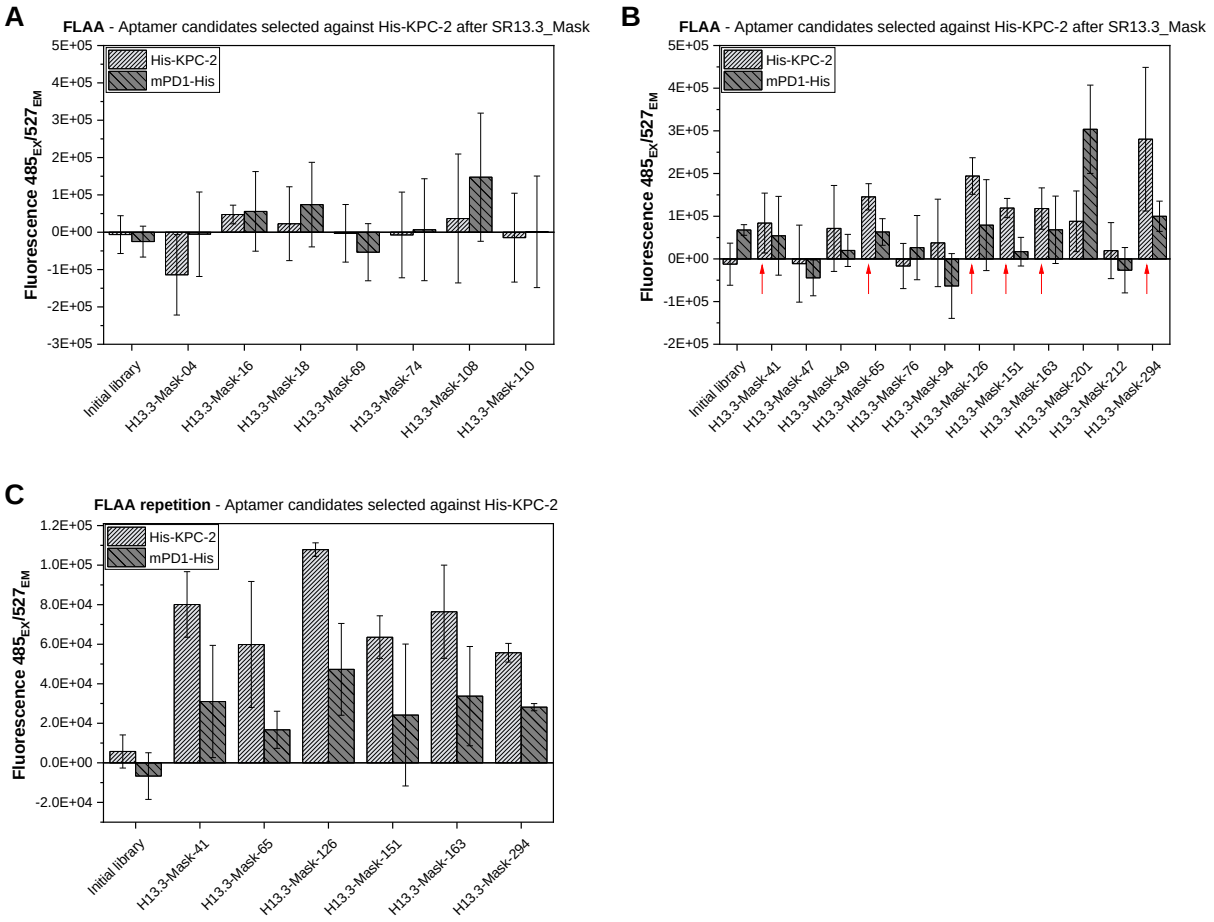

Figure 17: Characterization of aptamer candidates after SR13.3_Mask. (A-B) Aptamer candidates, selected against His-KPC-2 were tested for binding to His-KPC-2 and mPD1-His by FLAA. Fluorescence units measured with excitation at 485 nm and emission at 527 nm using EnVision® 2105 are shown. Aptamer candidates that showed higher fluorescence signals for His-KPC-2 than for mPD1-His as well as higher signals than the initial library are indicated with a red arrow. Fluorescence values of two target-coated and two negative control wells were averaged, and negative control values were subtracted. Error bars represent the square root of the sum of the variances of two target coated wells and two negative control wells. (C) For those promising aptamer candidates, FLAA was repeated and binding to His-KPC-2 was confirmed. Fluorescence values of three target-coated and three negative control wells were averaged, and negative control values were subtracted. Error bars represent the square root of the sum of the variances of three target-coated wells and three negative control wells.

Two aptamer candidates, KPC2-H13.3_Mask-41, the most enriched among His-KPC-2-binding sequences and KPC2-H13.3_Mask-126, with the highest fluorescence signal for His-KPC-2, were chosen for further characterization by SPR (see also 8.11). Both aptamers were rich in pyrimidines. The randomized regions were composed of 84% and 82% pyrimidines for KPC2-H13.3_Mask-41 and KPC2-H13.3_Mask-126, respectively. Both aptamers were immobilized on a SPR sensor chip. Two different concentrations of His-KPC-2 (100 nM and 500 nM) were injected (**Figure 18A**). Upon injection of 100 nM His-KPC-2 an almost linear

increase in RU was detectable. Here, binding may be indicated, yet it did not appear as an expected binding curve. However, upon injection of 500 nM a binding signal was shaped as expected. To test cross reactivity, 500 nM His-NDM-1 and mPD1-His were injected consecutively. Upon injection of His-NDM-1, a binding signal was obtained that was considerably lower than upon injection of His-KPC-2 (**Figure 18B)**. Injection of mPD1-His did not result in a binding signal at all (**Figure 18C**). As discussed in section 5.4.5, kinetic analysis with the aptamers immobilized as ligands and increasing concentrations of His-KPC-2 as analytes resulted in very high signal jumps for high concentrations of His-KPC-2, likely due to buffer incompatibility. Furthermore, even though higher concentrations of His-KPC-2 were injected, no binding curves were obtained. This may be caused by precipitation of the target molecule when dissolved in aptamer binding buffer in high concentrations. A buffer exchange failed due to precipitation of His-KPC-2. Thus, evaluation of kinetic SPR measurements was not possible. To further analyze binding, a sandwich assay was conducted with 5'-biotinylated aptamers KPC2-H13.3_Mask-41 and KPC2-H13.3_Mask-126 immobilized on a SA-MTP used as capture molecules and a HRP-labelled anti-His antibody as the detection molecule (see also 8.12.1). Signals derived from wells in which 5'-biotinylated aptamers KPC2-H13.3_Mask-41 and KPC2-H13.3 _Mask-126 were used as capture molecules exceeded that of the no aptamer control by factors 3.4 and 3.9 (**Figure 18D**). Hence, detection of 80 pmol His-KPC-2 was facilitated.

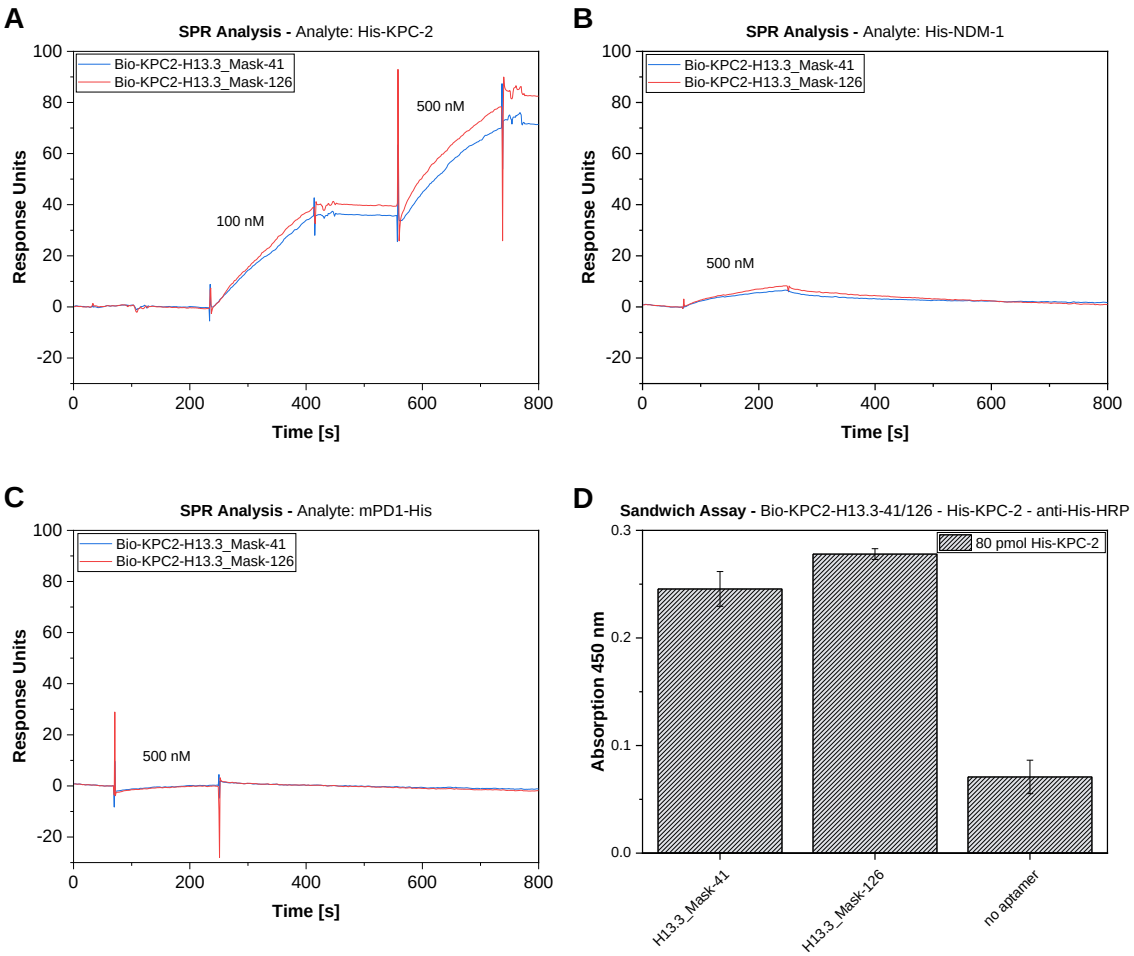

Figure 18: Analysis of KPC2-H13.3_Mask-41 and _Mask-126 by SPR and by an SA-MTP-based aptamer-antibody sandwich assay. (A-C) 5'-biotinylated aptamers KPC2-H13.3_Mask-41 and KPC2-H13.3_Mask-126 were immobilized on a SPR sensor chip. Response units over the course of 800 s are shown. (A) A single injection of 500 nM His-KPC-2 resulted in a binding curve while single injections of 500 nM (B) His-NDM-1 and (C) mPD1-His did not show binding. (D) Immobilization of 5'-biotinylated aptamers on a SA-MTP, incubation with 80 pmol His-KPC-2 and detection by a HRP-labeled anti-penta-His antibody resulted in absorption signals that exceeded that of the no-aptamer control. Absorption values measured at 450 nm using EnVision® 2105 are shown. Absorption values of three aptamer-coated and three negative control wells were averaged, and negative control values were subtracted. Error bars represent the square root of the sum of the variances of three aptamer-coated wells and three negative control wells

Hence, application of the masking approach resulted in the selection of at least two sequences that showed binding signals for His-KPC-2 in FLAA, and SPR. Lower binding signals were detected for mPD1-His in FLAA and no binding to mPD1-His was detected in SPR. SPR binding signals derived from injection of His-NDM-1 were considerably lower than for His-KPC-2. Kinetic SPR as well as MST measurements with high concentrations of His-KPC-2 were not possible due to buffer incompatibility. Yet, capture of His-KPC-2 by the aptamers and detection using an anti-penta-His antibody was possible. Thus, it is likely that aptamers were

selected that showed selective binding to KPC-2 rather than its N-terminal His-tag. Fluorescence signals derived from the sequences in FLAA were still low. Thus, the masking approach led to a successful selection of His-KPC-2 specific aptamers. However, selection of highly affine aptamers was likely not successful.

5.7. Implementation of KPC-2 Aptamers into an LFD

Nevertheless, a combination of 5'-biotinylated, guanine rich aptamer KPC2-H14-05 (54% guanines) and 5'-HS-triethylene glycol modified (referred to as thio-), pyrimidine rich aptamer KPC2-H13.3_Mask-41 (84% pyrimidines) were used for the development of a sandwich assay LFD by our project partner nal von minden GmbH (see also 8.12.2). 5'-biotinylated KPC2-H14-05 was immobilized on the membrane and thio-KPC2-H13.3_Mask-41 was immobilized on Au-NPs. A control line was not implemented in this assay. Preincubation of the Au-NP-aptamer conjugate with His-KPC-2 and application onto the membrane resulted in a visible test line for concentration ≥ 2 µg/ml when compared to the gold color card from Assure Tech. (Hangzhou) Co., Ltd. (**Figure 19**). Thus, as a sandwich assay-based detection was possible, it is likely that the two His-KPC-2 aptamers have different binding epitopes. Using these, a proof of concept for the development of an aptamer-aptamer sandwich LFD for the detection of His-KPC-2 was provided.

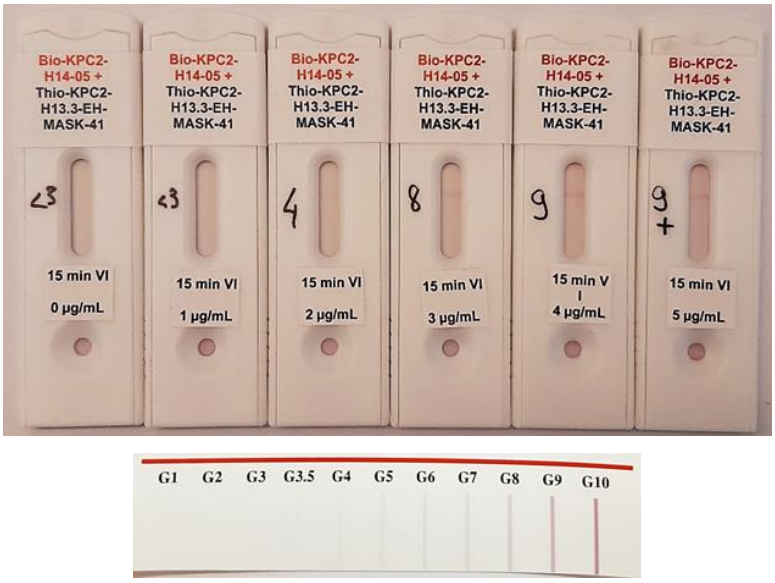

Figure 19: Aptamer-aptamer sandwich assay LFD. 5'-biotinylated-KPC2-H14-05 was immobilized on the membrane and 5'-thio modified KPC2-H13.3_Mask-41 was immobilized on Au-NPs. Preincubation of the aptamer-coated Au-NPs with different concentrations of His-KPC-2 and application on the membranes resulted in a detectable signal for concentrations ≥ 2 µg/ml, indicating different binding epitopes of the two His-KPC-2 aptamers (above). Signal intensities were compared to the gold color card (below). Numbers higher than 3 indicate a detectable signal.

5.8. Selection against His-NDM-1 with the Masking Approach

5.8.1. PCR and Affinity Analysis

Even though the masking approach likely did not result in the selection of an aptamer exceeding KPC2-H14-05 in affinity, it was successful in the prevention of strong enrichment of His-tag-binding sequences. Thus, the masking approach was chosen for the reselection against His-NDM-1, starting from SR10.1. Four selection rounds were conducted with either mPD1-His or mPD1-His and CFHR1-His as well as beads only as negative selections and masking with aptamer KPC2-H14-01(01)-FR. After only two SRs, PCR cycles required to obtain a signal derived from the elution fraction dropped from 15 after SR11.2_Mask to 10 after SR12.2_Mask (see also **Table 5**). The reduction in PCR cycles was detected despite an increase in stringency as the negative selection against mPD1-His was conducted with double the amount of mPD1-His compared to His-NDM-1. However, a control selection conducted as SR12.2_Mask_Control also showed a signal derived from the elution fraction after 10 PCR cycles as well. Thus, selection was continued for one SR with the same conditions as for SR11.2. PCR cycles required to obtain a signal derived from the elution fraction remained constant. One more selection round was conducted with increased stringency as the amount of His-NDM-1 was reduced by half while the amount of ssDNA and negative selection target mPD1-His remained constant. Furthermore, another negative selection against CFHR1-His at double the amount of His-NDM-1 was conducted. Thus, selection stringency was strongly increased (see also **Table 24**). Here, 12 PCR cycles were required to obtain a signal for the elution fraction. For a control selection conducted as SR14.2_Mask_Control, 15 PCR cycles were required (see also **Table 5**).

Table 5: PCR cycles required to obtain a signal from the elution fractions for selections against His-NDM-1 employing the masking approach to avoid His-tag binding.

SR	PCR cycles
11.2_Mask	15
12.2_Mask	10
12.2_Mask_Control	10
13.3_Mask	10
14.2_Mask	12
14.2_Mask_Control	15

Affinity of the ssDNA pool from SR14.2_Mask was tested by FLAA (see also 8.9). The ssDNA pool showed fluorescence values that exceeded that of the initial library by a factor of 5 (**Figure 20**).

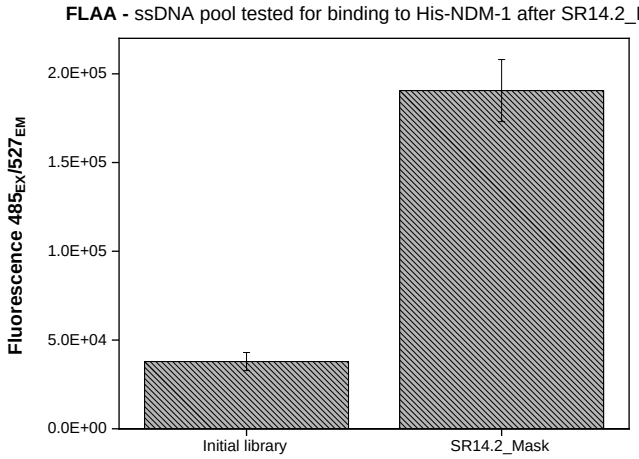

Figure 20: Characterization of the ssDNA pool after SR14.2_Mask. The ssDNA pool selected against His-NDM-1 was tested for affinity to the target by FLAA. Fluorescence units measured with excitation at 485 nm and emission at 527 nm using EnVision® 2105 are shown. The fluorescence signal derived from the ssDNA pool after SR14.2 exceeded that of the initial library. Fluorescence values of two target-coated and two negative control wells were averaged, and negative control values were subtracted. Error bars represent the square root of the sum of the variances of two target-coated wells and two negative control wells.

5.8.2. Next Generation Sequencing and Characterization of Aptamer Candidates

Affinity of the ssDNA pool was detected and thus, ssDNA pools from SR14.2_Mask and 14.2_Mask_Control were sequenced (see also 8.8). Enrichment of SR14.2_Mask was higher than for SR11.1 and 14.1, with 57.1% unique sequences. SR14.2_Mask_Control was also enriched, with unique sequences accounting for 50.9% of total sequences. The most enriched sequence after SR14.2_Mask accounted for 3.52% of total sequences. As for KPC-2 selections, the 100 most enriched sequences were screened for the His-tag-binding motif and were found to account for 1% of sequence counts. Further analysis of the randomized regions of the 100 most enriched sequences revealed five distinct motifs (**Appendix Table 6**) Sequences were grouped according to the motifs as sequence families. 20 representatives (see also **Table 14**), including members of the sequence families as well as the most enriched sequences, were synthesized on the condition that their percentage was higher for SR14.2_Mask than for SR14.2_Mask_Control. Furthermore, sequences including the His-tag-binding motif as well as non-binders from other selections or selection rounds were excluded.

After synthesis, as a first screening approach, all aptamers were tested for binding to His-NDM-1 and mPD1-His by FLAA (see also 8.9). Here, His-NDM-1 and mPD1-His were immobilized on non-directionally and incubated with aptamer candidates as well as the initial library. Aptamer candidates that showed higher binding signals for His-NDM-1 than for mPD1-His as well as higher signals than the initial library were NDM1-H14.2_Mask-16 (82 nt),

_Mask-19 (80 nt), _Mask-39 (79 nt), _Mask-42 (80 nt) and _Mask-43 (80 nt) (**Figure 21A-C**). These five aptamer candidates were chosen for further characterization. To decrease His-tag accessibility, His-NDM-1 was now immobilized via its N-terminal His-tag. Here, a stable fluorescence signal, exceeding that of the initial library, used as a negative control, was detected only for NDM1-H14.2_Mask-43 (**Figure 21D**).

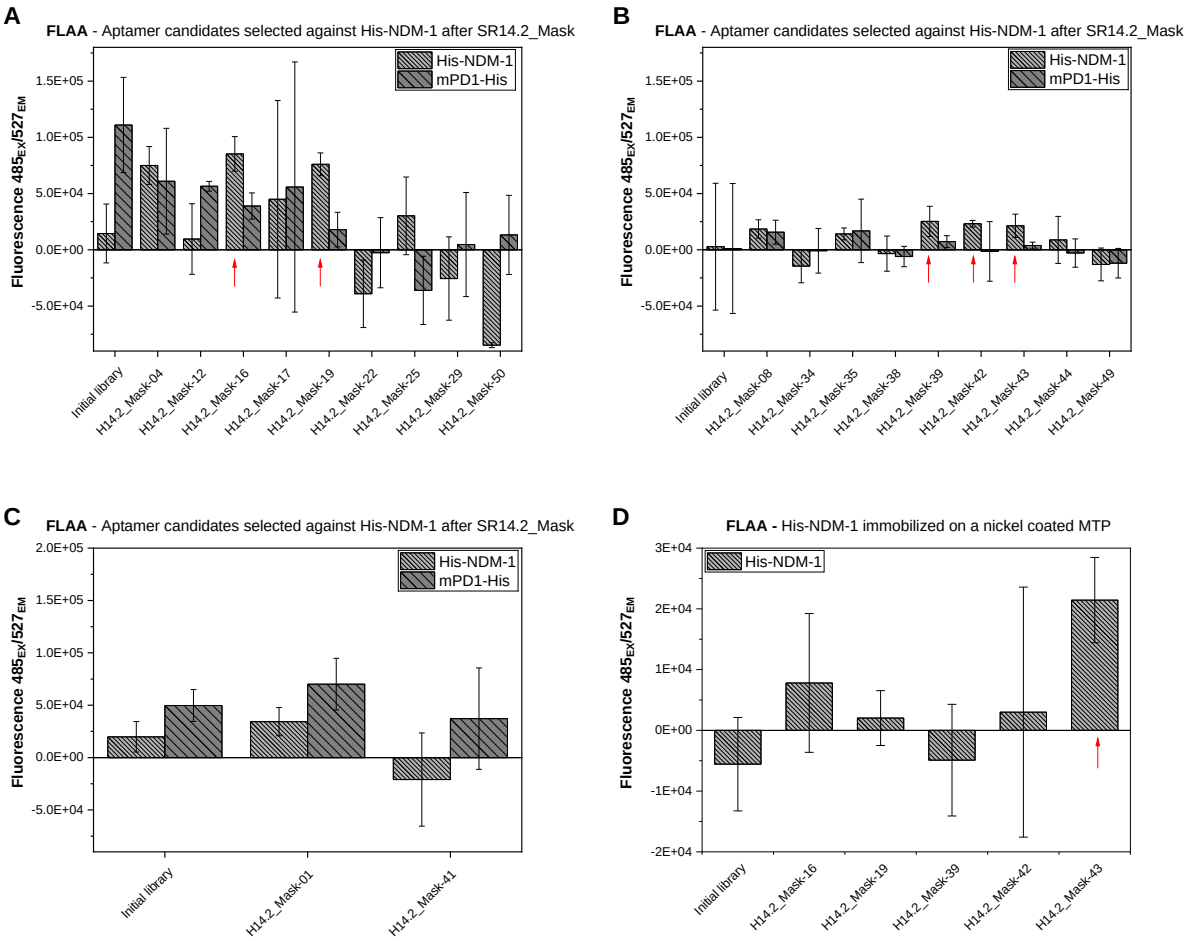

Figure 21: Characterization of aptamer candidates after SR14.2_Mask. Fluorescence units measured with excitation at 485 nm and emission at 527 nm using EnVision® 2105 are shown. (A-C) As a first screening approach, FLAA was conducted with His-NDM-1 and mPD1-His immobilized non-directionally and incubated with aptamer candidates selected against His-NDM-1 as well as the initial library. Aptamer candidates that showed higher fluorescence signals for His-NDM-1 than for mPD1-His are indicated with a red arrow. Those five promising candidates were chosen for further analysis. (D) To decrease accessibility of the N-terminal His-Tag, FLAA was conducted with His-NDM-1 immobilized via the His-tag and incubated with the five aptamer candidates and the initial library. A binding signal was obtained for NDM1-H14.2_Mask-43. (A-D) Fluorescence values of three target-coated and three negative control wells were averaged, and negative control values were subtracted. Error bars represent the square root of the sum of the variances of three target-coated wells and three negative control wells.

5.8.3. Kinetic Analysis and Sandwich Assay Development

As NDM1-H14.2_Mask-43 showed binding to His-NDM-1 in two different FLAA formats, it was chosen for quantitative aptamer characterization by SPR (see also 8.11) and MST (see also 8.10). For SPR, 5‘-biotinylated NDM1-H14.2_Mask-43 was synthesized and immobilized on an SPR sensor chip and increasing concentrations of His-NDM-1 were injected (**Figure 22A**). A K_D was calculated as $7.45 * 10^{-7}$ M (for kinetic data see also **Table 7** at the end of section 5.9.2). To investigate dependence of binding on the specific sequence, a 5’-biotinylated fully scrambled version of NDM1-H14.2_Mask-43 (ConSc) was designed and used as a negative control aptamer in SPR (see also **Table 14**). When compared to NDM1-H14.2_Mask-43, response units upon injection of His-NDM-1 were strongly decreased for the control aptamer ConSc (**Figure 22B**). Here, kinetic parameters could not be determined as the calculated k_a was outside of the measurable range. Thus, sequence-dependent binding of NDM1-H14.2_Mask-43 to His-NDM-1 was validated.

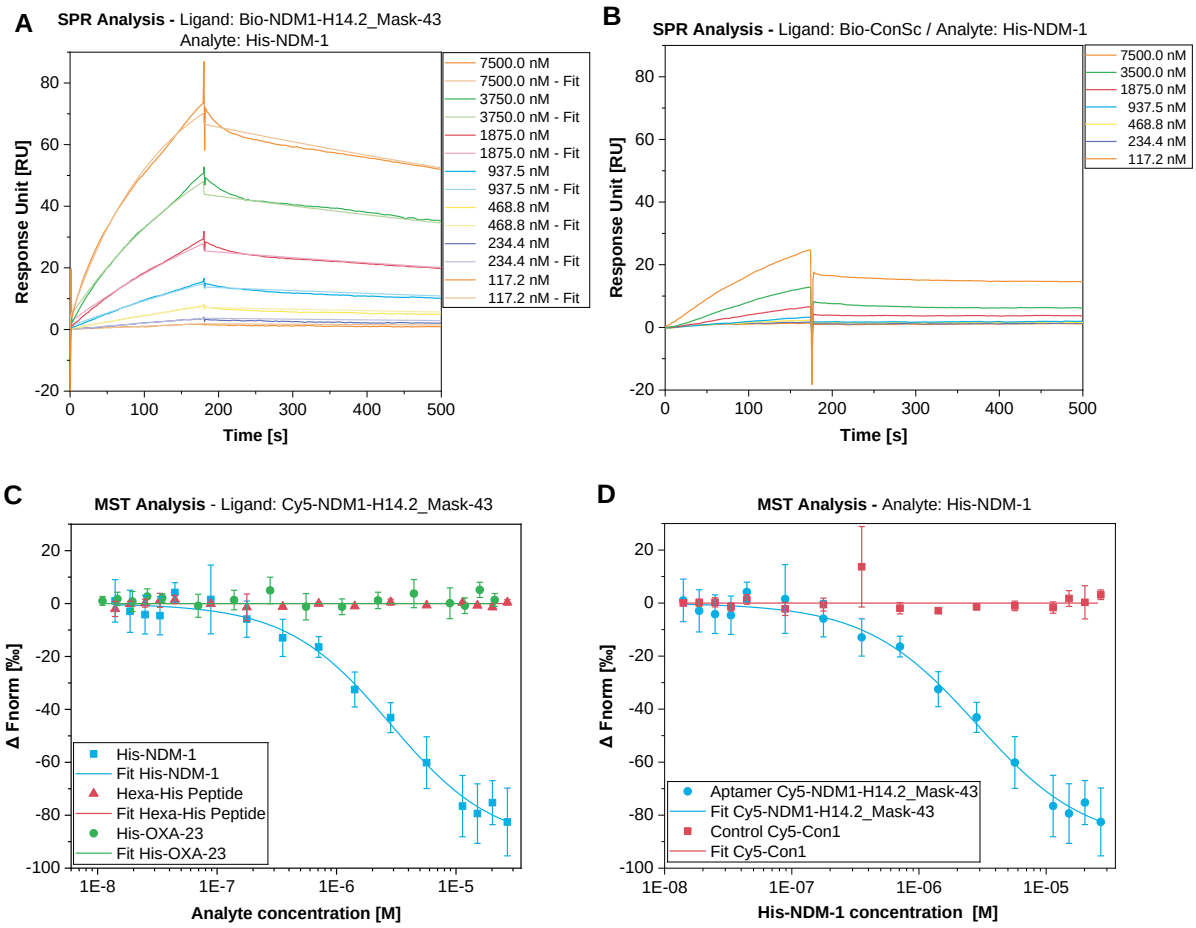

Figure 22: SPR and MST analysis of NDM1-H14.2_Mask-43 and control aptamers. (A-B) SPR analysis. Response units over the course of 500 s are shown for His-NDM-1 concentrations ranging from 117.2 – 7500 nM. 5'-biotinylated aptamers (A) NDM1-H14.2_Mask-43 and (B) ConSc were immobilized on SPR sensor chips. Kinetic parameters were assessed by injection of increasing amounts of His-NDM-1. Kinetic parameters are listed in **Table 7**. (C-D) MST analysis. ΔFnorm values in per mill are shown over analyte concentrations ranging from 32.3 - 0.017 µM (His-NDM-1 and hexa-His peptide) and 25.3 - 0.013 µM (His-OXA-23). Binding of 5'-Cy5 labeled aptamer (C) NDM1-H14.2_Mask-43 to His-NDM-1, His-OXA-23, and the hexa-His peptide as well as binding of (D) 5'-Cy5 labeled control aptamer Con1 to His-NDM-1 were assessed by MST. K_D-values are specified in **Table 7**. Error bars represent the standard deviation from three independent experiments.

To further assess specificity and sequence dependence of the binding event, NDM1-H14.2_Mask-43 as well as an unrelated control aptamer Con1 were synthesized 5'-Cy5-labelled and used for MST. Both aptamers were incubated with increasing concentrations of His-NDM-1. Furthermore, Cy5-NDM1-H14.2_Mask-43 was incubated with increasing concentrations of His-OXA-23 and the hexa-His peptide. No binding was detected for Cy5-NDM1-H14.2_Mask-43 to His-OXA-23 and the hexa-His peptide as well as for Cy5-Con1 to His-NDM-1. Only incubation of Cy5-NDM1-H14.2_Mask-43 with increasing concentrations of His-NDM-1 resulted in a binding curve. Here, a K_D-value of 2.82 * 10^{-6} M was

calculated by the software MO.Affinity Analysis (see also **Table 7** at the end of section 5.9.2). Hence, binding of NDM1-H14.2_Mask-43 to His-NDM-1 was detected. Moreover, NDM1-H14.2_Mask-43 did not bind to another His-tagged carbapenemase (His-OXA-23) nor to the hexa-His peptide, accounting for the specificity of the binding event. Furthermore, no binding of unrelated control aptamer Con1, further substantiating sequence dependence of binding.

Thus, an aptamer specific for NDM-1 could be selected using the masking approach. The aptamer was then used for the development of a sandwich assay. Here, truncated versions of the aptamer NDM1-H14.2_Mask-43 were synthesized. Due to high target consumption, these truncations were not kinetically characterized but directly tested in a sandwich assay format. The truncations were designed to lack either the forward (NDM1-H14.2_Mask-43**-F**, 62 nt) or reverse (NDM1-H14.2_Mask-43**-R**, 62 nt) or both (NDM1-H14.2_Mask-43**-FR**, 44 nt) primer binding sites. 5'-biotinylated NDM1-H14.2_Mask-43 and truncations thereof were immobilized as capture molecules, incubated with His-NDM-1 and detected using a polyclonal anti-NDM-1 antibody and a HRP-labelled secondary antibody (see also 8.12.1). Thus, an aptamer-antibody sandwich assay was set up that was independent of the N-terminal His-tag. Wells coated with either an unrelated control aptamer KPC2-H13.3_Mask-294 from the selection against His-KPC-2 and wells without aptamer-coating were used as negative controls. Signals derived from wells coated with 5'-biotinylated NDM1-H14.2_Mask-43 and derivates thereof exceeded that of the unrelated aptamer control by factors 2.1 (NDM1-H14.2_Mask-43), 1.7 (NDM1-H14.2_Mask-43-F), 2.4 (NDM1-H14.2_Mask-43-R) and 2.7 (NDM1-H14.2_Mask-43-FR). Thus, His-tag independent detection of His-NDM-1 appeared possible. However, the signal derived from the no aptamer control wells was comparably high to that derived from NDM1-H14.2 _Mask-43-F. The other derivates only exceeded that control by factors of 1.2 (NDM1-H14.2_Mask-43), 1.4 (NDM1-H14.2_Mask-43-R) and 1.6 (NDM1-H14.2_Mask-43-FR) (**Figure 23**). The signal derived from wells without aptamer-coating was calculated as the averaged signal derived from incubation with His-NDM-1, primary, and secondary antibody minus the averaged signals from wells incubated with the primary and secondary antibody only. Thus, the high signal intensity derived from this control is likely attributed to non-specific adsorption of His-NDM-1 to the surface of the biotin-blocked SA-MTP. Nevertheless, implementation of NDM1-H14.2_Mask-43 and derivates NDM1-H14.2_Mask-43-R and NDM1-H14.2 _Mask-43-FR in combination with the anti-NDM-1 antibody into LFDs is of future interest as unspecific adsorption of His-NDM-1 may not occur when using a different immobilization support.

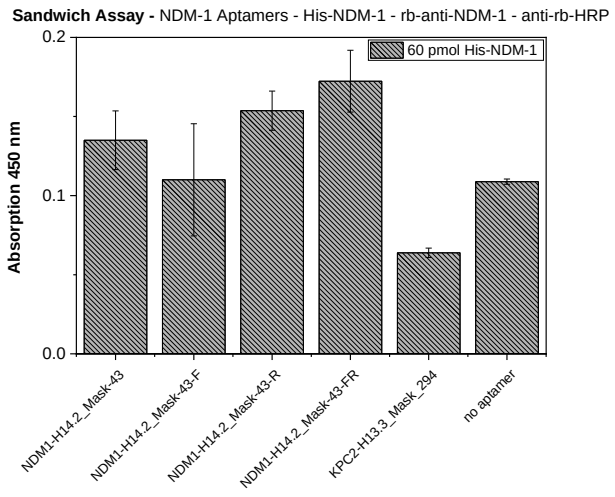

Figure 23: Evaluation of aptamer NDM1-H14.2_Mask-43 and truncated derivates by an MTP-based aptamer-antibody sandwich assay. Absorption values measured 450 nm using EnVision® 2105 are shown. 5'-biotinylated aptamers NDM1-H14.2_Mask-43, truncated derivates and control aptamer KPC2-H13.3_Mask-294 were immobilized on a SA-MTP. 60 pmol His-NDM-1 were captured by the aptamers and detected by an anti-NDM-1 antibody and a HRP labeled secondary antibody. Signals derived from wells coated with NDM1-H14.2_Mask-43 and truncated derivates exceeded those derived from wells coated with the control aptamer. Yet, high signals were also derived from the no aptamer control. Absorption values of three aptamer-coated and three negative control wells were averaged, and negative control values were subtracted. Error bars represent the square root of the sum of the variances of three aptamer-coated wells and three negative control wells.

5.9. Doped SELEX against His-NDM-1

5.9.1. PCR, Enrichment and Affinity Analysis

As NDM1-H14.2_Mask-43 turned out to be a suitable binding probe for detection of NDM-1, an approach was designed to increase its target affinity. A doped library was obtained in which the randomized region was kept constant for 79.5% percent. Each nucleotide within the 44 nt region was replaced in 5 - 8% of cases indicated by the respective number as specified by the supplier. The primer regions were kept 100% constant, resulting in a new, partially randomized library GTA TCT GGT GGT CTA TGG 667 685 866 765 586 878 686 888 868 885 886 888 856 865 66G CAT AGA CGA CGA AGA AC (see also **Table 14**). Selection was carried out for four selection rounds. Selection pressure was increased after each round by decreasing the target to ssDNA ratio, adding additional and prolonged washing steps, and by variations in negative selections against Dynabeads™ M-280 Tosylactivated and against immobilized mPD1-His (see also 8.2.3 and **Table 25**). Furthermore, target incubation was reduced to 30 minutes throughout the first two selections rounds, for 10 minutes in doped selection round (DSR) 3.1 and for twenty minutes in DSR4.1. PCR cycles required to obtain a signal for the elution fraction after gel electrophoresis increased from DSR1.1 to DSR2.1 from 10 to 15 PCR

cycles which is well in line with the increase in stringency. After DSR3.1 15 PCR cycles were also required even though the stringency was further increased (**Table 6**).

Table 6: PCR cycles required to obtain a signal from the elution fractions for doped SELEX against His-NDM-1 employing the masking approach to avoid His-tag binding.

DSR	PCR cycles
1.1_Mask	10
2.1_Mask	15
3.1_Mask	15
4.1_Mask	15
4.1_Mask_Control	15

Enrichment and affinity were tested by DANA (see also 8.7) and FLAA (see also 8.9). As expected, the doped library showed a slight signal of enrichment in DANA. DSR2.1 and DSR3.1 showed strong enrichment signals. In FLAA a negative signal was obtained for the doped library while a slightly positive signal was derived for the enriched pool after DSR3.1 (**Figure 24**).

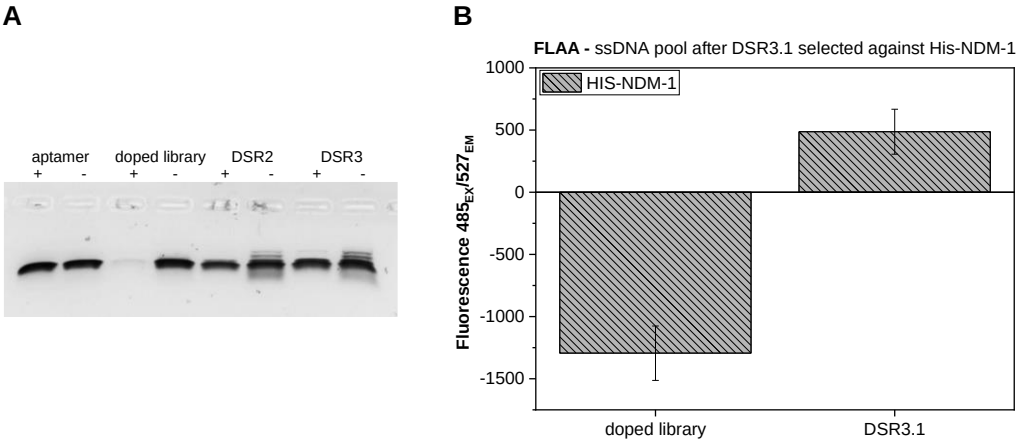

Figure 24: Enrichment and affinity analysis of DNA pools selected against His-NDM-1 by doped SELEX. (A) For enrichment analysis, signals obtained from reactions incubated with S1 nuclease (+) were compared to signals derived from reactions without S1 nuclease (-). DSR2.1 and DSR3.1 were found to be enriched. (B) The ssDNA pool after DSR3.1 was tested for affinity by FLAA. Fluorescence units measured with excitation at 485 nm and emission at 527 nm using Mithras² LB 943 are shown. The ssDNA from DSR3.1 showed slight affinity to His-NDM-1 when compared to the initial library. Fluorescence values of two target-coated and two negative control wells were averaged, and negative control values were subtracted. Error bars represent the square root of the sum of the variances of two target-coated wells and two negative control wells.

5.9.2. Next Generation Sequencing and Characterization of Aptamer Candidates

One more selection round, including a control selection was conducted. Here, for both the target selection as well as for the control selection 15 PCR cycles were required to obtain a PCR signal. Nevertheless, ssDNA pools from DSR3.1, DSR4.1 and DSR4.1_Control were sequenced. The DNA pools were strongly enriched with 20.0% unique sequences for DSR3.1, 15.0% for DSR4.1 and 17.0% for DSR4.1_Control. Sequence analysis of the randomized regions of the of the 100 most enriched sequences after DSR4.1 revealed three motifs that were highly abundant and two motifs that also occurred frequently (**Appendix Table 6**). NDM1-H14.2_Mask-43 was at position 37 after this doped SELEX. The previously identified His-tag-binding motif was not present among the 100 most enriched sequences. Sequences were grouped according to the motifs as sequence families. Members of the sequence families were picked, and six sequences were synthesized (see also **Table 14**) and tested for binding in FLAA (see also 8.9). His-NDM-1 was immobilized via the N-terminal His-tag and incubated with the aptamer candidates. The overall signal intensity was low. Binding signals exceeding that of the initial library were obtained for NDM1-DSR4_04 (84 nt), NDM1-DSR4_16 (80 nt) and NDM1-DSR4_74 (80 nt) (**Figure 25A**).

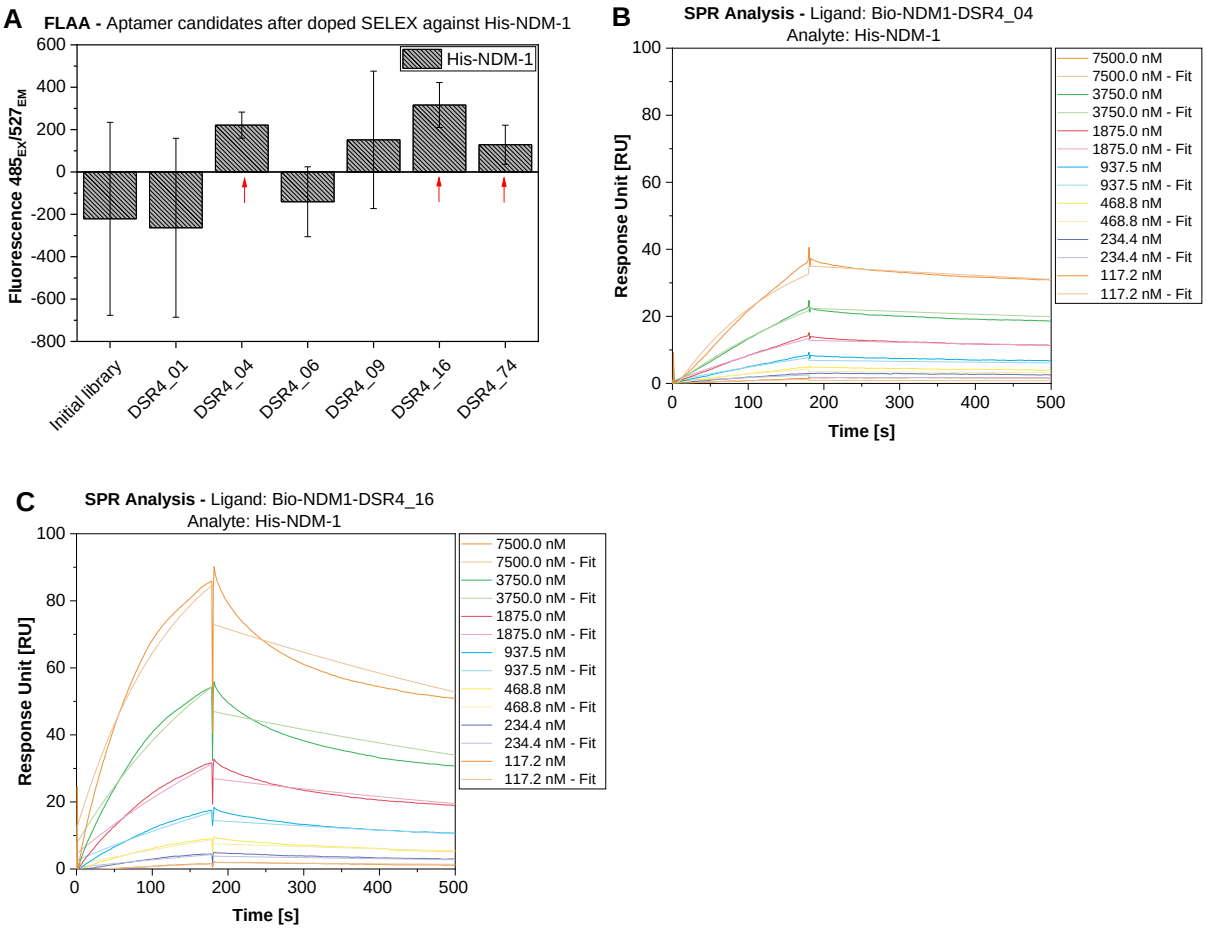

Figure 25: Characterization of aptamer candidates after DSR4.1. (A) Aptamer candidates selected against His-NDM-1 were tested for affinity to His-NDM-1 by FLAA. Fluorescence units measured with excitation at 485 nm and emission at 527 nm using Mithras² LB 943 are shown. His-NDM-1 was immobilized via its N-terminal His-tag. Aptamer candidates that showed binding signals exceeding that of the initial library are indicated by red arrows. Aptamer candidates (B) NDM1-DSR4_04 and (C) NDM1-DSR4_16 were characterized by SPR. Response units over the course of 500 s are shown for His-NDM-1 concentrations ranging from 117.2 - 7500 nM. 5'-biotinylated aptamers were immobilized on a SPR sensor chip and injected with increasing concentrations of His-NDM-1. Kinetic parameters are specified in **Table 7**. Fluorescence values of three target-coated and three negative control wells were averaged, and negative control values were subtracted. Error bars represent the square root of the sum of the variances of three target-coated wells and three negative control wells

NDM1-DSR4_16 and _74 shared sequence similarities while incubation with NDM1-DSR4_16 resulted in a higher fluorescence signal. Thus, only aptamer candidates NDM1-DSR4_04 and NDM1-DSR4_16, which showed very low sequence identity, were used for further characterization by SPR (see also 8.11). 5'-biotinylated aptamer candidates were immobilized on an SPR chip and injected with increasing concentrations of His-NDM-1 (**Figure 25B-C**). Here, K_Ds were calculated as $4.37 * 10^{-7}$ M for NDM1-DSR4_04 and $1.11 * 10^{-6}$ M for NDM1-DSR4_16 (for kinetic data see also **Table 7**). Both values are in a comparable range to

NDM1-H14.2_Mask-43. Thus, the selection of a considerably more affine binder was not successful. NDM1-DSR4_04 exhibited low sequence similarity to NDM1-H14.2_Mask-43. Thus, further characterization of this aptamer candidate may be of interest for the development of an aptamer-aptamer sandwich assay for the specific detection of NDM-1.

Table 7: Kinetic data and K_D-values of His-NDM-1 binding. Kinetic data of His-NDM-1 aptamers and scramble control aptamer ConSc were assessed by SPR. K_D-values of NDM-1 aptamer NDM1-H14.2_Mask-43 and unrelated control aptamer Con1, binding to His-NDM-1 were assessed by MST. NDM1-H14.2_Mask-43 was further tested for binding to the hexa-His peptide and His-OXA-23. Kinetic values: k_a = association constant, k_d = dissociation constant.

Method: SPR					
Ligand	**Analyte**	**k_a (1/Ms)**	**k_d (1/s)**	**K_D (M)**	**Chi² (RU²)**
Bio-NDM1-H14.2_Mask-43	His-NDM-1	$1.00*10^{3}$	$7.48*10^{-4}$	$7.45*10^{-7}$	0.70
Bio-ConSc		-	-	-	-
Bio-NDM1-DSR4_04		$0.87*10^{3}$	$3.78*10^{-4}$	$4.37*10^{-7}$	0.70
Bio-NDM1-DSR4_16		$0.91*10^{3}$	$1.00*10^{-3}$	$1.11*10^{-6}$	4.35

Method: MST			
Ligand	**Analyte**	**K_D (M)**	**K_D confidence (M)**
Cy5-NDM1-H14.2_Mask-43	His-NDM-1	$2.82*10^{-6}$	$3.77*10^{-7}$
	His-OXA-23	-	-
	Hexa-His peptide	-	-
Cy5-Con1	His-NDM-1	-	-

6. Discussion

6.1. Aptamer Selections using SELEX

SELEX is a versatile technique for the *in vitro* selection of high-affinity binders. Aptamers are relatively small in size, easy to synthesize and modify without batch-to-batch variations, heat-stable and of very low immunogenicity [109]. The *in vitro* selection process allows the selection against a wide variety of target molecules, including toxic and non-immunogenic agents as well as selection under non-physiological conditions [64,87]. All these features make aptamers valuable tools for many applications in the fields of diagnostics, therapeutics, or environmental analysis. A few aptamer-based products have already been introduced in clinical and industrial applications [110].

Besides its great benefits, the generation of aptamers by SELEX has some limitations hampering the selection of highly affine and specific aptamers. Firstly, aptamers are rather unstable in biological fluids. For therapeutic applications, costly modifications are required. Secondly, libraries used for selection are highly complex and the number of target-binding sequences within a nucleic acid library is usually low. Therefore, the selection of these few sequences by repeated target incubation usually requires PCR amplification of binding sequences prior to each selection round. A disadvantage of PCR-based DNA amplification is the possible occurrence of PCR bias. In the case of SELEX, PCR bias may result in the overrepresentation of weaker binding sequences in case their replication is more favored than that of binders with higher affinity. When using PCR to amplify DNA, bias cannot be fully bypassed. However, careful optimization of the PCR conditions can improve amplification outcome [81]. In this work, primers were designed regarding minimization of hairpin and dimer formation. In order to minimize byproduct formation, PCR cycles were kept low by making use of a three- to four-step PCR protocol with few cycles instead of a one-step protocol with many cycles. Thirdly, artifactual selection of sequences not binding to the target molecule but rather to, e.g., the selection matrix or additional moieties attached to the target molecule, like purification tags, is a risk that accompanies selection [110,111]. To reduce selection of non-target specific binders, negative selections, e.g., against the selection matrix or other molecules carrying the same additional moieties, are commonly recommended. Especially for cell-SELEX, negative selections are an essential part of the selection process as cells present high numbers of attractive side targets on their surfaces [77]. Negative selections against related molecules can also be used to increase specificity of the selected aptamers. Yet, negative selections have been reported to not always be sufficient to prevent enrichment of side target-binding sequences at least throughout cell-SELEX [48]. Moreover, not all target molecules are equally well suited for SELEX. The presence of hydrogen bond donors and acceptors

(e.g., hetero atoms like amine groups) as well as, positively charged groups, planarity and aromatic rings that allow π-π stacking are favorable [112,113]. Negatively charged groups as well as hydrophobic stretches make selection more difficult. When selecting against a difficult target, negative selections, especially against closely related molecules can exert strong selection pressure [114]. This may result in a loss of binding sequences. In this work, eleven selection rounds against His-tagged carbapenemases with negative selection against other His-tagged carbapenemases did not result in the identification of aptamers (further discussed in 6.1.1). Three additional selection rounds without negative selections against other proteins resulted in the strong enrichment of His-tag-binding sequences (further discussed in 6.1.2). Thus, strategies to avoid His-tag binding while facilitating selection of carbapenemase-binding aptamers were designed (further discussed in 6.1.3) and tested using His-KPC-2 as a model target (further discussed in 6.1.4). The most promising strategy was applied to selection against His-NDM-1 (further discussed in 6.1.5). Additionally, a doped SELEX was performed to enhance affinity (further discussed in 6.1.6).

6.1.1. First Selection Rounds against His-KPC-2 and His-NDM-1

In this work, eleven selection rounds against N-terminally His-tagged carbapenemases His-KPC-2 and His-NDM-1 did not result in target-binding sequences. Here, negative selections were conducted against the immobilization matrix Dynabeads™ M-280 Tosylactivated (SR1.1 - 11.1) and against carbapenemases His-NDM-1 in case of selection against His-KPC-2 and vice versa (SR5.1 - 11.1) as well as His-OXA-23 (SR8.1 - 11.1) (see also **Table 19** and **Table 20**). Negative selections against proteins from the same family were inter alia implemented to select for aptamers specific for one carbapenemases without cross reactivity to others. All three carbapenemases were tested for activity prior to selection and were found to be enzymatically active. Thus, native folding was assumed. Furthermore, activity of His-KPC-2 and His-NDM-1 was assessed after covalent coupling to Dynabeads™ M-280 Tosylactivated. Here, the color change was considerably lower (see also 5.2). This may be attributed to immobilization via primary amines on Dynabeads™ M-280 Tosylactivated. Primary amines are located at the N-terminus and at lysine residues in proteins. His-KPC-2 contains ten lysine residues in its primary sequences, two of which are a conserved active site residues (K73 and K234) [115]. His-NDM-1 contains nine lysines, none of which are considered key conserved side chains that coordinate metal ions in the active center. However, four of these lysines are part of the five active site loops forming the active site cavitiy (K124, K210, K213, K215) [116]. Immobilization via lysines that form the active centers or are located in close proximity to the active centers may affect carbapenemase activity. Furthermore, only 0.6 µg of His-NDM-1 and 0.9 µg of His-KPC-2 coupled to magnetic beads were tested compared to 1 µg

of each carbapenemases in solution. Thus, immobilization via lysines at or near the active center may have reduced enzyme activity resulting in a weaker color change. The lesser amount of protein used for analysis may also have contributed to the weaker signal. Nevertheless, remaining activity was detected. Hence, availability of active centers was likely.

Selection was monitored by PCR analysis of different fractions of the selection process, by enrichment and affinity analysis. Over the course of selection, PCR cycles required to obtain a signal in gel analysis from DNA derived from the elution fraction decreased for selections against both targets (see also 5.3.1). The decrease in PCR cycles suggests that more ssDNA was eluted from the beads even though the amount of ssDNA used for selection was decreased and the number and duration of washing steps was increased. Thus, an enrichment of sequences, potentially binding to the target molecule, was observed. Furthermore, PCR cycles required to obtain a signal for eluted ssDNA derived from the control selections exceeded those of the target selection. This indicated that the signal derived from the elution fraction of the target selections did not mainly derive from binding to the selection matrix (Dynabeads™ M-280 Tosylactivated). Enrichment of the ssDNA pools selected against His-KPC-2 and His-NDM-1 was tested by DANA and affinity was tested by FLAA (see also 5.3.2).

As PCR analysis indicated a positive progress over the course of selection and slight enrichment and affinity signals were obtained, NGS was performed. Compared to cloning and Sanger sequencing, NGS offers a broader information spectrum. Aptamers with desirable binding properties but low copy numbers may be missed by Sanger sequencing [117]. NGS approaches can be divided into short-read techniques and long-read techniques (see also 3.6.1). When sequencing long DNA stretches using short-read techniques, sequencing data must be reassembled [118]. In this case, long-read techniques such as nanopore sequencing can be beneficial. Yet, aptamers mostly do not exceed 100 nt in length and can be easily accommodated using short-read techniques. The most used short-read techniques are based on the mechanism of sequencing by synthesis employing amplification by polymerases. Here, amplification can occur as emulsion PCR or bridge amplification PCR. Incorporation of nucleotides can be analyzed using light emitted via an enzyme cascade (pyrosequencing), fluorescently labeled nucleotides with reversible termination chemistry (Illumina technology) or pH-shifts in microwells (Ion Torrent technology) [118]. All technologies are characterized by certain strengths and weaknesses. Major advantages of pyrosequencing are the comparably long read lengths of up to 800 bp and the bypassing of a chemical deblocking step which lowers the risk of premature chain termination. A limitation of pyrosequencing is that homopolymer regions are often misread. The same limitation applies for the Ion Torrent technology. Here, substitution errors are low, but incorporation of multiple

identical bases can result in a loss of signal linearity. The Illumina technology offers the possibility to accurately sequence homopolymer stretches due to the “one at a time” detection of nucleotides and its capability of paired-end sequencing. A limitation of the Illumina technology is the comparably low read length [95,119]. Yet, as aptamers are inherently short nucleic acids, limitations in read length are not limiting aptamer sequencing. Thus, in this work, Illumina dye sequencing was used for NGS. In addition to high sequence coverage, NGS facilitates the evaluation of binder evolution over the course of different selection rounds [81]. In this work, DNA pools from three (selection against His-KPC-2) or two (selection against His-NDM-1) consecutive selection rounds as well as a control selection of the final selection round (both targets) were sequenced (see also 5.3.3).

Bioinformatic analysis of the NGS data was performed by AptaAnalyzer™-SELEX. The software inter alia allows demultiplexing of the NGS data, calculation of pool enrichment, ranking of sequences enriched in the DNA pools, comparison of sequences enriched in different SRs, and graphical representation of sequence length and nucleotide distributions, for both full sequences and randomized regions [120]. However, identification of motifs and clustering as sequence families was performed without software support. Here multiple alignment programs like MAFFT [121], ClustalX [122] or the MEME Suite [123] may improve data analysis for future selections. In this work, analysis of the sequence data by AptanAnalyzer™-SELEX revealed pool enrichment that was higher for selection against His-KPC-2 than for selection against His-NDM-1, which is well in line with the results of DANA. The percentage of the most enriched sequences was low for both selections with 0.66% and 1.43% of total sequences for His-NDM-1 and His-KPC-2, respectively. Low enrichment of sequences may indicate that the DNA pools are not dominated by sequences with high affinity to the targets. However, enrichment is not necessarily defined by the accumulation of identical sequences but can also be described as the accumulation of different sequences bearing the same motif [96]. This type of enrichment is not covered by the AptaAnalyzer™-SELEX-based analysis of NGS data as sequences differing by only one nucleotide are counted as distinct sequences. Thus, it was assessed whether sequence motifs were enriched rather than complete sequences. The threshold for reoccurrence of a motif was set to at least three sequences carrying the motif. The threshold for nucleotides forming the motif to at least five, based on the usual length of DNA motifs in genomic analysis [107]. Upon identification of a motif, sequences carrying that motif were grouped as a sequence family. Yet, for both selections, only one reoccurring sequence motif was found within the randomized regions of the 50 most enriched sequences (see also **Appendix Table 6**). Furthermore, the percentage of sequences derived from sequencing a pool selected against a target molecule was compared to the percentage of the same sequences derived from sequencing a pool selected against Dynabeads™ M-280

Tosylactivated only. These non-target selections were termed control selections and aimed at detecting sequences that bind to the selection matrix rather than the target molecule immobilized on it. Thus, any sequence whose percentual abundance was higher for the control selection than the target selection was excluded.

16 aptamer candidates were synthesized and tested for binding to their respective target. Even though PCR analysis (see also 5.3.1) implicated a positive progression of selection, binding was not confirmed by FLAA and SPR (see also 5.3.3). Reasons for a false positive indication in PCR analysis may be attributed to the enrichment of unspecific binders or PCR bias [77,87]. Yet, as more PCR cycles were required for amplification of eluted DNA derived from the control selection when compared to the target selection, strong enrichment of matrix binders was not indicated. PCR bias may have participated in the enrichment of the DNA pools. One possible strategy to reduce PCR-bias is microfluidic droplet PCR that can be used to achieve single molecule amplification [124]. The implementation of this method may be of interest for future selections. Nevertheless, enrichment of sequences with high affinity to the target may also be achieved by the performance of more selection rounds or a change in the selection strategy. In this work, as no binders were identified and enrichment of single sequences and motifs was low, the selection strategy was changed.

6.1.2. Selection Rounds without Negative Selections against Carbapenemases

After eleven selection rounds, no aptamers were identified. Up to this point, six out of eleven selection rounds had been carried out with negative selections against His-tagged proteins from the same protein family. Here, the selection pressure caused by negative selections against related proteins may have been too high to achieve enrichment of target-binding aptamers. Thus, selection was continued with negative selections only against the immobilization matrix (Dynabeads™ M-280 Tosylactivated) while negative selections against related proteins were discontinued. After only two successive selection rounds enrichment was detected by DANA (see also 5.4.2). PCR analysis revealed that PCR cycles required to obtain a signal in gel electrophoresis had dropped even though SELEX parameters and thereby selection pressure was kept constant (see also 5.4.1). After one more selection round (SR14.1), affinity was tested and this time, binding signals of the ssDNA pools exceeded those of the initial library by factors greater than ten (see also 5.4.2). Thus, the abundance of strongly enriched sequences with desirable binding properties in the ssDNA pools was suspected.

NGS data of the final selection round showed that enrichment of 58.0% unique sequences for selection against His-KPC-2 and 64.8% unique sequences for selection against His-NDM-1. For a more detailed analysis of the NGS data, the randomized regions of the 50 most enriched

sequences were analyzed as described in section 6.1.1 and repeatedly occurring motifs were identified (see also **Appendix Table 6**). Further, striking sequence similarities between selections against the two targets were detected:

1. The most enriched sequence from selections against His-KPC-2 and His-NDM-1 were identical except for one nucleotide.
2. Of the six motifs identified for selection against His-KPC-2, four motifs were also identified for selection against His-NDM-1.
3. For selection against His-NDM-1, all motifs were also identified in the 50 most enriched sequences for selection against His-KPC-2.

The similarities in the enriched sequences may have been caused by several factors. Firstly, PCR bias may have led to the enrichment of sequences that were favored during amplification. Secondly, the immobilization support may be targeted, leading to the enrichment of sequences that bind to the immobilization support [77]. In both cases, the selection of aptamers that bind to the target proteins would have failed. However, the similarities in the enriched sequences may also be due to similarities in the proteins. In one case, it could be similar protein motifs to which the aptamers bind; in the other, it could be the purification tag. Similar protein motifs can be determined, e.g., from crystal structures. Crystal structures of KPC-2 and NDM-1 are available [115,125,126]. A PyMOL-based structural alignment can be found in **Appendix Figure 4**. Here, structural similarities were not striking. The program calculated a root-mean-square deviation (RMSD) of the atomic positions of 15.409 angstroms. Although the RMSD is not sufficient to exhaustively quantify structural similarity, a high RMSD serves as an indicator of low structural similarity [127]. Throughout selection, six rounds had been performed with negative selection against other His-tagged carbapenemases, lowering the likelihood for an enrichment of His-tag binders. As none the potential causes appeared very likely, testing of aptamer candidates was required to analyze which factor caused the enrichment of similar sequences in both selections.

Aptamer candidates from all sequence families were synthesized. In FLAA strong binding signals for KPC2-H14-01(01) and KPC2-H14-08 were detected. SPR analysis revealed cross reactivity with other His-tagged proteins and MST analysis showed binding to a synthetic hexa-His peptide (see also 5.4.3 and 5.4.4). Highly affine His-tag aptamers were selected, even after six selection rounds with negative selection against either one or two different His-tagged proteins. After only three consecutive SRs without negative selections, strong enrichment of His-tag-binding sequences was possible.

The aptamer candidates that had shown the highest fluorescence signals in FLAA turned out to bind the His-tags rather than the target molecules. Thus, aptamer candidates that had shown lower fluorescence signals were used for cross reactivity testing. Upon incubation with immobilized His-KPC-2 and mPD1-His, only aptamers KPC2-H14-05 and KPC2-H14-07 showed higher signals for His-KPC-2 than for mPD1-His. Detection of His-KPC-2 by KPC2-H14-05 in combination with a His-tag-binding antibody in an MTP-based sandwich assay was successful (see also 5.4.5). Thus, His-tag independent binding of KPC2-H14-05 to His-KPC-2 was likely and the aptamer was successfully implemented into an LFD (see 6.3). However, binding could not be confirmed by SPR and the signal intensity in FLAA and the MTP-based sandwich assay was low, indicating low target affinity (see also 6.2.2). Furthermore, no NDM-1 specific aptamer was identified. Accordingly, the selection strategy was changed again.

6.1.3. Development of New Selection Strategies

Eleven selection rounds with negative selections against His-tagged proteins from the same protein family did not result in strong enrichment of His-tag-binding sequences. However, carbapenemase binding sequences were not identified. Consecutive selection rounds without negative selections against His-tagged proteins resulted in the strong enrichment of His-tag-binding sequences. Thus, instead of continuing selection, a new strategy for the selection of carbapenemase aptamers was desirable.

One conceivable approach was cleavage of the His-tag and a restart of the selection. Some proteases such as enterokinase, factor Xa or thrombin can recognize and cleave specific cleavage sites which are inserted between the protein of interest and the tag [104]. However, nonspecific cleavage sites may compromise protein integrity [128]. More specific proteases are of viral origin such as rhinovirus 3C protease (3CP or PreScission) and tobacco etch virus (TEV) protease. Yet, some fusion proteins are inherently poor targets for TEV protease which may result in incomplete cleavage [129]. Furthermore, additional purification steps after cleavage often result in a reduction of protein yield. Importantly, commercially available protein targets may not or only at high costs be available with required cleavage sites. In this work, commercially available proteins had already been purchased without protease specific cleavage sites which, besides other limitations, omitted tag cleavage. Accordingly, other strategies were required.

In 2014, Even-Desrumeaux *et al.* published a selection strategy for phage display in which few rounds of selections were conducted to select for highly immunogenic but irrelevant epitope binders which were than used in excess to block unwanted epitopes throughout consecutive

selection rounds [130]. Parallels to the selection performed in this work, in which only a few selection rounds were sufficient to strongly enrich His-tag aptamers, were noted. Moreover, epitope masking, e.g., by existent aptamers, has been published [131] but was not applied to His-tags yet. Thus, masking of the His-tag was chosen as one strategy to be tested.

Additionally, competitive elution was a frequent result when searching for epitope directed selection in scientific literature. Here, usually the nucleic acid pools are eluted from the desired epitope by incubation with an excess of the target molecule or by other binders specific for the desired epitope [131-133]. No specific binders for KPC-2 and NDM-1 were available in the laboratory. It was concluded that competitive elution of unwanted sequences from the His-tag of the target proteins prior to unspecific urea elution may decrease enrichment of His-tag aptamers as well. Hence, competitive elution of His-tag-binding sequences by an excess of a defined His-tag binder was chosen as a second strategy.

The first two approaches were aimed at using aptamers directed against His-tags to either mask the His-tag or to competitively elute His-tag binders. Here, two options were conceivable. Firstly, usage of the His-tag binders selected throughout the first selection against His-KPC-2 and His-NDM-1 and secondly usage of already published His-tag-binding sequences. Already published aptamers targeting polyhistidine include the RNA aptamer Shot 47 that exhibited a K_D of $3.8 * 10^{-12}$ M when incubated with various concentrations of His-tagged macrophage migration inhibitory factor by SPR [134]. The aptamer exhibited highly affine binding. However, RNA is either costly in synthesis or requires an additional *in vitro* transcription step prior to use. Thus, DNA aptamers were favored. DNA aptamers 6H1, 6H5 and 6H7 were patented by Doyle *et al.* in 2005 [135]. Here, SPR analysis resulted in K_D-values that were in the range of $8.0 * 10^{-11}$ to $1.8 * 10^{-7}$ M depending on the aptamer and the His-tagged target used for analysis. The His-tag aptamer KPC2-H14-01(01) selected against His-KPC-2 and His-NDM-1 in this work and its derivates KPC2-H14-01(01)-R and KPC2-H14-01(01)-FR had also been used for K_D determination by SPR. Here, kinetic assessment had also been conducted with different His-tagged proteins. K_D-values calculated for binding to the different His-tagged proteins were in the range of $2.86 * 10^{-11}$ (KPC2-H14-01(01)-FR binding to CFHR1-His) to $1.06 * 10^{-8}$ (KPC2-H14-01(01)-R binding to His-NDM-1). Binding of 5'-Cy5 labelled full-length aptamer KPC2-H14-01(01) to the hexa-His peptide, characterized by MST, had resulted in a K_D of $2.81 * 10^{-8} \pm 3.9 * 10^{-9}$ M (see also 5.4.4). Thus, binding affinity was in a comparable range to already published DNA aptamers. Furthermore, dependence of the calculated K_D on the used His-tagged target molecule was also observed with KPC2-H14-01(01) and its truncated derivates. As KPC2-H14-01(01) had been selected for binding to His-KPC-2 and His-NDM-1 and characterized for binding to His-NDM-1, it seemed advisable to use a derivate of this aptamer for masking and competitive elution when reselecting against both targets. To

avoid amplification throughout the selection process, the fully truncated derivate KPC2-H14-01(01)-FR was used as the masking and competitive elution aptamer.

Finally, research on selections against other His-tagged proteins revealed that the proteins were often immobilized on Dynabeads™ His-Tag Isolation and Pulldown [89,136,137]. Immobilization via the His-tag can reduce accessibility of the His-tag. Dynabeads™ His-Tag Isolation and Pulldown deploy a cobalt-based immobilized metal affinity chromatography (IMAC) surface chemistry for the immobilization of His-tagged proteins. The basis of IMAC is a matrix on which metal chelating agents are covalently immobilized which form complexes with metal ions. Adsorption of proteins is based on coordination between an electron donor group in the protein and a metal ion on the surface. Histidine is the amino acid with the strongest affinity for metal ions. Thus, IMAC is frequently used for the purification of His-tagged proteins. While IMAC is an efficient way to purify His-tagged proteins, one disadvantage of IMAC is metal ion leakage [138] which may impact aptamer binding. Furthermore, the immobilization is not covalent and metal ions can serve as attractive targets for nucleic acid libraries [139]. Nevertheless, immobilization on Dynabeads™ His-Tag Isolation and Pulldown was chosen as a third method to evaluate prevention of selection of His-tag-binding sequences.

6.1.4. Selection against His-KPC-2 with different Selection Strategies

His-KPC-2 was chosen as the model target to test the three selection strategies described above. For His-KPC-2, highly affine aptamers had been published in the meantime [106] and thus proof of concept of a successful selection was presented. It was also decided that selection should not be started from the beginning but from a selection round with decent pre-enrichment. NGS data for SR9.1, 10.1 and 11.1 was available. For SR11.1 aptamer candidates had been tested for binding to His-KPC-2 and neither binding to the carba-penemase nor to the N-terminal His-tag had been detected. The motif GGG GGA CTG CTC GGG ATT GCG GA, was identified to be likely involved in His-tag binding (see also 5.6.2). In SR11.1, the motif was not detectable among the 100 most enriched sequences and enrichment was mediocre with 67.2% of unique sequences. Accordingly, ssDNA pools from SR11.1 were chosen as a starting point for restarting selection with the three strategies.

After three consecutive selection rounds, DNA pools were sequenced, and the 100 most enriched sequences were analyzed for enrichment of the potential His-tag-binding motif. Here, the competitive elution approach performed worse with 21.6% of total sequence counts within the 100 most enriched sequences that included the potential His-tag-binding motif. Compared to SR14.1 this accounts for a 2.4% reduction. The reduction was particularly surprising as the

competitive elution approach was accompanied by negative selections with an unrelated His-tagged protein while the initial selection was carried out without negative selections against His-tagged proteins in SRs 12.1 - 14.1. The bad performance may be attributed to the ratio of competitor to target. Competitive elution usually requires large molar excess of the competitor [140]. In this work a 10-fold molar excess of KPC2-H14-01(01)-FR over the immobilized protein was used which may not have been sufficient for successful competition. Testing competition with a larger molar excess of the competitive elution aptamer may be of future interest.

For the masking approach and immobilization on Dynabeads™ His-Tag Isolation and Pulldown a considerable reduction in the enrichment of the potential His-tag-binding motif was achieved. 0.7% and 2.7% of sequence counts within the 100 most enriched sequences included the potential His-tag-binding motif for the two strategies, respectively. The reduction was higher for the masking approach then for immobilization on Dynabeads™ His-Tag Isolation and Pulldown. Hence, aptamer candidates selected with the masking approach were tested for selective binding to His-KPC-2. For two aptamer candidates binding to His-KPC-2 was shown for His-KPC-2 but not for His-NDM-1 and mPD1-His in SPR. An MTP-based sandwich assay with a detection molecule binding to the His-tag was also successful (see also 5.6.3). Accordingly, the selection of aptamers binding to His-KPC-2, independent of the His-tag was likely (see also 6.2.2). Here the masking approach was rated the most promising based on the enrichment of the identified His-tag-binding motif. However, as shown for, e.g., NDM1-H14-02(04), KPC2-H14-15(18), KPC2-H14-18(25), and KPC2-H14-09(39), other motifs can be involved in His-tag binding as well (see also 5.4.5). Moreover, as the masking approach failed and was restarted with ssDNA from SR10.1 (see also 5.6.1) and sequenced after SR13.3, comparability was not unrestricted. Therefore, enrichment of the identified motif may be a good indicator for His-tag binding, as the motif was strongly enriched after SR13.1 and SR14.1 and the His tag aptamers bearing the motif were highly affine, but it is not an exhaustive criterion. Accordingly, testing of sequences selected with the immobilization on Dynabeads™ His-Tag Isolation and Pulldown approach is of future interest. For the subsequent selection against His-NDM-1, the two strategies were further compared. Both strategies have strengths and weaknesses. In the case of His-tag masking, the masking aptamer may interfere with target binding. Immobilization on Dynabeads™ His-Tag Isolation and Pulldown on the other hand makes use of non-covalent coupling which may interfere with storage of the immobilized target as target molecules may leak into the buffer. Furthermore, metal ion leakage may pose a problem throughout selection, as the aptamer binding buffer composition changes. Also, in case of a target protein that forms homodimers, some His-tags may display retained accessibility. NDM-1 has been reported to exist as a partial dimer [116].

Thus, immobilization via the His-tag may not be suitable to decrease accessibility of all His-tags for this target. Hence, after weighing the strengths and weaknesses of the two strategies and also considering the lowest enrichment of the His-tag motif, the masking approach was applied to selection against His-NDM-1

6.1.5. Selection against His-NDM-1 with Masking Approach

The masking approach turned out to be suitable for selection of aptamers binding to His-KPC-2 while not binding to other His-tagged proteins (see also 5.6.3). Furthermore, strong enrichment of the identified His-tag-binding motif was prevented. Thus, the approach was applied to selection against His-NDM-1. Unlike for His-KPC-2, NDM-1 specific DNA aptamers were neither identified after SR14.1 nor in the scientific literature. Further investigation on patent literature revealed two patented sequences, one that is claimed to bind NDM-1 from 2012 and one that is claimed to bind to NDM-1 and VIM-2 simultaneously from 2018 [141,142]. Here, specificity and sequence dependence were not assessed. Moreover, very little information on the used target protein, like the expression system or used purification tags, was published in the patent.

Thus, as an attempt to select for a NDM-1 specific, well characterized ssDNA aptamer, selection was restarted with ssDNA from SR10.1. After three consecutive selection rounds NGS data revealed that the potential His-tag-binding motif was enriched in 1% of sequences counts within the 100 most enriched sequences. Aptamer candidates from six sequences families were tested in FLAA. Here, only NDM1-H14.2_Mask-43 showed binding to His-NDM-1 in different FLAA formats (see also 5.8.2). SPR and MST analysis showed sequence dependent binding to His-NDM-1 with a binding affinity in the high nanomolar to low micromolar range. Binding to the hexa-His peptide and to another His-tagged carbapenemase – His-OXA-23 – was not detected (see also 5.8.3). Thus, a valuable binding probe for the detection of the highly prevalent and health hazardous carbapenemase NDM-1 was selected. However, the moderate affinity of NDM1-H14.2_43 may pose a problem for the detection of the resistance marker, as lower concentrations may be missed and result in false negative results. Various methods for the optimization of aptamer binding characteristics have been proposed. They include the introduction of artificial nucleotides, the joining of binding motifs from different aptamers, or the stabilization of aptamer structures e.g., by the introduction of locked nucleic acids [143].

6.1.6. Doped SELEX against His-NDM-1

Another potential strategy to enhance binding properties of selected aptamers is to perform a doped SELEX. Here, the sequence of a selected aptamer is partially randomized. Thereby, a new doped library is synthesized and used for several additional selection rounds [144]. In this work, a doped SELEX was performed as an attempt to select for more affine aptamers. The doped library was designed by partial randomization of the NDM-1 specific aptamer NDM1-H14.2_Mask-43. After only four rounds of selection employing the masking approach, the ssDNA pool was strongly enriched with 15% unique sequences. The 100 most enriched sequences were dominated by four distinct motifs (see also **Appendix Table 6**). Testing of aptamer candidates, however, revealed low overall signal intensities in FLAA (see also 5.9.1). Two aptamer candidates that showed binding signals in FLAA were kinetically analyzed. Here, K_D-values were either comparable to that of NDM1-H14.2_Mask-43 or higher (see also 5.9.2). Thus, the approach to select for more affine binders was not successful. Yet, future attempts to test whether one of these newly selected aptamers can be used in combination with NDM1-H14.2_Mask-43 should be made to create an aptamer-aptamer sandwich assay that can be implemented into a LFD. In addition, future attempts can be made to increase aptamer affinity. Here, repeating the doped SELEX with improved conditions could lead to more desirable results. The stringency of selection may be better tuned by lowering it in early rounds and increasing it only in later rounds [145]. Moreover, other SELEX strategies like the use of modified libraries, as in Click-SELEX, are of future interest [89].

6.1.7. General Conclusions Drawn from the Selection

The failure to select for high-affinity aptamers can be attributed to various factors influencing the outcome of selection. Firstly, target immobilization on a solid matrix bears certain risks. Immobilization of target proteins in high density can lead to artificially cooperative binding of weakly affine sequences that may displace high-affinity sequences [88]. On the other hand, low immobilization density may increase the likelihood for selecting for sequences that bind to the immobilization matrix. Thus, immobilization density is a critical factor that should be considered carefully in subsequent selections. Another important factor is the target molecule itself. Target purity is important for the selection of specific aptamers. In case of a protein target, the isoelectric point plays a role in the success of the selection. Ahmad *et al.* found that the affinity of selected aptamers was a function of the proteins isoelectric point (pI). Here, aptamer affinities increased with the proteins pI, with an aptamer against a protein target with a pI of 5.3 and net negative charge displayed the highest (least affine) K_D [146]. NDM-1 has a theoretical pI of 5.88 which may hamper selection of high affinity compared to proteins with higher pIs. Here, the expansion of the genetic code by introduction of artificial, potentially positively

charged bases may be favorable. Yet, introduction of artificial nucleotides increases selection and production costs. Finally, general factors impacting SELEX play a role as well. Choice of buffer conditions, nucleic acid to target ratio, and washing steps as well as PCR based amplification are factors that strongly influence SELEX outcomes. All selections against His-KPC-2 and His-NDM-1 were hampered by a strong tendency to byproduct formation in PCR. Additional purification steps were applied after almost every selection round which can be accompanied by the loss of sequence variety. Here, microfluidic droplet PCR (also discussed in 6.1.1) may be suitable as byproduct formation can be strongly reduced [124]. Moreover, using size separation on denaturing poly acryl amide gels instead of exonuclease digestion of the antisense strand for single strand synthesis may bypass the additional purification step. However, ssDNA yield of this method is often lower than for exonuclease digestion [147]. The design of an improved ssDNA library as well as optimization of the amplification process are of interest for future selections. Moreover, in future selections, the development of the nucleic acid pool may be more closely monitored by sequencing of ssDNA pools at earlier stages and more selection rounds [148]. Finally, the analysis of NGS data may also be improved. In this work, all sequences were analyzed for enrichment and ranked by their abundance in the ssDNA pools using the AptaAnalyzer™-SELEX. Here, variations in sequence length as well as overlapping sequences in different selection rounds or between target and control selections were analyzed. The 50 - 300 most enriched clones were then analyzed for reoccurring motifs. The motif analysis may be expanded to more sequences and potentially be supported by suitable software for future selections.

6.2. Aptamer Characterizations

As discussed before, next generation sequencing provides data on millions of sequences simultaneously [149]. Enrichment and motif analysis can aid to narrow down the data set to a set of potential aptamer candidates. These sequences now need to be tested for affinity and, if applicable, specificity to the target molecule. Adequate aptamer characterization is pivotal to determine whether an aptamer is suitable for the desired application [145]. Aptamer characterization can provide qualitative and quantitative as well as structural information on aptamer-target binding [150]. Qualitative aptamer binding studies can be used as a first screening approach to identify target binding sequences.

Qualitative analysis of target binding can either be performed in solution with methods like nitrocellulose filter binding assays or EMSA or with immobilized target molecules in methods like MTP assays or SPR. For nitrocellulose filter binding assays and EMSA, the aptamer candidate and the target molecules are incubated in solution and separation of target bound aptamer candidates from unbound aptamer candidates is facilitated either by binding to a

nitrocellulose filter or by gel electrophoresis [151,152]. Visualization of gel shifts and retained nucleic acids on the filter can be performed either by radiolabeling, by fluorescence labeling or by nucleic acids intercalating dyes. While radiolabeling is highly sensitive, it is also health hazardous and associated with high disposal costs. Thus, the use of other detection methods has become more frequent [153]. In MTP assays the target molecule is immobilized on an MTP either directly or via a linker while in SPR, either the target or the nucleic acid can be immobilized on a sensor chip. An example for a non-radioactive MTP assay is FLAA. FLAA makes use of the ssDNA specific fluorescent dye Quant-iT™ OliGreen™. The dye is basically non-fluorescent in the absence of ssDNA, while it becomes fluorescent when bound to ssDNA. The intensity of the signal is inter alia dependent on the length of the nucleic acid and its sequence. Thus, aptamer candidates, bound to the immobilized target molecule can be qualitatively detected by fluorescence [154]. For SPR measurements, the analyte – either binding partner that is not immobilized – is injected. Upon binding of the injected binding partner, the refractive index at the sensor surface increases, resulting in a change of the SPR angle (see also 8.11) [155]. Immobilization of the target molecule as the ligand and injection of various aptamer candidates as analytes can be used as a qualitative screening method. In this work, aptamer candidate screenings were performed by FLAA and SPR with immobilized target molecules as ligands on the sensor surface. The use of immobilized target molecules appeared expedient as selections were also performed with the target molecules immobilized on magnetic beads. The first screening was always conducted by FLAA (see also 5.3.3, 5.4.3, 5.6.3, 5.8.2, 5.9.2). Here, two to three technical replicates were performed. Some aptamer candidates were not chosen for further, quantitative characterization due to strong signal fluctuations. Here, a higher number of technical replicates would have allowed a more precise screening. However, technical replicates were limited because of the high costs of the target molecules. Aptamer candidates that performed well in screening assays were chosen for quantitative characterization.

Quantitative characterization of aptamers includes the calculation of dissociation constants and, if applicable, kinetic or thermodynamic parameters. Methods for the quantitative analysis of aptamer-target binding events are inter alia SPR, MST, ITC, bio-layer interferometry (BLI) and the switchSENSE® technology. SPR, BLI, and the switchSENSE® technology are techniques that are frequently used to directly determine kinetic parameters (association rate k_a and dissociation rate k_d) of the binding event [155-157]. Here, a strength of SPR and BLI is that no labels are required [155,156]. The use of labeled aptamers or target molecules may interfere with aptamer binding [158]. In contrast to SPR, MST can be used to quantitatively analyze an aptamer-target binding event in solution. Here, one binding partner is fluorescently labeled or intrinsically fluorescent while the other binding partner is titrated. The creation of a microscopic

temperature gradient allows the fluorescence-based tracking of molecules in the temperature gradient (see also 8.10). This phenomenon is called thermophoresis and is influenced by size, charge, and hydration shell. As virtually any binding event results in a change in one of these parameters, MST can be used to differentiate between unbound aptamers and aptamer-target complexes [159]. A strength of this method is the determination of binding characteristics in solution. ITC can be used to measure the thermodynamic parameters of a binding event. Changes in the power required to maintain equal temperatures in a sample and a reference cell upon addition of the ligand to the sample cell are measured. Binding affinity, enthalpy changes and stoichiometry can be calculated in this manner [160]. ITC can supply thermodynamic information on a binding event, immobilization as well as label-free. However, large amounts of both binding partners are usually required, lowering ITCs economic potential. In this work, aptamer candidates that had shown binding in qualitative screening assays were characterized by SPR and MST (see also 5.4.4, 5.8.3 and 5.9.2) to verify binding with immobilized aptamers as well as with both binding partners in solution.

Structural information on aptamer binding can be obtained as well. Methods that can be used for the structural elucidation of aptamer-target molecular complexes include X-ray crystallography, nuclear magnetic resonance (NMR) and circular dichroism (CD) spectroscopy [161]. In X-ray crystallography a sample is crystallized and the three-dimensional structure of the crystal is determined by exposure to an X-ray beam [162]. Crystal structures of aptamer-target complexes offer very detailed information on the interaction. Still, crystallization can be difficult. For NMR spectroscopy, isotope labeling is employed, and strong local magnetic fields are used to analyze the alignment of nuclei in an atom. Using NMR, high resolution structures can be obtained. However, the method is largely limited to complexes < 30 - 40 kDa due to the complexity of the data [161]. CD spectroscopy is based on differences in absorption of right and left-handed circularly polarized light by chiral molecules. Chirality in nucleic acids is sourced from asymmetric sugar moieties, helicity of secondary structures and long-range tertiary ordering. Structure elucidation via CD spectroscopy is mainly empiric-based. Still changes upon target binding can be detected [163]. In this work, structural data on the aptamers in complex with their respective targets has not been collected jet but may be of future interest. For interactions of carbapenemases with carbapenemase aptamers, X-ray crystallography may be expedient, while structures of complexes of the hexa-His peptide with His-tag binding aptamers may be solved by both X-ray crystallography and NMR.

6.2.1. Characterization of His-tag-binding Aptamers

In this work, first selection rounds with negative selections against other His-tagged carbapenemases did not result in the identification of aptamers. Yet, after three consecutive

selection rounds without negative selections against His-tagged carbapenemases, affinity testing revealed strong binding signals for 80 nt long KPC-2-H14-01(01) binding to both His-KPC-2 and His-NDM-1. Furthermore, 121 nt KPC2-H14-08 showed a stronger binding signal to His-KPC-2 (see also 5.4.3). Sequence analysis revealed that the randomized part of KPC2-H14-08 was a 3'-extension of the randomized part of KPC2-H14-01(01) by the randomized part of KPC2-H14-02. The 3'-extension may have aided in binding to His-KPC-2, as indicated by the higher signal in FLAA. However, the dye used for FLAA, Quant-it™ OliGreen® ssDNA Reagent, is not suitable for the simultaneous, quantitative comparison of different ssDNA sequences especially without the use of standard curves [164]. Longer ssDNA sequences may incorporate more dye which can result in a more intense fluorescence signal. Long sequences considerably increase synthesis cost and synthesis of longer oligonucleotides is more error prone [49] which may conflict with the intended use of the aptamer and with further characterization. Here, identification of truncated versions of aptamers that retain affine and specific binding is desirable. A commonly used approach for aptamer truncation is removing either the 5'-, the 3'- or both primer binding sites [165-167], as they may not always be required for structure formation. In this work, KPC2-H14-01(01) was shortened by the 5'-, the 3'- or both primer binding sites while KPC2-H14-08 was only shortened by both primer sites to achieve a reasonable aptamer length (85 nt). Full-length and truncated aptamers were tested for binding by SPR with immobilized His-tagged carbapenemases from Ambler classes A, B and C (His-KPC-2 and His-NDM-1, His-OXA-23) and an unrelated His-tagged protein (mPD1-His). Strong binding signals were obtained from all four channels (see also 5.4.3).

To further assess cross reactivity, KPC2-H14-01(01) and all truncated derivates were subjected to FLAA with three His-tagged (His-NDM-1, His-KPC-2, CFHR1-His) and one non-His-tagged protein (PAG) immobilized as targets. Binding was detected for all aptamers and all His-tagged but not the non-His-tagged protein targets, indicating His-tag binding. His-tag binding was confirmed for KPC2-H14-01(01) binding to a synthetic hexa-His peptide in MST. KPC2-H14-01(01) showed binding with a K_D-value in the mid nanomolar range, while the unrelated control aptamer of comparable size did not show any binding (see also 5.4.4). Kinetic evaluations of the His-tag aptamers KPC2-H14-01(01), KPC2-H14-01(01)-R and KPC2-H14-01(01)-FR with different His-tagged proteins revealed K_D-values that reached from the low nanomolar to the mid-picomolar range, depending on the aptamer and the His-tagged protein (see also 5.4.4). K_D values in the low nanomolar to mid picomolar range are comparable to many monoclonal antibodies [168]. Furthermore, differences in K_D-values for His-tag binding of different proteins are well in line with differences in His-tag accessibility [169]. Differences in K_D-values when using SPR and MST may be attributed to multiple factors. Firstly, kinetic SPR measurements were conducted with the aptamer immobilized on an SPR chip. Immobilization

of aptamers can influence the three dimensional structure and aptamer-ligand interaction [170]. Secondly, the aptamer modifications – 5'-biotin-triethylenglycol versus 5'-Cy5 – may have an impact on aptamer folding and thirdly, while in SPR the K_D is calculated from the ratio of k_d and k_a, usually kinetic parameters are not assessed in MST [171,172]. In MST, K_D is calculated by fitting the binding curve with a quadratic solution derived from the law of mass action and based on the definition of the K_D as

$$K_D = [\mathrm{B}] * [\mathrm{L}]/[\mathrm{BL}] \quad (2)$$

where [B] is the concentration of free binding sites of the fluorescent molecule, [L] the concentration of free ligand and [BL] is the concentration of complexes of [B] and [L] [173]. Nevertheless, His-tag binding was validated using different methods, and kinetic data revealed the high affinity of the His-tag aptamers.

6.2.2. Characterization of His-KCP-2-binding Aptamers

After SR14.1, the aptamer candidates that had exhibited high fluorescence signals in FLAA turned out to bind to the His-tags of His-KPC-2 and His-NDM-1. Characterization of further aptamer candidates resulted in the identification of KPC2-H14-05 which bound to His-KPC-2 but not mPD1-His in FLAA indicating target binding rather than His-tag binding. Moreover, KPC2-H14-05 was suitable for detection of His-KPC-2 in an MTP-based aptamer-antibody sandwich assay with an antibody targeting the His-tag (see also 5.4.5). Thus, His-tag independent KPC-2 binding was likely. However, binding could not be qualitatively validated by SPR and His-KPC-2 was not suitable for kinetic analysis. As fluorescence and absorbance signals in FLAA and the sandwich assay were comparably low, the affinity of KPC2-H14-05 high-affinity binding is unlikely. As discussed above the use of Quant-it™ OliGreen® ssDNA Reagent is not suitable for a quantitative analysis. Yet, a trend towards higher signals for more affine aptamers may be deduced. Thus, the selection of aptamers with higher affinity to His-KPC-2 was desirable. A quantification of signals can be achieved using radio-labeling and scintillation counting, instead of the fluorescent dye [153].

His-KPC-2 was chosen as the model target to test selection strategies designed to prohibit His-tag binding and facilitate carbapenemase binding. In addition to testing the strategies, the selection of higher affinity aptamers was also aimed at. After three selection rounds performed with the different strategies, aptamer candidates selected against His-KPC-2 using the masking approach were tested for binding to His-KPC-2 and mPD1-His. For six aptamer candidates, higher fluorescence signals were obtained for His-KPC-2 than for mPD1-His (see

also 5.6.3). However, overall signal intensities were even lower than for KPC2-H14-05. Thus, the selection of highly affine aptamers appeared rather unlikely. However, two aptamer candidates KPC2-H13.3_Mask-41 and KPC2-H13.3_Mask-126 which were both rich in pyrimidines (84% and 82%, see also 5.6.3) were characterization by SPR. Here, single injections of His-KPC-2, His-NDM-1, and mPD1-His resulted in binding signals only for His-KPC-2, accounting for the selection of KPC-2 specific aptamers (see also 5.6.3). As for KPC2-H14-05, a kinetic evaluation was not possible due to buffer incompatibility and precipitation of His-KPC-2. Yet a sandwich assay with immobilized KPC-2 specific aptamers for capture and a His-tag-binding antibody for detection facilitated the detection of 25 µg/ml His-KPC-2 in an MTP-based assay. Absorbance values were lower than for KPC2-H14-05 which is well in line with the signal intensity in FLAA. Thus, the approach to select for more affine aptamers likely failed.

Quantitative binding analysis was omitted for the His-KPC-2 aptamers because of insolubility of His-KPC-2 in the aptamer binding buffer in high concentrations. Here, future attempts to test affinity with methods like SPR, MST or ITC could be facilitated by the expression of His-KPC-2 with tags that increase protein solubility [174]. Affinity may be increased, e.g., by site-directed mutagenesis or the introduction of artificial nucleotides [100,175]. Also, a doped SELEX could be performed. However, as highly affine KPC-2 aptamers had been published in the meantime [106], it was primarily focused on selection of NDM-1 aptamers.

6.2.3. Characterization of His-NDM-1-binding Aptamers

Using the masking approach for selection against His-NDM-1, one aptamer candidate – NDM1-H14.2_Mask-43 – repeatedly showed binding signals to His-NDM-1 in FLAA employing different coupling chemistries (see also 5.8.2). This aptamer was further characterized by SPR and MST resulting in K_D-values of $7.45 * 10^{-7}$ M and $2.82 * 10^{-6}$ M, respectively (see also 5.8.3). Selectivity of the aptamer was probed by MST. Cross reactivity was neither detected for His-tagged carbapenemase His-OXA-23 nor for the hexa-His peptide. Taken together with higher fluorescence signals for His-NDM-1 than for mPD1-His and retained binding upon immobilization of His-NDM-1 via the His-tag, His-tag binding is unlikely. Furthermore, cross reactivity to another carbapenemase was not observed. Sequence dependence of binding was assessed by SPR with scramble control aptamer ConSc and by MST with unrelated control aptamer Con1. ConSc showed considerably lowered RU in SPR, and determination of kinetic parameters was not possible. In MST, no binding of Con1 to His-NDM-1 was observed. Thus, an aptamer with sequence dependent, moderate binding affinity to His-NDM1 but neither to the hexa-His peptide nor to another His-tagged carbapenemase was selected using the masking approach. As there are no well characterized ssDNA aptamers specifically binding to

NDM-1, NDM1-H14.2_43 may serve as a valuable probe for the detection of this highly prevalent and health hazardous carbapenemase. Truncations of the NDM-1 aptamer were designed and tested in an MTP-based sandwich assay but not yet kinetically characterized (see also 5.8.3). Kinetic characterization of the truncations is of future interest. Furthermore, probing cross reactivity to His-KPC-2 and other carbapenemases is another aspect that should be tested in the future. So far, cross reactivity was only tested for Ambler class C carbapenemase His-OXA-23.

As an attempt to select for aptamers with higher affinity to NDM-1, a doped SELEX was performed, based in the NDM-1 aptamer NDM1-H14.2_Mask-43. Here, aptamer candidates NDM1-DSR4-04 and -16 were characterized by FLAA and SPR. K_D-values were in a comparable range to NDM1-H14.2_Mask-43 (see also 5.9.2). Thus, NDM-1 specific aptamers with higher affinity to the target were not selected. However, future investigations may be conducted on whether a combination of NDM1-DSR4-04 and NDM1-H14.2_Mask-43, which have very little sequence similarity and may have different binding sites, is suitable for an aptamer-based sandwich assay. Furthermore, attempts to increase the aptamers affinities are of future interest. As discussed in section 3.6.4, the introduction of artificial nucleotides, like Clickmers or SOMAmers can be used to expand the chemical diversity of the nucleobases [69,101] and thereby potentially increase affinity. Site-directed mutagenesis is also a valuable tool to increase aptamer affinities [175]. Finally, repetition of the doped SELEX with less stringent SELEX conditions or restarting the selection with more focus on target immobilization and application of the masking approach from the beginning may also result in the identification of more affine aptamers.

6.3. Assay Development for Carbapenemase Detection

Detection of carbapenemase producing CRE is important, especially for infection control and interventions. Methods developed for this purpose are multifaceted and include e.g., broth microdilution metallo-β-lactamase screen, gradient MIC strips, multidisc mechanism testing, modified hodge test, Carba NP test, carbapenemase inactivation method, MALDI-TOF mass spectrometry, (real-time) PCR, microarrays, whole genome sequencing, and antibody-based LFDs [33]. While high complexity methods like real-time PCR, MALDI-TOF mass spectrometry and whole-genome sequencing deliver accurate results, they are not accessible for many users. Others, like the broth microdilution metallo-β-lactamase screen or gradient minimum inhibitory concentration strips require less equipment but are limited to a certain kind of carbapenemases [176,177]. Phenotypic tests that detect carbapenemase activity like Carba NP test, the modified hodge test and carbapenemase inactivation method are easily accessible and suitable for detection of most carbapenemases [34]. However, discrimination between

different types of carbapenemases cannot be facilitated. As discussed in sections 3.4 and 3.5, LFDs offer certain advantages for rapid, easy, and cost-effective on-site detection of carbapenemases. Various antibody-based LFDs for the detection of carbapenemases have been developed over the last years, including the commercially available multiplex LFDs NG-Test® CARBA-5 (NG-Biotech, Guipry-Messac, France), RESIST-5 K.O.N.V.I (Coris-Bio-Concept, Gembloux, Belgium) and CP-5 (ERA-Bio, Pittsford, USA). All three tests can be used for the simultaneous detection of KPC, OXA-48-like, NDM, VIM and IMP type carbapenemases. The tests were tested for sensitivity by Bernabeu *et al.* and all reached sensitivities of > 89.9% [178]. Thus, LFDs with high sensitivity have already been developed. Still, as discussed in section 3.6, aptamers display certain advantages over antibodies like high buffer stability, the ability to refold after denaturation and the lack of batch-to-batch variations [49]. Accordingly, the development of aptamer-based detection methods for the rapid, easy, cost-efficient, and robust on-site detection of carbapenemases is still desirable. In this work, His-KPC-2- and His-NDM-1-binding aptamers (also referred to as His-KPC-2 and His-NDM-1 aptamers) were selected and characterized for affinity and specificity. These aptamers were suitable for an MTP-based aptamer-antibody sandwich assay (see also 5.4.5 and 5.8.3) and implementation of His-KPC-2 aptamers into an aptamer-aptamer sandwich assay LFD was successful (see also 5.7). NG-Biotech published detection limits for the NG-Test® CARBA-5 LFD that were assessed with recombinantly expressed carbapenemases. Limits of detection were 600 pg/ml for the KPC type of carba-penemases, 300 pg/ml for the OXA and the VIM type, 200 pg/ml for the IMP type and 150 pg/ml for the VIM type [179]. Consequently, a comparison to the LFD developed in this work was possible (see also 6.3.2).

6.3.1. Carbapenemase-binding Aptamers in MTP-based Sandwich Assays

His-KPC-2-binding aptamers were identified after SR14.1 (KPC2-H14-05) and after SR13.3_Mask (KPC2-H13.3_Mask-41, KPC2-H13.3_Mask-126). Binding to the His-tag was assessed and found to be unlikely (see also 5.4.5 and 5.6.3). Thus, the His-KPC-2 specific aptamers were tested as capture molecules in an MTP-based sandwich assay. Detection was facilitated by a His-tag binding antibody. His-KPC-2 detection was facilitated for all three aptamers. The MTP-based assay employing a His-tag-binding antibody as the detection probe is not clinically relevant. However, it further substantiated the His-tag independent binding of the His-KPC-2 aptamers and showed that the aptamers were suitable for capturing His-KPC-2 in an MTP-based sandwich assay. Suitability for use as the detection molecule was tested for KPC2-H13.3_Mask-41 in an aptamer-aptamer sandwich assay format (see also 5.7 and 6.3.2).

Future research on whether the other two His-KPC-2 aptamer KPC2-H14-05 and KPC2-H13.3_Mask-126 also function as detection molecules should be conducted.

For His-NDM-1, NDM1-H14.2_Mask-43 was used for sandwich assay development. Here, a clinically relevant assay was set up by using a NDM-1 specific antibody as the detection molecules (see also 5.8.3). An aptamer-antibody sandwich assay format can be developed if the aptamer and antibody have different binding sites. Sandwich assay formats are known for their high specificity and sensitivity due to the requirement of binding for two different binding molecules [180]. In this work, signals derived from NDM1-H14.2_43 derivates as capture molecules and the NDM-1 specific antibody as the detection molecules exceeded those of an unrelated control aptamer. However, signals derived from the no aptamer control wells were only slightly lower than those derived from the NDM1-H14.2_43 derivates. As binding of the primary and secondary antibody was tested and excluded, non-specific binding of His-NDM-1 to the SA-MTP is likely and may be partially responsible for the signals derived from the NDM1-H14.2_43 derivates. Nevertheless, when compared to the control aptamer, detection of 17 µg/ml His-NDM-1 was facilitated. As part of future investigations, the sandwich assay may be tested using a different immobilization matrix and a limit of detection may be determined. Moreover, future implementation into an LFD is of interest as a different support is used.

6.3.2. The Implementation of His-KPC-2-binding Aptamers into an LFD

The combination of the guanine rich aptamer KPC2-H14-05 and thymine and cytosine rich aptamer KPC2-H13.3_Mask-41 was tested by our project partner nal von minden GmbH (see also 5.7). Here, the detection of ≥ 2 µg/ml His-KPC-2 was facilitated resulting, to our best knowledge, in the first reported aptamer-aptamer sandwich LFD for the detection of KPC-2. Yet, the aptamer-based LFD needs to compete with antibody-based LFDs for the detection of KPC-2. The NG-Test® CARBA-5 from NG Biotech exhibits a detection limit, tested with purified, recombinant KPC-2 of 600 pg/ml. The detection limit of the antibody-based LFD exceeds that of our test by far. Using a test device with high detection limits may result in false negative results. However, testing of the aptamer-aptamer sandwich LFD on bacterial isolates as well as testing other combinations and the development of a NDM-1 specific LFD may be of interest for future investigations.

6.4. Conclusions and Outlook

Eleven selection rounds against His-KCP-2 and His-NDM-1 with varying amounts of negative selections inter alia against other His-tagged carbapenemases did not result in the identi-

fication of carbapenemase-binding aptamers. Three consecutive rounds without negative selections against His-tagged carbapenemases resulted in the selection of highly affine His-tag aptamers. No NDM-1 and only one KPC-2 aptamer was identified. To facilitate selection of KPC-2 specific aptamers with more desirable binding features and to prohibit the selection of further His-tag aptamers three selection strategies were designed. Masking of the His-tag and competitive elution of His-tag-binding sequences with a truncated version of the previously selected His-tag aptamer KPC2-H14-01(01), and immobilization via the His-tag were tested. The masking approach turned out to be an appropriate strategy to select for His-KPC-2 aptamers that likely did not bind the His-tag. Two His-KPC-2 aptamers were implemented into an LFD and ≥ 2µg/ml of recombinantly expressed His-KPC-2 were detected. To compete with antibody-based LFDs, the limit of detection needs to be improved. Here, improvement of the aptamers is desirable. However, proof of concept of an aptamer-based carbapenemase detection system was shown.

Transfer of the masking approach to selection against His-NDM-1 resulted in the selection of the NDM-1 aptamer NDM1-H14.2_Mask-43. Kinetic data was assessed and cross reactivity to another His-tagged carbapenemase as well as to the hexa-His peptide was not detected. Sequence dependence of binding was shown. Thus, a strategy suitable for the selection of aptamers specifically binding to different carbapenemases while preventing His-tag binding is presented in this work. Furthermore, a NDM-1 aptamer was selected that may serve as a valuable tool for the detection of the prevalent and health hazardous carbapenemase NDM-1. A detection system based on this aptamer could potentially be used to contain transmission of carbapenem resistant bacteria and to facilitate appropriate treatment. However, the usability of NDM1-H14.2_Mask-43 is limited by its binding affinity in the high nanomolar to low micromolar range and the accompanying risk of false negative results. An attempt to increase aptamer affinity by performing doped SELEX failed to produce more affine binders. Yet, another aptamer with a dissociation constant comparable to NDM1-H14.2_Mask-43 was selected that showed low sequence similarity. Future attempts may focus on the further characterization of NDM1_DSR4-04 and the potential development of an aptamer-aptamer sandwich assay. Furthermore, other attempts to increase affinity, like the introduction of artificial nucleotides, e.g., Clickmers or SOMAmers, are conceivable even though synthesis costs may be elevated. Repeating doped SELEX with less stringent conditions or starting a new SELEX with more attention to target immobilization density and constant monitoring by NGS can also result in more affine aptamers.

Finally, future investigations on structural features of the His-KPC-2 and NDM-1 aptamers are also of interest. Elucidation of the binding epitopes may prove His-tag independent binding. Moreover, testing the ability of the aptamers to inhibit carbapenemases, either by inhibition

assays or by localization of the binding epitopes, can serve to evaluate whether the aptamers have therapeutic potential as well.

7. Material

Standard chemicals were purchased from Carl Roth GmbH + Co. KG, Karlsruhe, Germany or Merck KGaA, Darmstadt, Germany.

7.1. Buffers and Reagents

Buffers and reagents used for SELEX, PCR, other enzymatic reactions, gel electrophoresis and DNA purifications are specified in **Table 8** and **Table 9**.

Table 8: Buffers used in this work, their composition and providers.

Buffer	**Formulation**	**Provider**
5x GoTaq® Flexi Reaction Buffer	Without $MgCl_2$	Promega GmbH, Walldorf, Germany
10x Reaction Buffer (for Taq DNA Polymerase convenient)	With 30 mM $MgCl_2$	Biozym Scientific GmbH, Hessisch Oldendorf, Germany
5x Reaction Buffer (for S1 nuclease)	200 mM sodium acetate (pH 4.5 at 25 °C), 1.5 M NaCl and 10 mM $ZnSO_4$.	Thermo Fisher Scientific, Waltham, USA
Lambda Exonuclease Reaction Buffer (10X)	67 mM Glycine-KOH, 2.5 mM $MgCl_2$, 50 µg/ml BSA (pH 9.4 at 25°C)	New England Biolabs, Inc, Ipswich, USA
BP-TB	20 mM Tris-HCl [pH 7.4], 140 mM NaCl, 5 mM $MgCl_2$, 1 mM $CaCl_2$, 1 mM KCl, 0.1% [w/v] BSA, and 0.05% [v/v] Tween® 20	Self-made
BP-T	20 mM Tris-HCl [pH 7.4], 140 mM NaCl, 5 mM $MgCl_2$, 1 mM $CaCl_2$, 1 mM KCl, and 0.05% [v/v] Tween® 20	Self-made
BP-T*	20 mM Tris-HCl [pH 7.4], 140 mM NaCl, 5 mM $MgCl_2$, 1 mM $CaCl_2$, 1 mM KCl, and 0.005% [v/v] Tween® 20	Self-made
Buffer B	0.1 M sodium phosphate buffer, pH 8.5	Self-made
Buffer C	3 M ammonium sulphate in Buffer B	Self-made
2x Binding/Wash buffer	100 mM Sodium-Phosphate, pH 8.0, 600 mM NaCl, 0.02% [v/v] Tween® 20	Self-made
2x Pulldown Buffer	6.5 mM Sodium-phosphate, pH 7.4, 140 mM NaCl, 0.02% [v/v] Tween® 20	Self-made
Citrate-HCl buffer	0.1 M citric acid, 0.1 M Sodium citrate, pH 4.3	Made by project partner
Gold stabilization buffer	Colloidal gold stabilizer (6 g), 50 ml dd	Artron BioResearch Inc., Burnaby, Canada

ROTIPHORESE® 10x TBE-Buffer	1 M Tris-Borat, and 20 mM EDTA, pH 8.3.	Carl Roth GmbH + Co. KG, Karlsruhe, Germany
ROTI®Stock 10x PBS	Phosphate buffered saline, pH 7.4	Carl Roth GmbH + Co. KG, Karlsruhe, Germany
1x PBS-T	1:10 dilution of ROTI®Stock 10x PBS, 0.005% [v/v] Tween® 20	Self-made
Denaturing PAA loading dye	90% [v/v] formamide in 1x TBE with bromophenol blue	Self-made
Agarose loading dye	60% [v/v] glycerol in 1x TBE with 0.4% [w/v] xylene cyanol blue	Self-made
(Agowa) Binding Buffer BL (acetate)	No details available	LGC Limited, Teddington, UK
(Agowa) Wash buffer BN 2		
(Agowa) Elution Buffer BLM		

Table 9: Non-standard reagents used in this work.

Reagent	**Provider**
GelStar™ Nucleic Acid Gel Stain	Lonza Group, Basel, Switzerland
1% EtBr in aqueous solution	Merck KGaA, Darmstadt, Germany
Quant-iT™ OliGreen™	Thermo Fisher Scientific, Waltham, USA
1-Step Ultra TMB	Thermo Fisher Scientific, Waltham, USA
10x ROTI®Block	Carl Roth GmbH + Co. KG, Karlsruhe, Germany

7.2. Target Proteins, Enzymes and Antibodies

Table 10: Proteins used as targets for SELEX and aptamer characterizations.

Target Protein	Purification tag	Provider
His-NDM-1	N-terminal His-tag	Hölzel Diagnostica Handels GmbH, Köln, Germany
His-KPC-2		
His-OXA-23		
CFHR1-His	C-terminal His-tag	
mPD1-His		Abcam plc., Cambridge, UK
PAG	No tag	Supplied by project partner
Hexa-His peptide	No tag	BIOTREND Chemikalien GmbH, Köln, Germany

Table 11: Enzymes used for selection, enrichment assessment, library design and NGS preparation.

Enzyme	Provider
GoTaq® G2 Flexi DNA Polymerase	Promega GmbH, Walldorf, Germany
Taq DNA Polymerase convenient	Biozym Scientific GmbH, Hessisch Oldendorf, Germany
S1 Nuclease	Thermo Fisher Scientific, Waltham, USA
Lambda Exonuclease	New England Biolabs, Inc, Ipswich, USA
Perfect Match Enhancer	Agilent technologies, Inc., Santa Clara, USA

Table 12: Antibodies used for ELISA and MTP-based sandwich assays.

Antibody	Provider
Mouse-anti-Penta-His-HRP	Qiagen N.V., Venlo, Netherlands
Rabbit-anti-blaNDM-1 IgG	Cusabio Technology LLC, Houston, USA
Goat-anti-rabbit-IgG-HRP	Merck KGaA, Darmstadt, Germany

7.3. DNA Ladders

Table 13: DNA ladders used for gel electrophoresis.

Ladder	Provider
25 bp DNA Step Ladder	Promega GmbH, Walldorf, Germany
50 bp DNA Ladder	New England Biolabs, Inc, Ipswich, USA

7.4. Oligonucleotides

Libraries were purchased from Ella Biotech GmbH (Fürstenfeldbruck, Germany). Unmodified forward and reverse as well as 5'-phosporylated reverse Primers were purchased from TIB Molbiol Syntheselabor GmbH (Berlin, Germany). Aptamer candidates including aptamers with modifications (5'-biotinylated, 5'-thio and 5'-Cy5) were ordered from biomers.net GmbH (Ulm, Germany) and Integrated DNA Technologies Inc (Coralville, USA). All oligonucleotides were synthesized by standard solid-phase DNA synthesis and purified either by HPLC or standard desalting. Sequences of oligonucleotides used in this work are listed in **Table 14**.

Table 14: Names and sequences of oligonucleotides used in this work. Sequences are represented in 5'-3' direction. The potential His-tag-binding motif is highlighted in red. Other motifs, identified for the different selection rounds (**Appendix Table 6**) are highlighted in green.

Oligonucleotide	Sequence	Length [nt]
Libraries		
Initial library	GTATCTGGTGGTCTATGG – N(44) – GCATAGACGACGAAGAAC	80
Doped library	GTATCTGGTGGTCTATGG – 667685866765586878686888868885886888856865 66 – GCATAGACGACGAAGAAC	80
Library 42	AGGTAGAGGAGCAAGCCATC – N(42) – GATGCGTGATCGAACCTACC	82
Primers		
F44	GTATCTGGTGGTCTATGG	18
R44	GTTCTTCGTCGTCTATGC	18
Index01F	AGATGTATCCTGTCTCTTGTATCTGGTGG	29
Index01R	GACTACTACCTGTCTCTTGTTCTTCGTCG	29
Index02F	AGATGTATCCTCTGTGTTGTATCTGGTGG	29
Index02R	GACTACTACCTCTGTGTTGTTCTTCGTCG	29
Index03F	AGATGTATCCTTATCTCTGTATCTGGTGG	29
Index03R	GACTACTACCTTATCTCTGTTCTTCGTCG	29
Index04F	AGATGTATCCTCGTGTTTGTATCTGGTGG	29

Index04R	GACTACTACCTCGTGTTTGTTCTTCGTCG	29
Index05F	AGATGTATCCTTAGACGTGTATCTGGTGG	29
Index05R	GACTACTACCTTAGACGTGTTCTTCGTCG	29
Index06F	AGATGTATCCTCAGAGTTGTATCTGGTGG	29
Index06R	GACTACTACCTCAGAGTTGTTCTTCGTCG	29
Extension Primer F	CCTTGACGCCAGATGTATCC	20
Extension Primer R	GTATCCCGCTGACTACTACC	20
Aptamer candidates		
KPC2-H11-01	GTATCTGGTGGTCTATGGGGCGGGGGGAAACGAACGGGGGGATGGATCTCCTGCGGGGTGCATAGACGACGAAGAAC	77
KPC2-H11-03	GTATCTGGTGGTCTATGGGGAGGGGGGGCCTTTCATATCGGGGGGTGGTTCTGTGAGGGGAAGCATAGACGACGAAGAAC	80
KPC2-H11-05	GTATCTGGTGGTCTATGGGGGGGGGAATTAACACTTGGGGGGCGGGTAACGACCTGTGGGGTGCATAGACGACGAAGAAC	80
KPC2-H11-06	GTATCTGGTGGTCTATGGGCGGGGGCATCTGACTGAACTTCCGGGGGGTTGGTTACTGTGGGGCATAGACGACGAAGAAC	80
KPC2-H11-12	GTATCTGGTGGTCTATGGGGAGGGGGGGCCTTTCATATCGGGGGGTGGTTCTGTGAGGGGAAGCATAGACGACGAAGAACAGGCG GGCATAGACGACGAAGAAC	104
KPC2-H11-14	GTATCTGGTGGTCTATGGGCCGTAATGTATCTGGTGGTCTATGGGGCGGGGGGAAACGAACGGGGGGATGGATCTCCTGCGGGGT GCATAGACGACGAAGAAC	103
KPC2-H11-18	GTATCTGGTGGTCTATGGGGCGGGGGGAAACGAACGGGGGGATGGATCTCCTGCGGGGTGCATAGACGACGAAGAACAGGCGGGC ATAGACGACGAAGAAC	101
NDM1-H11-01	GTATCTGGTGGTCTATGGCCCGGGTCAACCGTTCTTCTCGTTTCCGTTATTTTGTCTTCTATGCATAGACGACGAAGAAC	80
NDM1-H11-02	GTATCTGGTGGTCTATGGCATAGACGACGAAGAACAGGACATTTTTGGTTTTTGGGTACTCCTCCGCATAGACGACGAAGAAC	83
NDM1-H11-03	GTATCTGGTGGTCTATGGCGGAGGTGTTCTGAGTAGTCAGTTCAAGTCGCTTAATTTTCGGGGCATAGACGACGAAGAAC	80
NDM1-H11-04	GTATCTGGTGGTCTATGGCACAGTGAAAATTCTTCGTCCCAATCTCTCTCTTCGACTCATATGCATAGACGACGAAGAAC	80
NDM1-H11-05	GTATCTGGTGGTCTATGGGTCGTCTCTTTTTTGTTGTTTTTTTTTGGTTTCCCGTGCATAGACGACGAAGAAC	73
NDM1-H11-06	GTATCTGGTGGTCTATGGCCCCGGAACCTTCGTCGATAGTTCTTCTCAACAGATACATTCCGGCATAGACGACGAAGAAC	80
NDM1-H11-07	GTATCTGGTGGTCTATGGCGGGACGTCGTCTAACGGTTCTTCTCTTGTCCTTTTTTGTGTGTGCATAGACGACGAAGAAC	80
NDM1-H11-08	GTATCTGGTGGTCTATGGCGGCGATAACAAAAAAAAAAACAAATTTGCTGTATCTGGTGGTCTATGGCATAGACGACGAAGAAC	84
NDM1-H11-26	GTATCTGGTGGTCTATGGCGAGGGGTGAGCTAAAAAAAAAAAAAAAATGTCCACGTCGTGGGGGGCATAGACGACGAAGAAC	81
KPC2-H14-01(01)	GTATCTGGTGGTCTATGGCGTCATAGGTACCATGGGGGACTGCTCGGGATTGCGGATTCATGGCATAGACGACGAAGAAC	80
KPC2-H14-02	GTATCTGGTGGTCTATGGCATAGACGACGAAGAACAGATCACCAGATACCCAGATACGGCATAGACGACGAAGAAC	76

NDM1-H14-02(04)	GTATCTGGTGGTCTATGGCCAGTATGGCTGTTCAAGTCTTCAGAGGGTCTGCTCGGGATTGCGCATAGACGACGAAGAAC	80
KPC2-H14-03	GTATCTGGTGGTCTATGGGCGGGGGCATCTGACTGAACTTCCGGGGGGGTTGGCTACTGTGGGGCATAGACGACGAAGAAC	80
NDM1-H14-03	GTATCTGGTGGTCTATGGCATAGACGACGAAGAACAGGACATTTTTGGTTTTTGGGTACTCCTCCGCATAGACGACGAAGAAC	83
NDM1-H14-04(06)	GTATCTGGTGGTCTATGGCATAGACGACGAAGAACAGCCGCAAAAAATAAAAGCCTAACGAGGGGCATAGACGACGAAGAAC	82
KPC2-H14-05	GTATCTGGTGGTCTATGGGGCGGGGGGAAACGAACGGGGGGATGGATCTCCTGCGGGGTGCATAGACGACGAAGAAC	77
NDM1-H14-05(12)	GTATCTGGTGGTCTATGGCCCCGGAACCTTCGTCGATAGTTCTTCTCAACAGATACATTCCGGCATAGACGACGAAGAAC	80
NDM1-H14-06(14)	GTATCTGGTGGTCTATGGCATAGACGACGAAGAACAACAAAAAGAGCGAACAAATCGGGGCTGGTGGGCATAGACGACGAAGAAC	85
KPC2-H14-07	GTATCTGGTGGTCTATGGGGAGGGGGGGCCTTTCATATCGGGGGGTGGTTCTGTGAGGGGAAGCATAGACGACGAAGAAC	80
NDM1-H14-07	GTATCTGGTGGTCTATGGCATAGACGACGAAGAACAGGCGGGCATAGACGACGAAGAACAGGCGGGCATAGACGACGAAGAAC	83
KPC2-H14-08	GTATCTGGTGGTCTATGGCGTCATAGGTACCATGGGGGACTGCTCGGGATTGCGGATTCATGGCATAGACGACGAAGAACAGATC ACCAGATACCCAGATACGGCATAGACGACGAAGAAC	121
KPC2-H14-09(39)	GTATCTGGTGGTCTATGGCATAGACGACGAAGAACAATAAGGGGCAAATCTATTTAATTGGGGAGAGCATAGACGACGAAGAAC	84
NDM1-H14-09(10)	GTATCTGGTGGTCTATGGCATAGACGACGAAGAACACTAACACGTTTTTTTACCTTATACTTGCGGGCATAGACGACGAAGAAC	84
NDM1-H14-10(13)	GTATCTGGTGGTCTATGGCGGCGATAACAAAAAAAAAAACAAATTTGCTGTATCTGGTGGTCTATGGCATAGACGACGAAGAAC	83
NDM1-H14-12(20)	GTATCTGGTGGTCTATGGCATAGACGACGAAGAACAGTGTATCTGGTGGTCTATGGCATAGACGACGAAGAAC	73
KPC2-H14-15(18)	GTATCTGGTGGTCTATGG CCCGGGTCAACCGTTCTTCTCGTTTCCGTTATTTTGTCTTCTATGCATAGACGACGAAGAAC	81
NDM1-H14-17	GTATCTGGTGGTCTATGGCGGAGGTGTTCTGAGTAGTCAGTTCAAGTCGCTTAATTTTCGGGGCATAGACGACGAAGAAC	80
KPC2-H14-18(25)	GTATCTGGTGGTCTATGGCAAACGTTCTGAGTTAGGCTTATTTTTCTCTCTTCCCTTCGCCGCATAGACGACGAAGAAC	79
KPC2-H14-19	GTATCTGGTGGTCTATGGCATAGACGACGAAGAACACATAGACGACGAAGAACACCAGATACCCAGATACGCATAGACGACGAAG AAC	88
KPC2-H14-01(01)-F	CGTCATAGGTACCATGGGGGACTGCTCGGGATTGCGGATTCATGGCATAGACGACGAAGAAC	62
KPC2-H14-01(01)-R	GTATCTGGTGGTCTATGGCGTCATAGGTACCATGGGGGACTGCTCGGGATTGCGGATTCATG	62
KPC2-H14-01(01)-FR	CGTCATAGGTACCATGGGGGACTGCTCGGGATTGCGGATTCATG	44
KPC2-H14-08-FR	CGTCATAGGTACCATGGGGGACTGCTCGGGATTGCGGATTCATGGCATAGACGACGAAGAACAGATCACCAGATACCCAGATACG	85
KPC2-H13.3_Mask-04	GTATCTGGTGGTCTATGGCATAGACGACGAAGAACAGGCGGGCATAGACGACGAAGAACAGGCGGGCATAGACGACGAAGAAC	83
KPC2-H13.3_Mask-16	GTATCTGGTGGTCTATGGCCGCCGAAATTTCATGAATCCGTATTTTCTTAACCTCTTTCTCCGCATAGACGACGAAGAAC	80
KPC2-H13.3_Mask-18	GTATCTGGTGGTCTATGGCGGAGGTGTTCTGAGTAGTCAGTTCAAGTCGCTTAATTTTCGGGGCATAGACGACGAAGAAC	80
KPC2-H13.3_Mask-41	GTATCTGGTGGTCTATGGCCGCATAATCGTTTCGTTCTCTCTTTTCTTTCTTTTCTCCCACCGCATAGACGACGAAGAAC	80
KPC2-H13.3_Mask-47	GTATCTGGTGGTCTATGGCGAGAAAAGTTCTGTCGTCTAAAAAGTTCTTGTCGTAATTCGGGGCATAGACGACGAAGAAC	80

KPC2-H13.3_Mask-49	GTATCTGGTGGTCTATGGCATAGACGACGAAGAACATGAAAGAGGTGTGGGGGTAAAACGGTCACGAGCATAGACGACGAAGAAC	85
KPC2-H13.3_Mask-65	GTATCTGGTGGTCTATGGCACACGCTAAAAGGAAATTAGAAGTCGTCTTGTATCTGGTGGTCTATGGCATAGACGACGAAGAAC	84
KPC2-H13.3_Mask-69	GTATCTGGTGGTCTATGGCGCCGAAAAAATTCACTATTACACAGATACGCACCAGATTTACAGCATAGACGACGAAGAAC	80
KPC2-H13.3_Mask-74	GTATCTGGTGGTCTATGGCATAGACGACGAAGAACACCATATACATCAGATACCCAGATACAGCATAGACGACGAAGAAC	80
KPC2-H13.3_Mask-76	GTATCTGGTGGTCTATGGCATAGACGACGAAGAACATTGCTCGTTTAAAAAAAAAAAATCTTACTCCGCATAGACGACGAAGAAC	85
KPC2-H13.3_Mask-94	GTATCTGGTGGTCTATGGCATAGACGACGAAGAACAACAAAAAGAGCGAACAAATCGGGGCTGGTGGGCATAGACGACGAAGAAC	85
KPC2-H13.3_Mask-108	GTATCTGGTGGTCTATGGCCAAAACAAAGAGTATAAACAGGGGGAGTGTATCTGGTGGTCTATGGCATAGACGACGAAGAAC	82
KPC2-H13.3_Mask-110	GTATCTGGTGGTCTATGGCGCAAAGGGACATATAACTCATAGTCGTCTGTATCTGGTGGTCTATGGCATAGACGACGAAGAAC	83
KPC2-H13.3_Mask-126	GTATCTGGTGGTCTATGGCGGCTTCTTCGAGTCCTTCCTTTTTTCCTTTTTTGTGTTTTTGTGCATAGACGACGAAGAAC	80
KPC2-H13.3_Mask-151	GTATCTGGTGGTCTATGGCGCAAAATGTCTCTTCGTTAGTATATTCATGTATCTGGTGGTCTATGGCATAGACGACGAAGAAC	83
KPC2-H13.3_Mask-163	GTATCTGGTGGTCTATGGCCCGCAAAGGAGTCTATTATGGATCGTTCGCTGTATCTGGTGGTCTATGGCATAGACGACGAAGAAC	85
KPC2-H13.3_Mask-201	GTATCTGGTGGTCTATGGCGCAGTGTTCGATGAGAGTCATTCAAAGCATGTATCTGGTGGTCTATGGCATAGACGACGAAGAAC	84
KPC2-H13.3_Mask-212	GTATCTGGTGGTCTATGGCATAGACGACGAAGAACACTTCCTTACTTTTTTTCCTTGGACGCGGCATAGACGACGAAGAAC	81
KPC2-H13.3_Mask-294	GTATCTGGTGGTCTATGGCCAAGGGAGGAAGATGAAGATCATAATAAATGTGTATCTGGTGGTCTATGGCATAGACGACGAAGAAC	86
NDM1-H14.2_Mask-04	GTATCTGGTGGTCTATGGCATAGACGACGAAGAACAATGAAACCCAATCCCTCTCCCCTTCGCCGCATAGACGACGAAGAAC	82
NDM1-H14.2_Mask-08	GTATCTGGTGGTCTATGGCCCCGGAACCTTCGTCGATAGTTCTTCTCAACAGATACATTCCGGCATAGACGACGAAGAAC	80
NDM1-H14.2_Mask-12	GTATCTGGTGGTCTATGGCCCCGTACCTATGACGCGCTTTTCTTTTTCTTATCTTTCCTTGTGCATAGACGACGAAGAAC	82
NDM1-H14.2_Mask-16	GTATCTGGTGGTCTATGGCCAACGAGAATCGGCAATCCTTAAACTGTGTATCTGGTGGTCTATGGCATAGACGACGAAGAAC	76
NDM1-H14.2_Mask-17	GTATCTGGTGGTCTATGGCATAGACGACGAAGAACAACCTTGAATCCAATTATCCCCAGCATAGACGACGAAGAAC	80
NDM1-H14.2_Mask-19	GTATCTGGTGGTCTATGGCCAAAATCCATCAATCCCGTTTTCATGTGCTCCGCTTACTCTTCGCATAGACGACGAAGAAC	78
NDM1-H14.2_Mask-22	GTATCTGGTGGTCTATGGCATAGACGACGAAGAACAGACCACTTATTTAATCCCACCCAGGCATAGACGACGAAGAAC	80
NDM1-H14.2_Mask-25	GTATCTGGTGGTCTATGGCCAGACTACTTTCAAAAACCAGACCATTTCATTTTAGTAAATCCGCATAGACGACGAAGAAC	80
NDM1-H14.2_Mask-29	GTATCTGGTGGTCTATGGCCAACAAATACAATTAACATGAAGCCGCCCTGTTTTTTCCTTCCGCATAGACGACGAAGAAC	80
NDM1-H14.2_Mask-34	GTATCTGGTGGTCTATGGCCAAGAATCCATCATATCTCCAATCCCAAGCTTTTATTTACTCAGCATAGACGACGAAGAAC	80
NDM1-H14.2_Mask-35	GTATCTGGTGGTCTATGGCCACAACATGAATCCGTTTCTAATTCCTTTTACCTTTTCTCTCAGCATAGACGACGAAGAAC	80
NDM1-H14.2_Mask-38	GTATCTGGTGGTCTATGGCAAGGGCGTTCTTCATCGGTTCTTCTCACATTTTCCTCCCACCAGCATAGACGACGAAGAAC	80
NDM1-H14.2_Mask-39	GTATCTGGTGGTCTATGGCGGAGGTCTAAAAAAAAAAAAACGCAATCCTATCTCATAATCCGCATAGACGACGAAGAAC	79
NDM1-H14.2_Mask-41	GTATCTGGTGGTCTATGGCGCTAGTTCTTCGCATCATTCCGCTTCCTTTCTTCTCCTTCTCCGCATAGACGACGAAGAAC	80

NDM1-H14.2_Mask-42	GTATCTGGTGGTCTATGGCATAGACGACGAAGAACACTACCCGCAAATTTTCACTGTAATCCGCATAGACGACGAAGAAC	80
NDM1-H14.2_Mask-43	GTATCTGGTGGTCTATGGCCGCTATCCGCAATCTGTCTCTTTTTCTTTATTCTTTTACTCACCGCATAGACGACGAAGAAC	80
NDM1-H14.2_Mask-44	GTATCTGGTGGTCTATGGCATAGACGACGAAGAACATGAATGATCAACTAAGGGATAGCAATCTCGGCATAGACGACGAAGAAC	84
NDM1-H14.2_Mask-49	GTATCTGGTGGTCTATGGGCCCGGACTAAAAATCAAAATCATATCGACCGCAATCCCTTTCCGCATAGACGACGAAGAAC	80
NDM1-H14.2_Mask-50	GTATCTGGTGGTCTATGGCGCATCCCTATCCCGTCTCTTTTTGTATTTTTATTTTTGTTTCCGCATAGACGACGAAGAAC	80
NDM1-H14.2_Mask-43-F	CCGCTATCCGCAATCTGTCTCTTTTCTTTATTCTTTTACTCACCGCATAGACGACGAAGAAC	62
NDM1-H14.2_Mask-43-R	GTATCTGGTGGTCTATGGCCGCTATCCGCAATCTGTCTCTTTTCTTTATTCTTTTACTCACC	62
NDM1-H14.2_Mask-43-FR	CCGCTATCCGCAATCTGTCTCTTTTCTTTATTCTTTTACTCACC	44
NDM1_DSR4_01	GTATCTGGTGGTCTATGGCGCAGTGTTCGATGAGAGTCATTCAAAGCATGTATCTGGTGGTCTATGGCATAGACGACGAAGAAC	84
NDM1_DSR4_04	GTATCTGGTGGTCTATGGCACACGCTAAAAGGAAATTAGAAGTCGTCTTGTATCTGGTGGTCTATGGCATAGACGACGAAGAAC	84
NDM1_DSR4_16	GTATCTGGTGGTCTATGGCCGCATAATCGTTTCGTTCTCTCTTTTCTTTCTTTTCTCCCACCGCATAGACGACGAAGAAC	80
NDM1_DSR4_09	GTATCTGGTGGTCTATGGGCACGCAACATTTTCGTCGTTACATCTCGTTGTATCTGGTGGTCTATGGCATAGACGACGAAGAAC	84
NDM1_DSR4_06	GTATCTGGTGGTCTATGGCGAGAAAAGTTCTGTCGTCTAAAAAGTTCTTGTCGTAATTCGGGGCATAGACGACGAAGAAC	80
NDM1_DSR4_74	GTATCTGGTGGTCTATGGCGGCTTCTTCGAGTCCTTCCTTTTTTCCTTTTTTGTGTTTTTGTGCATAGACGACGAAGAAC	80
Con1	GGGAATTCGAGCTCGGTACCGGCTGCTTTGCTGCAGATTTGTGGGTGGGTGGGTGGTGATCTGCAGGCATGCAAGCTTGG	80
ConSc	TTATAACCGGTTATACTGGTTGTTCCTAGATGCTTCATGATGCCCAACCTTTGTCCCTGGCCCTGACATGTTTCGACTAA	80

7.5. Immobilization Matrices and Purification Beads

Immobilization matrices were used for target immobilization throughout selection, DNA purification, aptamer characterization and for the development of an aptamer-based sandwich LFD. Immobilization matrices used in this work can be found in **Table 15**.

Table 15: Immobilization matrices used in this work.

Matrix	Specifications	Provider
Beads	Dynabeads™ M-280 Tosylactivated	Thermo Fisher Scientific, Waltham, USA
	Dynabeads™ His-Tag Isolation and Pulldown	
	sbeadex particle suspension (Agowa Beads)	LGC Limited, Teddington, UK
MTPs	Pierce™ Streptavidin Coated High-Capacity Plates, Clear, 96-Well	Thermo Fisher Scientific, Waltham, USA
	Greiner Bio-One FLUOTRAC™ High Binding 96-well Polystyrene Microplates	
	Pierce™ Nickel Coated Plates, Black, 96-Well	
Sensor chip	SPR Sensor Chips HC200M	GE healthcare, Chicago, USA
LFD	Unisart® CN140 Nitrocellulose Membrane	Sartorius AG, Göttingen, Germany
	300 * 60 mm , SMA 31.25 backing bard	Kinbio Tech.Co., Ltd, Shanghai, China
	300 * 24 mm , Polyester 6613 sample pad	Ahlstrom-Munksjö Oyj, Hellsinki, Finland
	300 * 17 mm , 222 absorbant pad	
	MK001, Hangzhou D2 test cassette	Hangzhou Jinyee Biotech. Co., Ltd, Hangzhou, China

7.6. Kits

Kits were used for DNA purifications, protein quantifications, activity assessment and library preparation as well as sequencing. Kits used in this work can be found in **Table 16**.

Table 16: Commercial kits used for DNA purification, protein quantification, activity assessment and NGS.

Kit	Usage	Provider
MinElute PCR Purification Kit	DNA purification	Qiagen N.V., Venlo, Netherlands
Micro BCA™ Protein-Assay-Kit	Protein quantification	Thermo Fisher Scientific, Waltham, USA
TruSeq DNA Nano	Library preparation	Illumina, Inc., San Diego, USA
Mini Seq Mid Output Kit	Sequencing	
RAPIDEC® CARBA NP	Carbapenemases activity assessment	bioMérieux, Marcy-l'Étoile, France

7.7. Devices, Consumables, and Software

Table 17: Devices used in this work.

Device	Type	Provider
Robotic workstation	KingFisher™ Duo Prime	Thermo Fisher Scientific, Waltham, USA
Robotic workstation	Biosprint 15	Qiagen N.V., Venlo, Netherlands
PCR cycler	Biometra TAdvanced	Analytik Jena GmbH, Jena, Germany
	Biometra TRIO	
UV/Vis Spectrometer	NanoPhotometer® NP80	Implen GmbH, München, Germany
Fluorometer	Qubit 4	Thermo Fisher Scientific, Waltham, USA
Gel documentation device with UV transilluminator	Biometra BioDoc Analyze	Analytik Jena GmbH, Jena, Germany
Agarose gel chambers	Model B1 and B1A EasyCast™ Mini Gel Electrophoresis System	Thermo Fisher Scientific, Waltham, USA
PAGE gel system	Miniprotean ® 3 Cell System	Bio-Rad Laboratories, Inc., Hercules, USA
SpeedVac vacuum concentrator	Pellet drying after DNA precipitation	Thermo Fisher Scientific, Waltham, USA
Thermomixer	Thermomixer C	Eppendorf, Hamburg, Germany
Centrifuge	5427R	
	miniSpin	
Sequencing system	MiniSeq™	Illumina, Inc., San Diego, USA
Microplate multimode reader	Mithras² LB 943	Berthold Technologies GmbH & Co. KG, Bad Wildbad, Germany
	EnVision® 2105	PerkinElmer Inc., Waltham, USA
SPR device	Biacore™ T200 facility	GE healthcare Bio Sciences AB, Uppsala, Sweden
MST device	Monolith NT.115	NanoTemper Technologies, Munich, Germany
Dispensing workstation	BioDot XYZ 3050	BioDot Inc, Irvine, USA
LFD analysis card	gold color card	Assure Tech.(Hangzhou) Co., Ltd, Hangzhou, China

Consumables for standard laboratory use were purchased from Sarstedt AG & Co. KG, Nümbrecht, Germany and Biozym Scientific GmbH, Hessisch Oldendorf, Germany. Consumables used for the robotic workstations were purchased from Thermo Fisher Scientific, Waltham, USA, and MST capillaries were purchased from NanoTemper Technologies, Munich, Germany. Consumable used for NGS were purchased from Illumina, Inc., San Diego, USA.

Table 18: Software used in this work.

Software	Usage	Provider / URL
Random DNA Sequence Generator	Primer design	Morris Maduro, University of California, Riverside, USA, http://www.faculty.ucr.edu/mmaduro/random.htm
OligoAnalyzer™ Tool	Primer evaluation	Integrated DNA Technologies, Inc., Coralville, USA
BioDoc Analyze software (version 2.2)	Gel documentation	Analytik Jena GmbH, Jena, Germany
Sequence Manipulation Suite – Shuffle DNA	Design of scramble control	Paul Stothard, University of Alberta, Canada, https://www.bioinformatics.org/sms2 /shuffle_dna.html
AptaAnalyzer™-SELEX	NGS data evaluation	AptaIT GmbH, Planegg, Germany
MO.Control software	MST measurement	NanoTemper Technologies, Munich, Germany
MO.Affinity Analysis Software	Evaluation of MST measurments	
Biacore™ T200 control software	SPR measurements	GE healthcare Bio Sciences AB, Uppsala, Sweden
BIAevaluation software (version 3.1)	Evaluation of SPR-Experiments	
EnVision Manager 1.14.3049.1193	Microplate multimode reader measurements	PerkinElmer Inc., Waltham, USA
MikroWin 2000		Berthold Technologies GmbH & Co. KG, Bad Wildbad, Germany
NanoPhotometer® software	UV/Vis measurements	Implen GmbH, München, Germany
Expasy	Compute pI, molecular weight, and extinction coefficients	SIB Swiss Institute of Bioinformatics, https://www.expasy.org/
ChemSketch (freeware)	Draw chemical structures	Advanced Chemistry Development, inc., Toronto, Canada
Origin® 2019	Create figures	OriginLab Corporation, Northampton, USA
CorelDRAW® 2019		Cascade Parent Ltd., Ottawa, Canada
PyMOL version 2.1	Protein structure visualization	DeLano Scientific LLC, Schrödinger Inc., New York City, USA

8. Methods

8.1. Target and Nucleic Acid Preparation

8.1.1. RAPIDEC® CARBA NP test

The RAPIDC® CARBA NP test exploits the pH shift upon hydrolysis of the carbapenemase substrate impenem. The test consists of five chambers (a – e). Chamber a contains phenol red as a pH indicator. Chamber b contains a turbidity control and chamber c contains a lysis buffer. Chamber d is the control without impenem, and chamber e contains the substrate impenem as well as zinc which is required for the activity of metallo-dependent carbapenemases. Solutions from chambers a and c are added to chambers d and e for activity assessment. In this work, RAPIDEC® CARBA NP test was used for activity testing of N-terminally His-tagged carbapenemases His-KPC-2, His-NDM-1 and His-OXA-23. The test was conducted following the manufacturer's instructions [181] with the exception that instead of a picked bacterial colony, 1 µg of purified carbapenemase solution or 0.6 - 0.9 µg of carbapenemases coupled to Dynabeads™ M-280 Tosylactivated were added to chamber c. Incubation was performed at 37 °C for 80 min. Activity was assessed by a color change from red to orange or yellow.

8.1.2. Immobilization of Proteins on Magnetic Beads

The immobilization of target and negative selection target proteins on magnetic beads throughout SELEX facilitates separation of bound from unbound sequences without the need for intermediate steps like centrifugation or filtration [182]. In this work, His-tagged carbapenemases or unrelated His-tagged proteins were immobilized on Dynabeads™ M-280 Tosylactivated. His-KPC-2 was also immobilized on Dynabeads™ His-Tag Isolation and Pulldown.

Immobilization on Dynabeads™ M-280 Tosylactivated

Dynabeads™ M-280 Tosylactivated are magnetic beads that carry reactive p-toluene-sulfonyl (Tosyl) groups on their surfaces. Tosylgroups react with primary amines or sulfhydryl groups and form a covalent linkage [183].

a. Immobilization in Buffer B

Carbapenemases His-KPC-2, His-NDM-1 and His-OXA-23 as well as C-terminally His-tagged proteins mPD1-His and CFHR1-His were immobilized on Dynabeads™ M-280 Tosyl-activated. Proteins were coupled in a ratio of 10 µg protein to 1 mg beads. Coupling reactions were prepared in a total volume of 160 µl in Buffer B. Prior to addition of the beads, 10 µl were set

aside for quantification by the BCA method. Upon addition of the beads, the remaining coupling reaction was incubated at 37°C overnight using a rotator. The next day, the supernatant was removed, 10 µl of the supernatant were set aside for quantification, beads were washed thrice and stored in 1x PBS-T in the volume that was equivalent to the volume of beads used in the beginning.

b. Immobilization in Buffer C

As the first coupling attempt of His-OXA-23 in Buffer B failed, coupling was tried again in Buffer C. Since the 3 M ammonium sulfate contained in Buffer C interferes with the BCA measurement for protein quantification, the A_{280} methods was used for subsequent protein quantification. Therefore, higher concentrations of His-OXA-23 had to be used in the coupling reaction to make sure protein concentrations prior to and after coupling were quantifiable. Here, 20 µg His-OXA-23 per mg beads were used in a total volume of 160 µl. Further coupling steps were preceded as described for immobilization in Buffer B.

Immobilization on Dynabeads™ His-Tag Isolation and Pulldown

Immobilization on Dynabeads™ His-Tag Isolation and Pulldown is based on the non-covalent interaction of polyhistidine with cobalt-based IMAC chemistry on the beads' surface [184]. In this work His-KPC-2 was coupled to Dynabeads™ His-Tag Isolation and Pulldown throughout SR11.2_ Co^{2+}-NTA - 14.2_ Co^{2+}-NTA. Here, His-KPC-2 was coupled in a ratio of 10 µg protein to 250 mg beads. Coupling reactions were prepared in a total volume of 87 µl in 1x Binding/Wash buffer. Prior to addition of the beads, 10 µl were set aside for quantification by the BCA method. Upon addition of the beads, the remaining coupling reaction was incubated for 10 min on a roller at room temperature. Supernatant was removed and 10 µl were set aside for quantification. Beads were washed thrice with 1x Binding/Wash buffer and stored in 3.2x the volume of beads used in the beginning in 1x Pulldown buffer.

8.1.3. Quantification of Coupling Efficiency

BCA Method

Protein concentrations were determined in the supernatant prior to and after coupling to different magnetic beads by the BCA method. Bichinonic acid (BCA), as its water-soluble sodium salt, is a reagent specific for Cu^{+}. Proteins that are incubated with an alkaline solution containing Cu^{2+} ions can form complexes with the copper ions which are then reduced to Cu^{+}. Two BCA molecules form a purple-colored complex with one Cu^{+} ion that absorbs light at a wavelength of 562 nm [185]. As the amount of reduced Cu^{2+} is proportional to the amount of protein in the solution, a calibration series can be used to quantify a known protein in a solution.

In this work, BCA assay was performed using the Micro BCA™ Protein assay kit. A calibration series was prepared from stock solutions of the proteins that was to be quantified with six concentrations ranging from 0 - 100 ng. Micro BCA™ Protein assay reagents were prepared as follows: 25 parts of Micro reagent A were mixed with 24 parts of Micro reagent B and 1 part of Micro reagent C. 10 µl of the Micro BCA™ Protein assay reagent mixture was added to 10 µl of protein solution prior to beads coupling, supernatant after beads coupling as well as to each calibration solution. The reactions were incubated for 1 h at 60°C and 350 rpm. Subsequently absorption was measured at 562 nm using IMPLEN NP80 Nanophotometer®. A calibration curve as well as protein concentrations in ng/µl prior to and after beads coupling were calculated by NanoPhotometer® Software.

A_{280} Method

The A_{280} method makes use of the intrinsic light absorbance by the amino acids tryptophan and tyrosine, as well as by disulfide bonded cystine residues. The method is less sensitive than the BCA method. However, pretreatment of the samples is not required. According to the amount of absorbing amino acids, a molecular extinction coefficient (E_{molar}) can be calculated for native proteins measured at 280 nm in water [186].

$$E_{molar}\,[M^{-1}cm^{-1}] = n(Trp) * 5500\,M^{-1}cm^{-1} + n(Tyr) * 1490\ M^{-1}cm^{-1} + n(Cystine) * 125\ M^{-1}cm^{-1} \quad (3)$$

With E_{molar} and the molecular weight of a specific protein, the theoretical absorption of a 1 mg/ml solution at 280 nm ($A_{0.1\%}$) can be calculated.

$$A_{0.1\%}\left[\frac{l}{g}\right] = \frac{E_{molar}\,[M^{-1}cm^{-1}] * L\,[cm]}{molecular\ weight\,[g * mol^{-1}]}, with\ L = path\ length \quad (4)$$

Assuming a path length of 1 cm, the protein concentration can then be calculated as

$$Concentration\ of\ protein\ sample\ \left[\frac{g}{l}\right] = \frac{measured\ A_{280}}{A_{0.1\%}[l * g^{-1}]}. \quad (5)$$

For quantification of His-OXA-23, its molecular weight , E_{molar} as well as $A_{0.1\%}$ were calculated as 31801.71 g/mol, 43430 M^{-1} cm^{-1} and 1.370 l * g^{-1} using the ExPASy tool ProtParam [187]. Calculation was carried out under the assumption that all cysteine residues are reduced. Absorption was measured at 280 nm using IMPLEN NP80 Nanophotometer®. Buffer C was used for blank measurement. Protein concentrations in ng/µl prior to and after beads coupling were calculated by NanoPhotometer® Software.

Calculation of Coupling Efficiency

The concentration of protein bound to the beads as well as the coupling efficiency were further calculated independent of the protein quantification strategy as follows:

$$\Delta\, Concentration\, [\frac{ng}{\mu l}] = concentration\ prior\ to\ coupling - concentration\ after\ coupling \quad (6)$$

$$Concentration\, \left[\frac{\mu g\ protein}{\mu l\ beads}\right] = \frac{\Delta\ conc. * \mu l\ reaction\ volume * 1000}{\mu l\ beads} \quad (7)$$

$$Concentration\, \left[\frac{pmol\ protein}{\mu l\ beads}\right] = Concentration\, \left[\frac{\mu g\ protein}{\mu l\ beads}\right] * \frac{1}{MW(protein)[kDa]} * 1000 \quad (8)$$

$$Coupling\ efficiency = \left(100 - \frac{concentration\ after\ coupling}{concentration\ prior\ to\ coupling}\right) * 100 \quad (9)$$

8.1.4. Enzyme-linked Immunosorbent Assay (ELISA)

ELISA exploits the specific binding of an antibody to its antigen. For ELISA, enzyme-labeled antibodies or antigens are used to generate a detectable signal [188]. Horse radish peroxidase (HRP) is a widely used enzyme label in immunoassays. It catalyzes the following general redox reaction,

$$SubH_2\ (red) + H_2O_2 \rightarrow Sub\ (Ox) + 2\ H_2O \quad (10)$$

with Sub = substrate molecule. A possible chromogenic substrate for HRP is 3,3',5,5'-tetra-methylbenzidine (TMB). Its reaction with H_2O_2 in the presence of HRP results in a colored product. After stopping the reaction with H_2SO_4, absorbance can be measured at 450 nm [189]. In this work, first immobilizations of His-NDM-1 and His-KPC-2 on Dynabeads™ M-280 Tosylactivated were further verified by ELISA. Here, a HRP-labeled mouse-anti-Penta-His antibody was used for detection of the His-tagged proteins. 0.27 mg of either uncoupled beads, beads theoretically coupled to 0.86 pmol His-NDM-1 or beads theoretically coupled to 2.8 pmol His-KPC-2 were washed thrice with 800 µl PBS-T, using a robotic workstation. Beads were transferred into a new strip and incubated with 100 µl of the HRP-labeled anti-His antibody, diluted 1:600 in 1x ROTI®Block solution for 30 min. Subsequently, beads were washed thrice with PBS-T and transferred to 100 µl of 1-Step Ultra TMB. After approximately 5 min of color reaction, the reaction was stopped with 50 µl 2 M H_2SO_4, strips were placed on a magnet and

supernatants were transferred into a clear 96 well MTP. Absorbance was measured at 450 nm using the Mithras² LB 943 Monochromator Multimode Microplate Reader.

8.1.5. Nucleic Acid Library Design

For the design of the primer regions, random 18 nt sequences were generated using the Maduro Labs Random DNA Sequence Generator software. The size of DNA was set to 18 bp and the GC content (between 0 and 1) to 0.5. Resulting sequences were analyzed using IDT OligoAnalyzer™ software. Here, target type was set to DNA, oligo concentration to 1 µM, dNTP concentration to 0.4 µM, Na^+ concentration to 0 mM and Mg^{2+} concentration to 4 mM to match PCR1 conditions (see also 8.3.2).

8.2. Systematic Evolution of Ligands by Exponential Enrichment (SELEX)

8.2.1. General SELEX Procedure

The theoretical background of the SELEX procedure was already discussed in section 3.6.1. In this work, aptamer selection was carried out semi automatically as previously described [62,70]. Prior to every selection round, ssDNA was diluted to its final concentration in aptamer binding buffer. The binding buffer for selections against His-KPC-2 and His-NDM-1 (SR1.1 - 14.1) was BP-TB. For doped SELEX against His-NDM-1, BSA was excluded from the buffer formulation resulting in binding buffer BP-T. To achieve optimal folding, diluted ssDNA was activated by heating to 92 °C for 3 min followed by slowly cooling down to room temperature for approximately 30 min. For negative selections against beads only, ssDNA was incubated with Dynabeads™ M-280 Tosylactivated or Dynabeads™ His-Tag Isolation and Pulldown for 20 min in binding buffer. Negative selections against other His-tagged carbapenemases or unrelated His-tagged proteins were performed for either 20 min or 1 h. Subsequently, ssDNA was incubated with the target molecule and different numbers of washing steps were performed. For all selections against His-KPC-2 and His-NDM-1, except for doped SELEX against His-NDM-1, target incubation was performed for 1 h at room temperature. Washing was performed 2x in 1000 µl and 1 - 2x in 400 µl binding buffer for SR1 and 2. For consecutive SRs, washing was performed 2x in 500 µl and 3 - 9x in 200 µl binding buffer. For exact numbers and duration of washing steps for each SR refer to **Table 19 - 25**. Elution was performed by incubation (target- and negative selection target-coated beads as well as uncoupled beads used for negative selection against beads only) with 8 M urea in binding buffer at 65 °C and 900 rpm. Supernatants were transferred to another tube and beads were washed with the same amount of ddH_2O. Subsequently, eluted ssDNA as well as ssDNA from the last washing step, was precipitated by addition of 1.125x its volume of isopropyl alcohol,

0.15x its volume 3 M $C_2H_3NaO_2$ and 1 µl glycogen and incubation at -20 °C overnight. Precipitation reactions were centrifuged at 15,700x g for 1 h at 4 °C. Supernatant was removed and washed twice with 80% EtOH for 10 min at 15,700x g at 4 °C. Supernatants were removed and pellets were dried for 10 min using a SpeedVac vacuum concentrator at room temperature. Finally, dried pellets were dissolved in 20 µl ddH_2O and used for PCR.

8.2.2. Negative Selections and different Approaches to Prevent His-tag binding

For first selections against His-KPC-2 and His-NDM-1, from SR1 on, negative selections were performed against varying amounts of uncoupled Dynabeads™ M-280 Tosylactivated. From SR5.1 - 11.1, negative selections were performed against His-NDM-1 for selection against His-KPC-2 and against His-KPC-2 for selection against His-NDM-1. From SR8.1 - 11.1 negative selections were also performed against His-OXA-23. All negative selections were performed for 20 min. From SR12.1 - 14.1 negative selections against other His-tagged carbapenemases were stopped and only negative selections against uncoupled Dynabeads™ M-280 Tosylactivated were continued. Exact numbers of negative selections as well as amounts of negative selection targets can be found in **Table 19** and **Table 20**. After SR14.1, for both selections against His-KPC-2 and His-NDM-1, His-tag-binding sequences were strongly enriched. Thus, different strategies were tested to prevent enrichment of His-tag-binding sequences using the model target His-KPC-2. For all three approaches, negative selections were performed against uncoupled beads as well as unrelated His-tagged protein mPD1-His immobilized on Dynabeads™ M-280 Tosylactivated. Furthermore, selection of His-tag-binding sequences was to be prevented by

1. Preincubation of the His-KPC-2 coated Dynabeads™ M-280 Tosylactivated with a 10-fold excess of the His-tag-binding aptamer KPC2-H14-01(01)-FR (masking approach)

2. Competitive elution of His-tag-binding sequences after target incubation by incubation with a 10-fold excess of the His-tag-binding aptamer KPC2-H14-01(01)-FR

3. Coupling of His-KPC-2, via its N-terminal His-tag to Dynabeads™ His-Tag Isolation and Pulldown instead of Dynabeads™ M-280 Tosylactivated.

Here, the ssDNA pool from SR11.1 was chosen for restart of the selections. The masking approach failed after two rounds of selection and was restarted with ssDNA from SR10.1. Selection was carried out as described for the initial selections with the exception that for the masking and competitive elution approach not only the ssDNA pool but also masking / elution aptamer KPC2-H14-01(01)-FR, in a 10-fold excess over His-KPC-2, was diluted in binding buffer and activated. For the masking approach, target-coated beads were incubated with

10-fold excess of the masking aptamer prior to incubation with the ssDNA pool. For the competitive elution approach incubation with 10x excess of KPC2-H14-01(01)-FR was conducted after target incubation and washing steps. For the immobilization via the N-terminal His-tag, selection was carried out against His-KPC-2 coupled to Dynabeads™ His-Tag Isolation and Pulldown. Negative selections against beads only were conducted against Dynabeads™ His-Tag Isolation and Pulldown while negative selections against mPD1-His were performed with mPD1-His coupled to Dynabeads™ M-280 Tosylactivated. For number of negative selections as well as amounts of negative selection targets and masking / elution aptamer refer to **Table 21 - 24**.

The masking approach was later chosen for the selection of an NDM-1 specific aptamer. Here, ssDNA from SR10.1 (selected against His-NDM-1) was used to restart selection. Negative selections were performed either against mPD1-His or against mPD1-His and CFHR1-His immobilized on Dynabeads™ M-280 Tosylactivated. The masking approach was performed as described above.

8.2.3. Doped SELEX against His-NDM-1

To select for more affine binders to His-NDM-1, a doped library was designed originating from NDM1-H14.2_Mask-43. The primer binding regions were kept constant, while each nucleotide within the 44 nt random region was replaced by each of the three other nucleotides in 5 - 8% of sequences. The doped library was used for four rounds of selection with varying ssDNA to beads ratios (see **Table 25**). Selection was carried out as described for the masking approach with the exception that target incubation was performed for 30 min for doped selection round (DSR) 1.1 and 2.1, 10 min for DSR3.1 and 20 min for DSR4.1. The numbers of negative selections as well as amounts of negative selection targets and masking aptamer are specified in **Table 25**.

Table 19 - 25 list the parameters of different selections against His-KPC-2 and His-NDM-1.

Table 19: Parameters of SELEX for His-KPC-2: SR1.1 - 14.1

SR	ssDNA [pmol]	His-KPC-2-coated beads [pmol]	His-KPC-2-coated beads [µl]	Beads only [µl]	His-NDM-1-coated beads [pmol]	His-OXA-23-coated beads [pmol]	Washing steps [min]
1.1	1000	100	10.1	1x 10.1	-	-	3x 3
2.1	200	40	4	2x 4			4x 3
1.2	1000	100	11.1	1x 11.1			3x 3
2.2	200	40	4.4	2x 4.4			4x 3
3.1	120	40	4.4	2x 4.4, 1x 8.8			4x 3, 1x 10
4.1	80	40	4.4	2x 4.4, 1x 8.8			5x 3, 1x 10, 1x 20
4.1_Control	80	-	4.4	2x 4.4, 1x 8.8, selection: 4.4			5x 3, 1x 10, 1x 20
5.1	80	40	4.4	2x 4.4, 1x 8.8	40		5x 3, 1x 10, 1x 20, 1x 30
5.1_Control	80	-	4.4	2x 4.4, 1x 8.8, selection: 4.4	40		5x 3, 1x 10, 1x 20, 1x 30
6.1	80	40	6	1x 6 + 1x 12	40		6x 3, 1x 10, 1x 20, 1x 30
7.1	80	40	6	1x 6 + 1x 12	40		6x 3, 1x 10, 1x 20, 1x 30
7.1_Control	80	-	6	1x 6 + 1x 12, selection: 6	40		6x 3, 1x 10, 1x 20, 1x 30
8.1	80	40	10.8	1x 5.1 + 1x 10.2 + 1x 15.3	40	40	8x 3, 1x 10, 1x 20, 1x 30
9.1	80	40	8.7	1x 8.7 + 1x 17.4+ 1x 26.1	40	40	8x 3, 1x 10, 1x 20, 1x 30
9.1_Control	80	-	-	1x 8.7 + 1x 17.4+ 1x 26.1, selection: 8.7	40	40	8x 3, 1x 10, 1x 20, 1x 30
10.1	80	40	8.7	1x 8.7 + 1x 17.4+ 1x 26.1	80	80	8x 3, 1x 10, 1x 20, 1x 30
11.1	80	40	2.8	1x 2.8 + 1x 5.6 + 1x 8.4	80	80	8x 3, 1x 10, 1x 20, 1x 30
11.1_Control	80	40	-	1x 2.8 + 1x 5.6 + 1x 8.4, selection: 2.8	80	80	8x 3, 1x 10, 1x 20, 1x 30
12.1	80	40	3.7	1x 11.1 + 1x 7.4 + 1x 3.7	-	-	8x 3, 1x 10, 1x 20, 1x 30
12.1_Control	80	40	-	1x 11.1 + 1x 7.4 + 1x 3.7, selection: 3.7	-	-	8x 3, 1x 10, 1x 20, 1x 30
13.1	80	40	4.1	1x 12.3 + 1x 8.2 + 1x 4.1	-	-	8x 3, 1x 10, 1x 20, 1x 30
14.1	80	40	4.1	1x 12.3 + 1x 8.2 + 1x 4.1	-	-	8x 3, 1x 10, 1x 20, 1x 30
14.1_Control	80	40	-	1x 12.3 + 1x 8.2 + 1x 4.1, selection: 4.1	-	-	8x 3, 1x 10, 1x 20, 1x 30

Table 20: Parameters of SELEX for His-NDM-1: SR1.1 - 14.1

SR	ssDNA [pmol]	His-NDM-1-coated beads [pmol]	His-NDM-1-coated beads [µl]	Beads only [µl]	His-KPC-2-coated beads [pmol]	His-OXA-23-coated beads [pmol]	Washing steps [min]
1.1	1000	100	13.2	1x 13.2	-	-	3x 3
1.2	1000	100	13.2	1x 13.2			3x 3
2.1	200	40	5.6	2x 5.6			4x 3
3.1	200	40	5.3	2x 5.3 + 1x 10.6			4x 3, 1x 10
3.1_Control	200	-	-	2x 5.3 + 1x 10.6, selection: 5.3			4x 3, 1x 10
4.1	120	40	5.3	2x 5.3 + 1x 10.6			5x 3, 1x 10, 1x 20
5.1	120	40	3.8	1x 3.8 + 1x 7.6	40		5x 3, 1x 10, 1x 20
5.1_Control	120	-	-	1x 3.8 + 1x 7.6, selection: 3.8	40		5x 3, 1x 10, 1x 20
6.1	120	40	3.8	1x 3.8 + 1x 7.6	40		5x 3, 1x 10, 1x 20, 1x 30
6.1_Control	120	-	-	1x 3.8 + 1x 7.6, selection: 3.8	40		5x 3, 1x 10, 1x 20, 1x 30
7.1	120	40	3.8	1x 3.8 + 1x 7.6	40		6x 3, 1x 10, 1x 20, 1x 30
6.2	120	40	5.1	1x 5.1 + 1x 10.2	40		6x 3, 1x 10, 1x 20, 1x 30
6.2_Control	120	-	-	1x 5.1 + 1x 10.2, selection: 5.3	40		6x 3, 1x 10, 1x 20, 1x 30
7.2	120	40	5.1	1x 5.1 + 1x 10.2	40		8x 3, 1x 10, 1x 20, 1x 30
7.2_Control	120	-	-	1x 5.1 + 1x 10.2, selection: 5.3	40		8x 3, 1x 10, 1x 20, 1x 30
8.1	80	40	5.1	1x 5.1 + 1x 10.2 + 1x 15.3	40	40	8x 3, 1x 10, 1x 20, 1x 30
8.1_Control	80	-	-	1x 5.1 + 1x 10.2 + 1x 15.3, selection: 5.3	40	40	8x 3, 1x 10, 1x 20, 1x 30
9.1	80	40	3.4	1x 3.4 + 1x 6.8 + 1x 10.2	40	40	8x 3, 1x 10, 1x 20, 1x 30
10.1	80	40	8.5	1x 8.5 + 1x 17 + 1x 25.5	80	80	8x 3, 1x 10, 1x 20, 1x 30
10.1_Control	80	40	-	1x 8.5 + 1x 17 + 1x 25.5, selection: 8.5	80	80	8x 3, 1x 10, 1x 20, 1x 30
11.1	80	40	3.4	1x 3.4 + 1x 6.8 + 1x 10.2, selection: 3.4	80	80	8x 3, 1x 10, 1x 20, 1x 30
11.1_Control	80	40	-	1x 3.4 + 1x 6.8 + 1x 10.2, selection: 3.4	80	80	8x 3, 1x 10, 1x 20, 1x 30
12.1	80	40	3.8	1x 11.4 + 1x 7.6 + 1x 3.8	-	-	8x 3, 1x 10, 1x 20, 1x 30
12.1_Control	80	40	-	1x 11.4 + 1x 7.6 + 1x 3.8, selection: 3.8	-	-	8x 3, 1x 10, 1x 20, 1x 30
13.1	80	40	5.3	1x 15.3 + 1x 10.6 1x 5.3	-	-	8x 3, 1x 10, 1x 20, 1x 30
13.2	80	40	5.3	1x 15.3 + 1x 10.6 1x 5.3	-	-	8x 3, 1x 10, 1x 20, 1x 30
13.2_Control	80	40	-	1x 15.3 + 1x 10.6 1x 5.3, selection: 5.3	-	-	8x 3, 1x 10, 1x 20, 1x 30
14.1	80	40	5.3	1x 15.3 + 1x 10.6 1x 5.3	-	-	8x 3, 1x 10, 1x 20, 1x 30
14.1_Control	80	40	-	1x 15.3 + 1x 10.6 1x 5.3, selection: 5.3	-	-	8x 3, 1x 10, 1x 20, 1x 30

Table 21: Parameters of SELEX for His-KPC-2: SR11.2 - 13.3 with the His-tag masking.

SR	ssDNA [pmol]	His-KPC-2-coated beads [pmol]	His-KPC-2-coated beads [µl]	Beads only [µl]	mPD1-His-coated beads [pmol]	Masking aptamer [pmol]	Washing steps [min]
12.2_Mask	80	20	2.6	1x 5.2 + 1x 2.6	20	200	6x 3, 1x 10, 1x 20, 1x 30
13.2_Mask	80	20	2.6	1x 5.2 + 1x 2.6	20	200	6x 3, 1x 10, 1x 20, 1x 30
11.2_Mask	80	20	2.6	1x 5.2 + 1x 2.6	20	200	6x 3, 1x 10, 1x 20, 1x 30
12.3_Mask	80	20	2.6	1x 5.2 + 1x 2.6	20	200	6x 3, 1x 10, 1x 20, 1x 30
13.3_Mask	80	20	3.8	1x 5.2 + 1x 2.6	80	200	6x 3, 1x 10, 1x 20, 1x 30
13.3_Mask_Control	80	20	3.8	1x 5.2 + 1x 2.6, selection: 2.6	80	200	6x 3, 1x 10, 1x 20, 1x 30

Table 22: Parameters of SELEX for His-KPC-2: SR11.2 - 13.3 with competitive elution

SR	ssDNA [pmol]	His-KPC-2-coated beads [pmol]	His-KPC-2-coated beads [µl]	Beads only [µl]	mPD1-His-coated beads [pmol]	Elution apt. [pmol]	Washing steps [min]
12.2_Comp	80	20	2.6	1x 5.2 + 1x 2.6	20	200	6x 3, 1x 10, 1x 20, 1x 30
13.2_Comp	80	20	2.6	1x 5.2 + 1x 2.6	20	200	6x 3, 1x 10, 1x 20, 1x 30
14.2_Comp	80	20	2.6	1x 5.2 + 1x 2.6	20	200	6x 3, 1x 10, 1x 20, 1x 30
14.2_Comp_Control	80	20	2.6	1x 5.2 + 1x 2.6, selection: 2.6	20	200	6x 3, 1x 10, 1x 20, 1x 30

Table 23: Parameters of SELEX for KPC-2: SR11.2 - 13.3 with His-KPC-2 coupled to Dynabeads™ His-Tag Isolation and Pulldown (Co^{2+}-NTA)

SR	ssDNA [pmol]	His-KPC-2-coated beads [pmol]	His-KPC-2-coated beads [µl]	Beads only [µl]	mPD1-His-coated beads [pmol]	Washing steps [min]
12.2_Co^{2+}-NTA	80	20	1	1x 2 + 1x 1	20	6x 3, 1x 10, 1x 20, 1x 30
13.2_ Co^{2+}-NTA	80	20	1	1x 2 + 1x 1	20	6x 3, 1x 10, 1x 20, 1x 30
14.2_ Co^{2+}-NTA	80	20	1	1x 2 + 1x 1	20	6x 3, 1x 10, 1x 20, 1x 30

Table 24: Parameters of SELEX for His-NDM-1: SR 11.2 - 14.2 with the masking approach

SR	ssDNA [pmol]	His-NDM-1-coated beads [pmol]	His-NDM-1-coated beads [µl]	Beads only [µl]	mPD1-His-coated beads [pmol]	CFHR1-His-coated beads [pmol]	Masking aptamer [pmol]	Washing steps [min]
11.2_Mask	80	40	4	1x 8 + 1x 4	40	-	400	6x 3, 1x 10, 1x 20, 1x 30
12.2_Mask	80	40	4	1x 8 + 1x 4	80		400	6x 3, 1x 10, 1x 20, 1x 30
12.2_Mask_Control	80	-	-	1x 8 + 1x 4, selection: 4	80		400	6x 3, 1x 10, 1x 20, 1x 30
13.3_Mask	80	40	4	1x 8 + 1x 4	40	40	400	6x 3, 1x 10, 1x 20, 1x 30
14.2_Mask	80	20	2	1x 4 + 1x 2	40	40	200	6x 3, 1x 10, 1x 20, 1x 30
14.2_Mask_Control	80	20	-	1x 4 + 1x 2, selection: 2	40	40	200	6x 3, 1x 10, 1x 20, 1x 30

Table 25: Parameters of doped SELEX for His-NDM-1: DSR1.1 - 4.1, with the masking approach

DSR	ssDNA [pmol]	His-NDM-1-coated beads [pmol]	His-NDM-1-coated beads [µl]	Beads only [µl]	mPD1-His-coated beads [pmol]	Masking aptamer [pmol]	Washing steps [min]
1.1_Mask	1000	100	20	1x 20	1000	1000	3x 3
2.1_Mask	62.5	2.5	0.5	1x 0.5	2.5	79	3x3, 1x 30
3.1_Mask	100	2	0.4	1x 0.4	1x 2.5 +1x 5	79	2x3, 1x 10, 1x 30
4.1_Mask	85	1	0.6	1x 0.6 + 1x 1.2	2	79	2x3, 1x 15, 1x 30
4.1_Mask_Control	85	-	-	1x 0.6 + 1x 1.2, selection: 0.6	2	79	2x3, 1x 15, 1x 30

**For DSR 4.1 coupled and uncoupled beads were diluted 1:10 prior to use*

8.3. Polymerase Chain Reaction (PCR)

PCR was first reported in 1986 by Mullis *et al.* [190]. The reaction involves repetitive cycles of denaturation of a template DNA molecule, hybridization of two oligonucleotides (primers) to the different strands and DNA polymerase extension of the product they prime. To date, PCR has undergone some improvements like the use of thermostable polymerases such as taq polymerase from the extreme thermophile *Thermus aquaticus* rendering the addition of fresh polymerase after each amplification cycle unnecessary [191]. In this work, PCR was performed using a Biometra Trio cycler for 100 µl reactions and a Biometra TAdvanced for 200 µl reactions. The general PCR program is specified in **Table 26**. Two different polymerases were used throughout this work. The polymerases can be used interchangeably. While GoTaq® G2 Flexi DNA Polymerase was used for preliminary experiments, the work was continued using Taq DNA Polymerase convenient for cost reasons. For all PCRs, a no template control (NTC) was prepared in which the volume of template solution was replaced with the corresponding volume of ddH_2O. After each PCR amplification, PCR products were analyzed by gel electrophoresis.

Table 26: General PCR program

General PCR program		
Step	T [°C]	t [min]
1. Initial Denaturation	94	3.0
2. Denaturation	94	1.0
3. Annealing	55	0.5
4. Elongation	72	0.5
5. Repeat	Go to 2.	xx
6. Final elongation	72	3.0
7. Hold	4	∞

8.3.1. Gradient PCR for Library Design

Primers designed for the library used for selection (see **Table 14**, referred to as initial library) were tested for non-specific amplification either without template DNA or with 300 ng of library 42. Library 42 (see **Table 14**) contained different primer binding sites than the initial library. Non-specific amplification was tested at three different annealing temperatures. Master mixes were prepared as specified in **Table 27** and annealing was tested at 56 °C, 61 °C and 66 °C. Amplification was stopped and PCR products were analyzed by gel electrophoresis after 10, 20, 30 and 40 cycles. After library synthesis, optimal annealing was tested. Reactions were prepared as specified in **Table 27** with 300 ng of the library as template DNA. Annealing was tested at 55°C, 60°C and 65°C. A non-template control was prepared amplified at an

annealing temperature of 55°C. Amplification was stopped and PCR products were analyzed by gel electrophoresis after 10 and 20 PCR cycles. After 20 PCR cycles DNA was purified by Agowa purification and DNA concentration was measured using IMPLEN NP80 Nano-Photomer®.

Table 27: Preparation of the reaction mixtures for primer and library PCR.

Primer and library PCR	
1x [µl]	Reagent
20	5x Colorless GoTaq® Flexi Buffer
10	25 mM $MgCl_2$
4	10 mM dNTPs
1	100 µM Primer DSP-F44
1	100 µM Primer DSP-R44
1	5 U/µl GoTaq® G2 Flexi DNA Polymerase
0.5	1 U/µl Perfect Match PCR Enhancer
X	ddH_2O
100 - Y	Final master mix volume

Y = Volume of PCR product containing 300 ng DNA

X = Final volume - Y - sum (volume of other components)

8.3.2. Analytical PCR1

After the selection step, PCR was performed to analyze selection progress and to produce sufficient amounts of DNA for the next round of selection. Precipitated ssDNA from the selection step was amplified to compare PCR products of different fractions as well as in some cases PCR products from target selection with PCR products from control selections. Reactions of the first PCR (PCR1) were prepared as specified in **Table 28**. 20 µl of ssDNA from different fractions were added as a template. Final reactions at a total volume of 100 µl were amplified as specified in **Table 26**. For most selection rounds, amplification was started with 9 - 10 PCR cycles, analyzed by gel electrophoresis and more cycles were added until a PCR product with a signal intensity comparable to the used DNA ladder was achieved. PCR products of the elution fraction were then purified using the MinElute PCR Purification Kit. DNA concentration was measured using IMPLEN NanoPhotometer®.

Table 28: Preparation of reaction mixtures for analytical PCR (PCR1).

PCR1	
1x [µl]	Reagent
10	10x Reaction Buffer with 30 mM $MgCl_2$
4	25 mM $MgCl_2$
4	10 mM dNTPs
1	100 µM Primer DSP-F44
1	100 µM Primer DSP-R44
1	5U/µl Taq DNA Polymerase convenient
0.5	1 U/µl Perfect Match PCR Enhancer
58.5	ddH_2O
80	Final master mix volume

8.3.3. Further Amplifications throughout the SELEX Process

The further amplification strategy was dependent on the formation of byproducts throughout the PCR1. A three- to four-step PCR strategy with few PCR cycles was applied to reduce byproduct production in comparison to a one-step PCR strategy with many PCR cycles. If no byproducts were formed in PCR1, 2x 100 µl PCR2a reaction was prepared and amplified. 200 ng of PCR product from PCR1 were used as template DNA in PCR2a. To generate sufficient amounts of dsDNA for ssDNA synthesis and use for the next round of selection, PCR products from PCR2a or PCR3a were further amplified. Here, 10 - 25x 200 µl PCR2b or PCR3b reactions were prepared. 10 µl of unpurified PCR2a or PCR3a products were used as template DNA and amplified with 5 - 7 PCR cycles. All PCRs following PCR1 were carried out with the use of a 5'-phosphorylated reverse primer to facilitate ssDNA synthesis after PR2b/PCR3b. In case of byproduct formation, 3x 200 µl PCR2a-gel reactions were prepared with addition of 150 - 200 ng PCR1 product as template DNA and amplified with 5 - 7 PCR cycles. PCR2a-gel product was purified using the MinElute PCR Purification Kit (see also 8.5.1) to reduce the sample volume prior to PAGE purification (see also 8.5.3). After PAGE purification, 2x 100 µl PCR3a were prepared with 150 - 200 ng gel purified template DNA and amplified with 5 – 7 PCR cycles. Reaction mixtures for PCR2a, 3a, 2a-gel, 2b and 3b were prepared as specified in **Table 29** and **Table 30**.

Table 29: Preparation of reaction mixtures for PCR2a and 3a.

PCR2a, PCR3a	
1x [µl]	Reagent
10	10x Reaction Buffer with 30 mM $MgCl_2$
4	25 mM $MgCl_2$
4	10 mM dNTPs
1.5	100 µM Primer DSP-F44
1.5	100 µM Primer Phos-DSP-R44
0.5	5 U/µl Taq DNA Polymerase convenient
0.5	1 U/µl Perfect Match PCR Enhancer
X	ddH_2O
100 - Y	Final master mix volume

Y = 10 µl PCR2a/3a product

X = Final volume - Y - sum (volume of other components)

Table 30: Preparation of reaction mixtures for PCR2a-gel, PCR2b, and PCR3b.

PCR2a-gel, PCR2b, PCR3b	
1x [µl]	Reagent
20	10x Reaction Buffer with 30 mM $MgCl_2$
8	25 mM $MgCl_2$
12	10 mM dNTPs
3	100 µM Primer DSP-F44
3	100 µM Primer Phos-DSP-R44
1	5 U/µl Taq DNA Polymerase convenient
0.5	1 U/µl Perfect Match PCR Enhancer
X	ddH_2O
200 - Y	Final master mix volume

Y = Volume of PCR product containing 200 ng DNA

X = Final volume - Y - sum (volume of other components)

8.3.4. PCR for Next Generation Sequencing

The TruSeq DNA Nano kit used for library preparation for Illumina dye sequencing is designed to produce inserts of 350 or 550 bp. The ssDNA pools consist of sequences which consist of only 80 nt. Here, the risk of losing sequences throughout bead-based purification steps was high. Thus, a two-step PCR was performed in which the pools were extended to 136 nt to facilitate library preparation with adjustments. Furthermore, an index was introduced that was used for sequence analysis. Different index primers were used for the first amplification. The primers consisted of 29 nt of which 11 nt were complementary to the primer binding sites of the DNA pools. 200 ng of dsDNA either after gel purification or PCR3b were used as a template. One no template control was prepared usually using index primer 1. PCR reactions were prepared as specified in **Table 31**.

Table 31: Preparation of the master mix and the final reaction mixture for index PCR. Conv. = convenient,

Index PCR Master Mix	
1x [µl]	Reagent
10.0	10x Reaction Buffer with 30 mM $MgCl_2$
4.0	25mM $MgCl_2$
4.0	10mM dNTPs
1.0	5U/µl Taq DNA Polymerase conv.
0.5	1U/µl Perfect Match PCR Enhancer
68.5	ddH_2O
88	Total volume Master Mix

Index PCR final reaction	
1x [µl]	Reagent
10	200 ng dsDNA + ddH_2O or ddH_2O
88	Master Mix
1	100 µM index primer F
1	100 µM index primer R
100	Total volume

Amplification was performed using the PCR program specified in **Table 26** with 6 - 8 PCR cycles. Amplification success was monitored by agarose gel electrophoresis, the final PCR product was purified using the MinElute kit and concentration was measured using IMPLEN NP80 Nanophotometer®. 200 ng of the obtained PCR products were used for Extension PCR. Here, 20 nt long primers were used of which 10 nt were complementary to the index primers. PCR reactions were prepared as specified in **Table 32**.

Table 32: Preparation of reaction mixtures for extension PCR.

Extension PCR	
1x [µl]	Reagent
10	10x Reaction Buffer with 30 mM $MgCl_2$
4	25 mM $MgCl_2$
4	10 mM dNTPs
2	100 µM Primer Extension Primer F
2	100 µM Primer Extension Primer R
1	5 U/µl Taq DNA Polymerase convenient
0.5	1 U/µl Perfect Match PCR Enhancer
X	ddH_2O
100 - Y	Final master mix volume

Y = Volume of PCR product containing 200 ng DNA

X = Final volume - Y - sum (volume of other components)

Amplification was performed using the PCR program specified in section 8.3 with 7 PCR cycles, followed by addition of 2.5 U Taq DNA Polymerase and 6 further PCR cycles. Amplification success was monitored by agarose gel electrophoresis, the final PCR product was purified using the MinElute PCR Purification Kit (see also 6.5.1) and concentration was measured using IMPLEN NP80 Nanophotometer®. Finally, 150 ng of both Index PCR and Extension PCR products were analyzed by PAGE.

8.4. Gel Electrophoresis

DNA electrophoresis describes the migration of DNA in a medium under the influence of an electric field [192]. The electrophoretic mobility of macromolecules in solution depends on the total charge of the molecule as well as the ratio between the applied force by an electric field and the resistance to its motion due to friction with the solvent. For large DNA molecules, this motion is independent of molecular size. Thus, porous gels, in which small DNA molecules migrate faster than larger one, are used as supporting media [193]. In this work, DNA electrophoresis was performed on either on agarose gels or polyacrylamide gels to visualize PCR products or DNA prior to and after single strand synthesis (see also 8.6), for PAGE purification (see also 8.5.3) and for enrichment analysis by DANA (see also 8.7).

8.4.1. Agarose Gel Electrophoresis

Agarose gels were used for analysis of PCR products or enrichment assessment by DANA. For agarose gels, 2% agarose was dissolved in 1x TBE and heated in a microwave until dissolved. After a few min of cooling down, 0.05 µl of 1% ethidium bromide solution per ml gel solution for PCR analysis or 0.025 µl GelStar™ Nucleic Acid Gel Stain per ml gel solution for DANA were added. Liquid agarose solution containing the respective dye was casted into gel slides and was left to harden for approximately 30 min. 6 - 12 µl DNA containing solutions were mixed with 1 - 2 µl 10x loading dye and applied onto the gel, which was run for approximately 45 min at 100 - 120 V. 1x TBE was used as a running buffer. For DNA detection, gels were irradiated at 254 nm UV light and photographed using the BioDoc Analyze gel documentation system. Signal intensities of the PCR products were compared to signal intensity of 4 µl 50 bp DNA Ladder.

8.4.2. Polyacrylamide Gel Electrophoresis (PAGE)

Polyacrylamide gels (PAA gels) were used for analysis of single strand production as well as for PAGE purifications. A solution containing 30% ROTIPHORESE® Gel 40 (29:1) solution, adding up to a final of acrylamide concentration of 12%, TBE at a final concentration of 1x and 7 M urea was prepared. 12.5 ml per gel were polymerized with 62.5 µl ammonium persulfate (APS) and 6.25 µl Tetramethylethylenediamine (TEMED) using the BioRad Mini-PROTEAN® Tetra cell system with 1.5 mm spacer plates and combs. DNA samples as well as 3 µl of 25 bp DNA Step Ladder were prepared by adding 8 µl (for samples < 8 µl) or equivalent amounts (for samples > 8µl) of 2x denaturing PAA loading dye. All samples, except for the ladder, were heated to 90°C for 10 min. Heated 1x TBE was used as running buffer. Samples were loaded onto the gel and run at 80 V for approximately 30 min followed by 120 V until the bromophenol

blue front reached the lower edge of the gel. For analytical purposes and after PAGE purification, PAA gels were stained by a 15-min-long incubation in 1x TBE including 0.05 µl of 1% ethidium bromide solution per ml TBE solution. For DNA detection, gels were irradiated at 254 nm UV light and photographed BioDoc Analyze gel documentation system.

8.5. DNA Purifications

DNA was purified after most PCR steps as well as after single strand production. MinElute and Agowa purifications were performed to remove PCR or single strand production components such as polymerase or lambda exonuclease. PAGE purification was performed to remove PCR byproducts with different molecular sizes. 1.5 µl of purified DNA were used for concentration measurement using IMPLEN NP80 NanoPhotometer®.

8.5.1. MinElute Purification

After PCR1, PCR2a-gel and NGS preparation PCRs, resulting dsDNA was purified using the MinElute PCR Purification Kit according to the manufacturer's specifications except for the addition of 1.6% (v/v) 3 M $C_2H_3NaO_2$ to the binding reaction. PCR1 products were eluted in 30 µl elution buffer. For PCR2a-gel, the PCR product solution was split onto 2 columns which were both eluted with 17.5 µl elution buffer.

8.5.2. Agowa Purification

Bead-based Agowa purification was performed after PCR2b, PCR3b and after single strand production. Here, reaction volumes were too high to perform MinElute. Thus, bead-based purification using a robotic workstation was performed. Purification was performed utilizing a KingFisher™ microtiter 96 deepwell plate and KingFisher™ Duo Prime robotic workstation. Reactions were prepared as specified in **Table 33** and purification was performed automated by the robotic workstation.

Table 33: Agowa purification steps.

Step	Step number	Duration [min]	Row	Volume [µl]	Reagents	Temp [°C]
Bind	1	12	A/E	400 - 600	DNA sample	RT
				24 - 36	sbeadex particle solution	
				320 - 480	Agowa binding buffer	
Wash 1	2	5	B/F	400	Agowa washing buffer	
Wash 2	3	5	C/G	400	ddH_2O	
Elution 2	5	2	D/H	80	ddH_2O	
Elution 1	4	5	Elution strip	120	Agowa elution buffer	55
				20	ddH_2O	

After purification, solutions from rows D/H and from the elution strip were pipetted into a tube and DNA concentration was measured using IMPLEN NP80 NanoPhotomer®.

8.5.3. PAGE Purification

For PAGE purification, PCR2a-gel products were purified by MinElute. 200 ng for analytical purposes, the remaining 2 - 10 µg of DNA and 3 µl of 25 bp DNA step ladder were prepared as described in section 8.4.2. To facilitate proper separation of DNA sequences with different molecular sizes for as large amounts as 2 - 10 µg, 2 - 3 gel pockets were merged by cutting the separating gel pieces. Samples were applied onto the gel and run as described in section 8.4.2. After electrophoresis, DNA was visualized by UV shadowing (254 nm) on a silica gel plate. The desired band was cut out, placed in 1.5 ml tube, and covered with 700 µl of 0.3 M $C_2H_3NaO_2$, pH 5.2 for DNA extraction. After incubation for 1 h at 70°C and 600 rpm, using a thermomixer the supernatant was transferred into a 2 ml tube and approximately 350 µl of fresh 0.3 M $C_2H_3NaO_2$ were added. The amount of fresh 0.3 M $C_2H_3NaO_2$ depended on the size of the gel piece as it needed to be covered by the fluid. This procedure was repeated twice after another 1.5 and 2 h of incubation. Subsequently, the supernatant was divided into 2x 2 ml tubes and precipitated as described in section 8.2.1. After precipitation centrifugation and washing was performed as described in section 8.2.1. Yet, dried pellets were dissolved in 10 µl ddH_2O each and pooled in a fresh tube. DNA concentration was measured, and the purified DNA was used for amplification as PCR3b.

8.6. Single Strand Synthesis

Single stranded DNA was synthesized utilizing lambda exonucleases ability to selectively digest the 5' phosphorylated strand of dsDNA in 5'-3' direction [73]. PCR2b or PCR3b products, purified by Agowa purification, were supplemented with 10% (v/v) 10x reaction buffer lambda

exonuclease. Prior to addition of lambda exonuclease, 7 µl were put aside for subsequent PAGE analysis. 1.5 U/µg dsDNA lambda exonuclease were added and incubated for 30 min to 1 h at 37°C and 300 rpm. After incubation, lambda exonuclease was heat inactivated at 75°C for 10 min. 7 µl were put aside for subsequent PAGE analysis and ssDNA was Agowa purified. Finally, 7 µl of DNA prior to and after single strand synthesis as well as 100 ng of Agowa purified ssDNA were analyzed by PAGE.

8.7. Diversity Assay for Nucleic Acids (DANA)

DANA is based on the ability of S1 nuclease to digest ssDNA but not dsDNA [194]. Here, prior to S1 nuclease incubation, dsDNA is denatured at a temperature well above its melting point, followed by cooling down for rehybridization for a defined amount of time. Upon S1 incubation, remaining ssDNA is digested while dsDNA remains intact. Discrimination between strongly enriched and highly diverse DNA pools is possible if the rehybridization time frame is set to an amount of time in which strongly enriched pools can rehybridize while highly diverse pools remain single stranded for the most part. In this work, dsDNA from PCR2b or PCR3b was used for DANA. Double stranded DNA from different DNA libraries was used as a highly diverse negative control while dsDNA of an unrelated aptamer was used as a positive control. Double stranded DNA samples were prepared as follows: 500 ng of dsDNA were supplemented with 10 µl 5x S1 buffer and ddH_2O to achieve a final volume of 50 µl. The reactions were split up as two reactions of 25 µl each and heated to 98 °C for 3 min for denaturation followed by 65 °C for 5 min for (partial) rehybridization. In the meantime, S1 nuclease was diluted to 0.2 U/µl in 1x S1 buffer. After the rehybridization step, the PCR program was stopped to immediately add either 0.5 U S1 in 2.5 µl 1x S1 buffer (+) or 2.5 µl 1x S1 buffer (-). Partially rehybridized DNA was then incubated with S1 nuclease or buffer for 30 min at 65 °C. Subsequently, 2 µl of 0.5 M EDTA were added to stop the reaction. Of all reactions, 12 µl were supplemented with 1.2 µl 10x agarose loading dye and loaded onto a 2% agarose gel containing GelStar™ Nucleic Acid Gel Stain. The gel was run and analyzed as described in section 8.4.2

8.8. Next Generation Sequencing (NGS) - Illumina Dye Sequencing

The term next generation sequencing refers to highly parallel or high-output sequencing techniques that produce high amounts of data [195]. Illumina dye sequencing is based on the concept of sequencing by synthesis (SBS). SBS is characterized by three basics steps which are fragmentation of the DNA or RNA by physical shearing (1), generation of a “sequencing library” by addition of platform specific adaptors at both ends of the DNA or RNA fragments (2) and hybridization to covalently surface-bound oligonucleotides with complementarity to the

adaptors followed by clonal on-surface amplification of the bound fragment (3) [93]. Clonal clusters are formed, and one DNA strand is removed to yield single-stranded templates with uniform orientation. The 3'-ends of the DNA are blocked and a sequencing primer hybridizes to the adaptor. 4 differently labeled or three differently labeled and one unlabeled, 3'-blocked (d)NTPs are added and used for extension in the presence of a polymerase. After incorporation, the flow cell is read out piecewise by imaging. The terminator and the fluorophore are removed and a new cycle is started [196]. In this work, ssDNA pools were prepared for sequencing via a two-step PCR to yield a dsDNA product extended by 48 nt. The library prep was performed using the TruSeq DNA Nano kit partially according to the manufacturer's specifications. The library prep workflow includes 6 steps, namely fragment DNA (1), repair ends and select library size (2), adenylate 3' ends (3), ligate adapters (4), enrich DNA fragments (5), check, normalize and pool libraries (6). The following changes were made to the workflow, to accustom the workflow to the short sequences used for NGS. Step 1 was left out as DNA pools after extension PCR were already at the size used for sequencing. For step 2, the Repair Ends procedure was performed as described in the manual. However, the Select Library Size was accustomed. Here, the manual suggests a two-step clean up to remove large and small DNA fragments. As the used fragments were of only one length, only the second clean up step was performed to remove reagents from the Repair Ends procedure. Here, the ratio of beads volume to sample volume was accustomed to the size of the fragments and used in a ratio of 1.3 µl beads per 1 µl sample. Steps 3, 4 and 5 were performed as described in the manual. However, clean-up procedures after steps 4 and 5 were performed with a bead to sample ratio of 1.2µl per 1µl. Step 6 was performed as specified by the manufacturer. Quantification of the library was performed with a Qubit Fluorometer as specified by the manufacturer. Sequencing was performed using the Mini Seq Mid Output Kit on a Miniseq sequencing platform. Paired end mode was chosen with 150 reads per direction and data was bioinformatically analyzed using AptaAnalyzer™-SELEX.

8.9. Fluorescent-dye Linked Aptamer Assay (FLAA)

FLAA is an MTP-based assay that can be used to test the affinity of aptamer candidates or ssDNA pools. The assay makes use of the ssDNA specific fluorescent dye Quant-iT™ OliGreen™ which is basically nonfluorescent in the absence of ssDNA, while it becomes fluorescent when bound to ssDNA. Target molecules are immobilized on an MTP and incubated with the respective aptamer candidate or ssDNA pool. After certain washing steps a dilution of the fluorescent dye is added to the plate and after incubation, fluorescence is measured [154]. In this work, carbapenemases were either immobilized on Greiner Bio-One FLUOTRAC™ High Binding 96-well Polystyrene Microplates or on Pierce™ Nickel Coated 96

well plates. In both cases, carbapenemases were diluted to 0.6 µg per well in a total volume of 100 µl in PBS and applied onto the plates. 100 µl PBS were applied to negative control wells. Target incubation was conducted for 3h at 23°C and 300 rpm and 18 °C without shaking overnight for Greiner Bio-One FLUOTRAC™ High Binding 96-well Polystyrene Microplates and for 1h at 23 °C and 300 rpm for Pierce™ Nickel Coated MTP. Single stranded DNA was diluted to 0.4 - 1 µM in a total volume of 100 µl per well in aptamer binding buffer and activated as described before to achieve optimal folding by denaturation and refolding. After target incubation MTPs were washed twice with PBS-T and once with aptamer binding buffer. 100 µl activated ssDNA was applied to each well and incubated for 1h at 23°C and 300 rpm. Meanwhile, Quant-iT™ OliGreen™ was diluted 1:200 in aptamer binding buffer. After three consecutive washing steps with aptamer binding buffer, 100 µl Quant-iT™ OliGreen™ dilution were applied to each well and incubated for 12 - 20 min. Fluorescence was measured thrice (excitation 485 nm, emission 527 nm) using either Mithras² LB 943 Monochromator multimode microplate reader or EnVision® 2105 multimode plate reader. Two or three target-coated, and negative control wells were incubated with the same ssDNA sample as technical replicates. Fluorescence values were averaged, and negative control values were subtracted. Error bars represent the square root of the sum of the variances of two or three target-coated wells and two or three negative control wells.

8.10. MicroScale Thermophoresis (MST)

MST is an immobilization-free technique for the analysis of binding events. It is based on a phenomenon called thermophoresis which is the directed movement of molecules in a temperature gradient. Thermophoresis is influenced by size, charge, and hydration shell of a molecule in a liquid medium. Virtually any binding event is accompanied by changes in at least one of these factors, allowing for the characterization of binding events. In a typical MST setup, an infrared laser is used to create a microscopic, local temperature gradient in which a fluorescently labeled binding partner moves either alone or in complex with another, unlabeled molecule. Titration of the unlabeled binding partner allows for the calculation of dissociation constants [159]. In this work, constant concentrations of 5'-Cy5-labelled aptamers KPC2-H14-01(01), NDM1-H14.2-Mask_43, and Con1 were incubated with varying concentrations of unlabeled His-NDM-1, His-OXA-23, and/or the hexa-His peptide. For characterization of KPC2-H14-01(01) binding to the hexa-His peptide, Cy5-KPC2-H14-01(01) and Cy5-Con1 were diluted to 20 nM. A serial dilution of the hexa-His peptide (8960 - 2.72 nM) was prepared and 10 µl of each aptamer and hexa-His peptide solution were mixed. For characterization of NDM1-H14.2_Mask-43, selectively binding to His-NDM-1, aptamers Cy5-NDM1-H14.2_Mask-43 and Cy5-Con1 were diluted to 42 nM in BP-TB and activated as

described before. Serial dilutions of His-NDM-1, the hexa-His peptide (both 32.3 - 0.017 µM), and His-OXA-23 (25.3 - 0.013 µM) were prepared, and 1 µl of each aptamer was mixed with 5 µl of ligand solution. For all dilutions, BP-TB was used. Binding experiments were performed with 40 - 70% excitation power and 40 - 60% MST power using standard capillaries. Measurements were performed on Monolith NT.115. The recorded fluorescence was normalized to ΔF_{norm} in per mill and fitted utilizing the K_D formula derived from the law of mass action by MO.Affinity Analysis software as previously described [44]. All measurements were performed in triplicates.

8.11. Surface Plasmon Resonance Spectroscopy (SPR)

SPR is a label-free method that can be exploited to analyze kinetic features of a binding event. SPR exploits the phenomenon of surface plasmon resonance which occurs when a photon of incident light strikes a metal surface. At a certain angle of incidence, some of the light energy excites electrons in the metal layer which then move. These movements are called plasmons and propagate parallel to the metal surface. The angle at which surface plasmon resonance occurs is dependent on the refractive index of the material near the metal surface. Thus, changes in the refractive index near the metal surface, e.g., through binding events, require adjustment of the SPR angle. For SPR measurements, one binding partner is immobilized on an SPR sensor chip and the other binding partner is injected. Upon binding of the injected binding partner, the refractive index at the sensor surface increases, resulting in a change of the SPR angle. In an SPR experiment, signal changes are described as response units (RU) where one RU corresponds to an angle shift of 10^{-4} degrees [155]. In this work, SPR was performed with immobilized carbapenemase and unrelated His-tagged protein for aptamer candidate screening after SR11.1 and for truncations of promising aptamer candidates after SR14.1. Kinetic measurements were further conducted on the His-tag aptamer KPC2-H14-01(01) and derivates thereof. The His-NDM-1 specific aptamer NDM1-H14.2_Mask-43 and scramble control aptamer ConSc as well as two His-NDM-1 binding sequences after doped selection were kinetically characterized by SPR. Finally, single injections were used as an attempt to characterize weak binder KPC2-H14-05 and two KPC-2 binding sequences, selected with the masking approach. All kinetic measurements as well as single injections were performed with 5'-biotinylated aptamers, immobilized on SPR sensor chips. All measurements were performed using a BIAcore T200 facility. The system was operating at 25 °C and at flow rates of 10 - 30 µl/min. BP-T* was used as the running buffer and for aptamer dilutions. HC200M sensor chips were primed twice with ddH_2O and activated with 0.2 M 1-ethyl-3-(3-dimethylaminopropyl) carbodiimide (EDC) and 0.1 M N-hydroxy-succinimide (NHS) for 180 s. Regenerations were performed with 20 mM Na_2CO_3.

For measurements with immobilized proteins, immobilization was performed via amine coupling for 180 s and the chip was blocked with 1 M ethanolamine for 420 s at a flow rate of 20 µl/min. Proteins were diluted to 5 - 30 µg/ml in acetate buffer and immobilized at different pHs. Protein concentrations as well as pH of immobilization are specified in **Table 34**. Aptamer candidates were activated, diluted to 1 µM and injected with 180 s association and 300 s dissociation at a flow rate of 30 µl/min.

Table 34: Concentration and pH for immobilization of target proteins.

Protein	Concentration [µg/ml]	pH
mPD1-His	15	5.0
His-NDM-1	15	6.0
His-KPC-2	30	6.5
His-OXA-23	5	6.5

For kinetic measurements, 20 - 30 µg/ml NeutrAvidin in 10 mM acetate buffer was immobilized via amine coupling at a pH of 5.5 for 120 s. The chip was blocked with 1 M ethanolamine for 420 s at a flow rate of 20 µl/min. 5'-biotinylated aptamers were diluted to 1 µM, activated, and further diluted to 0.1 µM. Aptamer immobilization was performed at a flow rate of 10 µl/min and stopped at approximately 100 RU. Remaining NeutrAvidin binding sites were blocked with 40 µM biotin for 120 s at a flow rate of 20 µl/min. Analytes were diluted to their final concentration and injected to both the ligand-bound channels and the reference channel. For kinetic measurements injections were performed with 180 s association and 600 s dissociation at a flow rate of 30 µl/min. Kinetic parameters were calculated using BIAevaluation software. For the attempt to characterize the weak binder KPC2-H14-05 as well as KPC2-H13.3_Mask-41 and KPC2-H13.3_Mask-126, 100 nM His-KPC-2 was injected for 180s. After 60 s, 500 nM of His-KPC-2 were injected for 180 s. 500 nM His-NDM-1 and mPD1-His were injected for 180 s with a dissociation for 600 s.

8.12. Sandwich Assays

Sandwich assays are composed of three key elements – the analyte, recognition molecules and a reporter molecule. Reporter molecules, for example enzymes, fluorescence tags, redox tags or radioactive isotopes, are usually attached to a recognition molecule. Upon or in response to binding of an analyte to the recognition molecules a signal becomes measurable, indicating the presence of the analyte in a sample. Sandwich assays play an important role in the fields of bio detection, clinical diagnostics, environmental monitoring, and quality control as the requirement for binding of at least two recognition molecules to one analyte make them highly specific [197].

8.12.1. MTP-based Sandwich Assays

In this work, sandwich assays were inter alia performed in an MTP format. 5'-biotinylated aptamers were immobilized on SA-coated MTP as capture probes. The analytes were added for a first analyte recognition by the capture probes. Detection was facilitated by incubation with HRP-labelled antibodies, as a second analyte recognition step, followed by addition of the HRP substrate TMB and absorption measurement at 450 nm. For detection of His-KPC-2 and His-NDM-1, 5'-biotinylated aptamers KPC2-H14-05, KPC2-H13.3_Mask-41, and _Mask-126 and NDM1-H14.2_Mask-43 were diluted to 250 nM in aptamer binding buffer and activated. 25 pmol of activated aptamer were applied per well to six wells per aptamer (3x detection wells and 3x negative control wells) and incubated for 1h. Six further wells were incubated with BP-T (3x His-KPC-2 only detection wells and 3x negative control wells). Wells were washed thrice and blocked with 5000 pmol biotin for another hour. For detection of His-KPC-2, 100 µl BP-T, either supplemented with 80 pmol His-KPC-2 or without supplementation, were added to either detection or negative control wells. After 1 h of incubation, 100 µl of a HRP-labeled anti-penta-His antibody, diluted 1:600 in BP-T, were added per well and incubated for 30 min. For detection of His-NDM-1, 100 µl BP-T, either supplemented with 60 pmol His-NDM-1 or without supplementation, were added to either detection or negative control wells. After 1 h of incubation, 100 µl of a polyclonal rabbit-anti-NDM-1 antibody, diluted 1:5000 in 1x Rotiblock, was added per well and incubated for 30 min. After washing thrice, wells were incubated with a HRP-labeled, secondary anti-rabbit antibody, diluted 1:1000 in 1x RotiBlock, for 30 min. After antibody incubation, wells were washed thrice and incubated with 100 µl TMB solution until a blue color was detected. The reaction was stopped by addition of 50 µl 2 M H_2SO_4 and absorption was measured at 450 nm by EnVision® 2105 multimode plate reader. All incubation and washing steps were performed at 23°C and 300 rpm using a thermomixer. Washing was performed for 90 sec with BP-T. Measurements were performed as triplicates. Absorption values were averaged, and signals derived from negative control wells were subtracted. Error bars reflect the standard deviation of detection wells plus the standard deviation of negative control wells.

8.12.2. Lateral Flow Device (LFD)-based Sandwich Assay

Additionally, an aptamer-based sandwich assay LFD was developed by Katharina Fedorov from our project partner nal von minden GmbH. The preparation and testing of the LFD was divided into four steps.

Conjugate preparation

Conjugation was carried out according to a modified version of the protocol established by Deka *et al.* [198]. For conjugation of 5'-HS-TEG modified KPC2-H13.3_Mask-41 with gold particles (~ 40 nm, OD 1,776) at pH 5.0, the aptamer (v = 30 µl; c = 0.1 nmol/µl) was activated as described before. Afterwards, the aptamer was mixed with 1 ml of gold particles and left for 10 min. The conjugation requires acidic pH, which was achieved by adding 1.5 ml citrate-HCl buffer of pH 4.31. After 30 min of incubation, 20 µl (11-Mercaptoundecyl)-tetraethylenglykol (MUTEG) was added to the mixture and incubated for another 10 min. This step is required to stabilize the conjugate and to saturate free binding sites of the colloid. The solution was centrifuged two times at 15,000x g and the supernatant was discarded to remove unbound aptamers and MUTEG molecules from the functionalized gold particles. Subsequently, the pellet was washed by resuspension in 1000 µl ddH_2O and centrifugation at 15,000x g for 30 min. After determination of the pellet volume, 5.92 µl gold stabilization buffer was added and filled up to 59.2 µl with ddH_2O.

Membrane coating

For the coating solution 1.4 nmol 5'-biotinylated KPC2-H14-05 were activated as described before. After addition of 420 pmol NeutrAvidin, the solution was shaken at 500 rpm at room temperature for 25 min. Subsequently, 5 pmol biotin and 3.5 µl 10x aptamer binding buffer were added and filled up to 35 µl with ddH_2O. The coating solution was incubated at room temperature and 500 rpm for another 25 min. The membrane was placed and pressed onto the backing card. After adjustment of the dispenser, the card with the membrane was placed onto the dispenser table. Theron, 1 µl/cm (16 pmol/4 mm) coating solution was applied onto the membrane. The membrane was dried in the incubator at 40 °C and a relative humidity of 10% over night (> 12 h).

Assembling

Assembling of the uncut sheet was performed by attaching the absorbent pad above and the sample pad (pretreated with 1% Tween-20) beneath the coated membrane onto the backing card. The absorbent pad and the sample pad were placed on the backing card in a manner that ensures overlapping with the membrane. Afterwards, the uncut sheets were cut in 4 mm strips, which were inserted in the test cassettes.

Test performance: Sandwich assay

To perform the sandwich assay, six testing reactions were pipetted into Eppendorf tubes. Each reaction contained 1 µl Tween-20 (10%), 1 µl 10x aptamer binding buffer, 2 µl of the conjugate and either 0, 1, 2, 3, 4 or 5 µl of His-KPC-2 (0.1 mg/ml) filled up to 100 µl with ddH_2O. The testing reactions were vortexed and incubated for 15 min at room temperature before pipetting onto the test cassettes. The results were determined after 10 min by using the gold color card.

9. References

1 Slaught, M., Rasmussen, M., Bougie, D. & Aster, R. Immune thrombocytopenia induced by beta-lactam antibiotics: Cross-reactions of responsible antibodies with other beta-lactam drugs. *Transfusion* **61**, 1600-1608, doi:10.1111/trf.16295 (2021).

2 Bruch, R. *et al.* Clinical on-site monitoring of ss-lactam antibiotics for a personalized antibiotherapy. *Sci Rep* **7**, 3127, doi:10.1038/s41598-017-03338-z (2017).

3 Palacios, A. R., Rossi, M. A., Mahler, G. S. & Vila, A. J. Metallo-beta-Lactamase Inhibitors Inspired on Snapshots from the Catalytic Mechanism. *Biomolecules* **10**, doi:10.3390/biom10060854 (2020).

4 Mai-Prochnow, A., Clauson, M., Hong, J. & Murphy, A. B. Gram positive and Gram negative bacteria differ in their sensitivity to cold plasma. *Sci Rep* **6**, 38610, doi:10.1038/srep38610 (2016).

5 Scheffers, D. J. & Pinho, M. G. Bacterial cell wall synthesis: new insights from localization studies. *Microbiol Mol Biol Rev* **69**, 585-607, doi:10.1128/MMBR.69.4.585-607.2005 (2005).

6 Cho, H., Uehara, T. & Bernhardt, T. G. Beta-lactam antibiotics induce a lethal malfunctioning of the bacterial cell wall synthesis machinery. *Cell* **159**, 1300-1311, doi:10.1016/j.cell.2014.11.017 (2014).

7 Lima, L. M., Silva, B., Barbosa, G. & Barreiro, E. J. beta-lactam antibiotics: An overview from a medicinal chemistry perspective. *Eur J Med Chem* **208**, 112829, doi:10.1016/j.ejmech.2020.112829 (2020).

8 Fleming, A. On the antibacterial action of cultures of a penicillium, with special reference to their use in the isolation of B. influenzae. 1929. *Bull World Health Organ* **79**, 780-790 (2001).

9 Lowy, F. D. Antimicrobial resistance: the example of Staphylococcus aureus. *J Clin Invest* **111**, 1265-1273, doi:10.1172/JCI18535 (2003).

10 Marcy, S. M. & Klein, J. O. The isoxazolyl penicillins: oxacillin, cloxacillin, and dicloxacillin. *Med Clin North Am* **54**, 1127-1143 (1970).

11 Abraham, E. P. & Newton, G. G. The structure of cephalesporin C. *Biochem J* **79**, 377-393, doi:10.1042/bj0790377 (1961).

12 Essack, S. Y. The development of beta-lactam antibiotics in response to the evolution of beta-lactamases. *Pharm Res* **18**, 1391-1399, doi:10.1023/a:1012272403776 (2001).

13 El-Shorbagi, A. N. & Chaudhary, S. Monobactams: A Unique Natural Scaffold of Four-membered Ring Skeleton, Recent Development to Clinically Overcome Infections by Multidrug-resistant Microbes. *Lett Drug Des Discov* **16**, 1305-1320, doi:10.2174/1570180816666190516113202 (2019).

14 Brown, A. G., Corbett, D. F., Eglington, A. J. & Howarth, T. T. Structures of olivanic acid derivatives MM 4550 and MM 13902; two new, fused β-lactams isolated from Streptomyces olivaceus. *Journal of the Chemical Society, Chemical Communications*, 523-525 (1977).

15 Kahan, J. S. *et al.* Thienamycin, a New Beta-Lactam Antibiotic .1. Discovery, Taxonomy, Isolation and Physical-Properties. *J Antibiot* **32**, 1-12 (1979).

16 Moellering Jr, R. C., Eliopoulos, G. M. & Sentochnik, D. E. The carbapenems: new broad spectrum β-lactam antibiotics. *J Antimicrob Chemoth* **24**, 1-7 (1989).

17 El-Gamal, M. I. *et al.* Recent updates of carbapenem antibiotics. *Eur J Med Chem* **131**, 185-195, doi:10.1016/j.ejmech.2017.03.022 (2017).

18 McKenna, M. The last resort: health officials are watching in horror as bacteria become resistant to powerful carbapenem antibiotics--one of the last drugs on the shelf. *Nature* **499**, 394-397 (2013).

19 Podolsky, S. H. The evolving response to antibiotic resistance (1945-2018). *Palgr Commun* **4**, doi:10.1057/s41599-018-0181-x (2018).

20 Lutgring, J. D. Carbapenem-resistant Enterobacteriaceae: An emerging bacterial threat. *Semin Diagn Pathol* **36**, 182-186, doi:10.1053/j.semdp.2019.04.011 (2019).

21 Munita, J. M. & Arias, C. A. Mechanisms of Antibiotic Resistance. *Microbiol Spectr* **4**, doi:10.1128/microbiolspec.VMBF-0016-2015 (2016).
22 Armand-Lefevre, L., Andremont, A. & Ruppe, E. Travel and acquisition of multidrug-resistant Enterobacteriaceae. *Med Mal Infect* **48**, 431-441, doi:10.1016/j.medmal.2018.02.005 (2018).
23 Nordmann, P., Naas, T. & Poirel, L. Global spread of Carbapenemase-producing Enterobacteriaceae. *Emerg Infect Dis* **17**, 1791-1798, doi:10.3201/eid1710.110655 (2011).
24 Reygaert, W. C. An overview of the antimicrobial resistance mechanisms of bacteria. *AIMS Microbiol* **4**, 482-501, doi:10.3934/microbiol.2018.3.482 (2018).
25 Naas, T. & Nordmann, P. Analysis of a carbapenem-hydrolyzing class A beta-lactamase from Enterobacter cloacae and of its LysR-type regulatory protein. *Proc Natl Acad Sci U S A* **91**, 7693-7697, doi:10.1073/pnas.91.16.7693 (1994).
26 Tilahun, M., Kassa, Y., Gedefie, A. & Ashagire, M. Emerging Carbapenem-Resistant Enterobacteriaceae Infection, Its Epidemiology and Novel Treatment Options: A Review. *Infect Drug Resist* **14**, 4363-4374, doi:10.2147/IDR.S337611 (2021).
27 Suay-Garcia, B. & Perez-Gracia, M. T. Present and Future of Carbapenem-resistant Enterobacteriaceae (CRE) Infections. *Antibiotics (Basel)* **8**, doi:10.3390/antibiotics8030122 (2019).
28 Paterson, D. L. & Bonomo, R. A. Extended-spectrum beta-lactamases: a clinical update. *Clin Microbiol Rev* **18**, 657-686, doi:10.1128/CMR.18.4.657-686.2005 (2005).
29 Arnold, R. S. *et al.* Emergence of Klebsiella pneumoniae carbapenemase-producing bacteria. *South Med J* **104**, 40-45, doi:10.1097/SMJ.0b013e3181fd7d5a (2011).
30 Miriagou, V. *et al.* Imipenem resistance in a Salmonella clinical strain due to plasmid-mediated class A carbapenemase KPC-2. *Antimicrob Agents Chemother* **47**, 1297-1300, doi:10.1128/AAC.47.4.1297-1300.2003 (2003).
31 Yigit, H. *et al.* Carbapenem-resistant strain of Klebsiella oxytoca harboring carbapenem-hydrolyzing beta-lactamase KPC-2. *Antimicrob Agents Chemother* **47**, 3881-3889, doi:10.1128/AAC.47.12.3881-3889.2003 (2003).
32 Nordmann, P. *et al.* Identification and screening of carbapenemase-producing Enterobacteriaceae. *Clin Microbiol Infect* **18**, 432-438, doi:10.1111/j.1469-0691.2012.03815.x (2012).
33 Lutgring, J. D. & Limbago, B. M. The Problem of Carbapenemase-Producing-Carbapenem-Resistant-Enterobacteriaceae Detection. *J Clin Microbiol* **54**, 529-534, doi:10.1128/JCM.02771-15 (2016).
34 Kon, H. *et al.* Multiplex lateral flow immunochromatographic assay is an effective method to detect carbapenemases without risk of OXA-48-like cross reactivity. *Ann Clin Microbiol Antimicrob* **20**, 61, doi:10.1186/s12941-021-00469-0 (2021).
35 Hammoudi, D., Moubareck, C. A. & Sarkis, D. K. How to detect carbapenemase producers? A literature review of phenotypic and molecular methods. *J Microbiol Methods* **107**, 106-118, doi:10.1016/j.mimet.2014.09.009 (2014).
36 Boutal, H. *et al.* A multiplex lateral flow immunoassay for the rapid identification of NDM-, KPC-, IMP- and VIM-type and OXA-48-like carbapenemase-producing Enterobacteriaceae. *J Antimicrob Chemother* **73**, 909-915, doi:10.1093/jac/dkx521 (2018).
37 Glupczynski, Y. *et al.* Prospective evaluation of the OKN K-SeT assay, a new multiplex immunochromatographic test for the rapid detection of OXA-48-like, KPC and NDM carbapenemases. *J Antimicrob Chemother* **72**, 1955-1960, doi:10.1093/jac/dkx089 (2017).
38 Boutal, H. *et al.* Development and Validation of a Lateral Flow Immunoassay for Rapid Detection of NDM-Producing Enterobacteriaceae. *J Clin Microbiol* **55**, 2018-2029, doi:10.1128/JCM.00248-17 (2017).
39 Koczula, K. M. & Gallotta, A. Lateral flow assays. *Essays Biochem* **60**, 111-120, doi:10.1042/EBC20150012 (2016).
40 Eltzov, E. *et al.* Lateral Flow Immunoassays - from Paper Strip to Smartphone Technology. *Electroanal* **27**, 2116-2130, doi:10.1002/elan.201500237 (2015).

41 Li, H. Y. *et al.* Advances in detection of infectious agents by aptamer-based technologies. *Emerg Microbes Infect* **9**, 1671-1681, doi:10.1080/22221751.2020.1792352 (2020).
42 Song, K. M., Lee, S. & Ban, C. Aptamers and Their Biological Applications. *Sensors-Basel* **12**, 612-631, doi:10.3390/s120100612 (2012).
43 Rajendran, M. & Ellington, A. D. Selection of fluorescent aptamer beacons that light up in the presence of zinc. *Anal Bioanal Chem* **390**, 1067-1075, doi:10.1007/s00216-007-1735-8 (2008).
44 Sass, S. *et al.* Binding affinity data of DNA aptamers for therapeutic anthracyclines from microscale thermophoresis and surface plasmon resonance spectroscopy. *Analyst* **144**, 6064-6073, doi:10.1039/c9an01247h (2019).
45 Dreymann, N. *et al.* Inhibition of Human Urokinase-Type Plasminogen Activator (uPA) Enzyme Activity and Receptor Binding by DNA Aptamers as Potential Therapeutics through Binding to the Different Forms of uPA. *Int J Mol Sci* **23**, doi:10.3390/ijms23094890 (2022).
46 Escudero-Abarca, B. I., Suh, S. H., Moore, M. D., Dwivedi, H. P. & Jaykus, L. A. Selection, characterization and application of nucleic acid aptamers for the capture and detection of human norovirus strains. *Plos One* **9**, e106805, doi:10.1371/journal.pone.0106805 (2014).
47 Yu, X. F., Chen, F., Wang, R. H. & Li, Y. B. Whole-bacterium SELEX of DNA aptamers for rapid detection of E. coli O157:H7 using a QCM sensor. *Journal of Biotechnology* **266**, 39-49, doi:10.1016/j.jbiotec.2017.12.011 (2018).
48 Wu, X. *et al.* Cell-SELEX aptamer for highly specific radionuclide molecular imaging of glioblastoma in vivo. *Plos One* **9**, e90752, doi:10.1371/journal.pone.0090752 (2014).
49 Adachi, T. & Nakamura, Y. Aptamers: A Review of Their Chemical Properties and Modifications for Therapeutic Application. *Molecules* **24**, doi:10.3390/molecules24234229 (2019).
50 Kim, Y. J., Kim, Y. S., Niazi, J. H. & Gu, M. B. Electrochemical aptasensor for tetracycline detection. *Bioprocess Biosyst Eng* **33**, 31-37, doi:10.1007/s00449-009-0371-4 (2010).
51 Amouzadeh Tabrizi, M., Shamsipur, M. & Farzin, L. A high sensitive electrochemical aptasensor for the determination of VEGF(165) in serum of lung cancer patient. *Biosens Bioelectron* **74**, 764-769, doi:10.1016/j.bios.2015.07.032 (2015).
52 Wu, L., Zhang, X., Liu, W., Xiong, E. & Chen, J. Sensitive electrochemical aptasensor by coupling "signal-on'' and "signal-off'' strategies. *Anal Chem* **85**, 8397-8402, doi:10.1021/ac401810t (2013).
53 Huang, R., Xi, Z., Deng, Y. & He, N. Fluorescence based Aptasensors for the determination of hepatitis B virus e antigen. *Sci Rep* **6**, 31103, doi:10.1038/srep31103 (2016).
54 Lu, Z. S., Chen, X. J. & Hu, W. H. A fluorescence aptasensor based on semiconductor quantum dots and MoS2 nanosheets for ochratoxin A detection. *Sensor Actuat B-Chem* **246**, 61-67, doi:10.1016/j.snb.2017.02.062 (2017).
55 Katiyar, N., Selvakumar, L. S., Patra, S. & Thakur, M. S. Gold nanoparticles based colorimetric aptasensor for theophylline. *Anal Methods-Uk* **5**, 653-659, doi:10.1039/c2ay26133b (2013).
56 Birader, K. *et al.* Colorimetric aptasensor for on-site detection of oxytetracycline antibiotic in milk. *Food Chem* **356**, 129659, doi:10.1016/j.foodchem.2021.129659 (2021).
57 Lian, Y., He, F., Wang, H. & Tong, F. A new aptamer/graphene interdigitated gold electrode piezoelectric sensor for rapid and specific detection of Staphylococcus aureus. *Biosens Bioelectron* **65**, 314-319, doi:10.1016/j.bios.2014.10.017 (2015).
58 Chen, X. J., Bai, X. J., Li, H. Y. & Zhang, B. L. Aptamer-based microcantilever array biosensor for detection of fumonisin B-1. *Rsc Adv* **5**, 35448-35452, doi:10.1039/c5ra04278j (2015).
59 Yan, S. R. *et al.* A review: Recent advances in ultrasensitive and highly specific recognition aptasensors with various detection strategies. *Int J Biol Macromol* **155**, 184-207, doi:10.1016/j.ijbiomac.2020.03.173 (2020).
60 Tuerk, C. & Gold, L. Systematic Evolution of Ligands by Exponential Enrichment - Rna Ligands to Bacteriophage-T4 DNA-Polymerase. *Science* **249**, 505-510, doi:DOI 10.1126/science.2200121 (1990).

61 Ellington, A. D. & Szostak, J. W. Invitro Selection of Rna Molecules That Bind Specific Ligands. *Nature* **346**, 818-822, doi:DOI 10.1038/346818a0 (1990).
62 Wochner, A., Cech, B., Menger, M., Erdmann, V. A. & Glokler, J. Semi-automated selection of DNA aptamers using magnetic particle handling. *Biotechniques* **43**, 344-+, doi:10.2144/000112532 (2007).
63 Mencin, N. *et al.* Optimization of SELEX: comparison of different methods for monitoring the progress of in vitro selection of aptamers. *J Pharm Biomed Anal* **91**, 151-159, doi:10.1016/j.jpba.2013.12.031 (2014).
64 Stoltenburg, R., Reinemann, C. & Strehlitz, B. FluMag-SELEX as an advantageous method for DNA aptamer selection. *Anal Bioanal Chem* **383**, 83-91, doi:10.1007/s00216-005-3388-9 (2005).
65 Bianchini, M. *et al.* Specific oligobodies against ERK-2 that recognize both the native and the denatured state of the protein. *J Immunol Methods* **252**, 191-197, doi:10.1016/s0022-1759(01)00350-7 (2001).
66 Theis, M. G. *et al.* Discriminatory aptamer reveals serum response element transcription regulated by cytohesin-2. *Proc Natl Acad Sci U S A* **101**, 11221-11226, doi:10.1073/pnas.0402901101 (2004).
67 Lao, Y. H., Chiang, H. Y., Yang, D. K., Peck, K. & Chen, L. C. Selection of aptamers targeting the sialic acid receptor of hemagglutinin by epitope-specific SELEX. *Chem Commun (Camb)* **50**, 8719-8722, doi:10.1039/c4cc03116d (2014).
68 Geiger, A., Burgstaller, P., vonderEltz, H., Roeder, A. & Famulok, M. RNA aptamers that bind L-arginine with sub-micromolar dissociation constants and high enantioselectivity. *Nucleic Acids Res* **24**, 1029-1036, doi:DOI 10.1093/nar/24.6.1029 (1996).
69 Rohloff, J. C. *et al.* Nucleic Acid Ligands With Protein-like Side Chains: Modified Aptamers and Their Use as Diagnostic and Therapeutic Agents. *Mol Ther Nucleic Acids* **3**, e201, doi:10.1038/mtna.2014.49 (2014).
70 Wochner, A. *et al.* A DNA aptamer with high affinity and specificity for therapeutic anthracyclines. *Analytical Biochemistry* **373**, 34-42, doi:DOI 10.1016/j.ab.2007.09.007 (2008).
71 Boiziau, C., Dausse, E., Yurchenko, L. & Toulme, J. J. DNA aptamers selected against the HIV-1 trans-activation-responsive RNA element form RNA-DNA kissing complexes. *J Biol Chem* **274**, 12730-12737, doi:10.1074/jbc.274.18.12730 (1999).
72 Williams, K. P. & Bartel, D. P. PCR product with strands of unequal length. *Nucleic Acids Res* **23**, 4220-4221, doi:10.1093/nar/23.20.4220 (1995).
73 Null, A. P., Hannis, J. C. & Muddiman, D. C. Preparation of single-stranded PCR products for electrospray ionization mass spectrometry using the DNA repair enzyme lambda exonuclease. *Analyst* **125**, 619-625, doi:DOI 10.1039/a908022h (2000).
74 Baba, S. A., Jain, S. & Navani, N. K. A reliable, quick and universally applicable method for monitoring aptamer SELEX progress. *Gene* **774**, 145416, doi:10.1016/j.gene.2021.145416 (2021).
75 Ellington, A. D. & Szostak, J. W. Selection in vitro of single-stranded DNA molecules that fold into specific ligand-binding structures. *Nature* **355**, 850-852, doi:10.1038/355850a0 (1992).
76 Jones, S., Daley, D. T., Luscombe, N. M., Berman, H. M. & Thornton, J. M. Protein-RNA interactions: a structural analysis. *Nucleic Acids Res* **29**, 943-954, doi:10.1093/nar/29.4.943 (2001).
77 Kohlberger, M. & Gadermaier, G. SELEX: Critical factors and optimization strategies for successful aptamer selection. *Biotechnol Appl Biochem*, doi:10.1002/bab.2244 (2021).
78 Vorobyeva, M. A., Davydova, A. S., Vorobjev, P. E. & Venyaminova, A. G. Key Aspects of Nucleic Acid Library Design for in Vitro Selection. *Int J Mol Sci* **19**, doi:10.3390/ijms19020470 (2018).
79 Kratschmer, C. & Levy, M. Effect of Chemical Modifications on Aptamer Stability in Serum. *Nucleic Acid Ther* **27**, 335-344, doi:10.1089/nat.2017.0680 (2017).

80 Tolle, F., Rosenthal, M., Pfeiffer, F. & Mayer, G. Click Reaction on Solid Phase Enables High Fidelity Synthesis of Nucleobase-Modified DNA. *Bioconjug Chem* **27**, 500-503, doi:10.1021/acs.bioconjchem.5b00668 (2016).
81 Komarova, N. & Kuznetsov, A. Inside the Black Box: What Makes SELEX Better? *Molecules* **24**, doi:10.3390/molecules24193598 (2019).
82 Musheev, M. U. & Krylov, S. N. Selection of aptamers by systematic evolution of ligands by exponential enrichment: addressing the polymerase chain reaction issue. *Anal Chim Acta* **564**, 91-96, doi:10.1016/j.aca.2005.09.069 (2006).
83 Chen, M. *et al.* Development of Cell-SELEX Technology and Its Application in Cancer Diagnosis and Therapy. *Int J Mol Sci* **17**, doi:10.3390/ijms17122079 (2016).
84 Stoltenburg, R., Nikolaus, N. & Strehlitz, B. Capture-SELEX: Selection of DNA Aptamers for Aminoglycoside Antibiotics. *J Anal Methods Chem*, doi:10.1155/2012/415697 (2012).
85 Yang, Q., Goldstein, I. J., Mei, H. Y. & Engelke, D. R. DNA ligands that bind tightly and selectively to cellobiose. *Proc Natl Acad Sci U S A* **95**, 5462-5467, doi:10.1073/pnas.95.10.5462 (1998).
86 Boese, B. J. & Breaker, R. R. In vitro selection and characterization of cellulose-binding DNA aptamers. *Nucleic Acids Res* **35**, 6378-6388, doi:10.1093/nar/gkm708 (2007).
87 Stoltenburg, R., Reinemann, C. & Strehlitz, B. SELEX-A (r)evolutionary method to generate high-affinity nucleic acid ligands. *Biomol Eng* **24**, 381-403, doi:10.1016/j.bioeng.2007.06.001 (2007).
88 Ozer, A., Pagano, J. M. & Lis, J. T. New Technologies Provide Quantum Changes in the Scale, Speed, and Success of SELEX Methods and Aptamer Characterization. *Mol Ther-Nucl Acids* **3**, doi:10.1038/mtna.2014.34 (2014).
89 Pfeiffer, F. *et al.* Identification and characterization of nucleobase-modified aptamers by click-SELEX. *Nat Protoc* **13**, 1153-1180, doi:10.1038/nprot.2018.023 (2018).
90 Wlotzka, B. *et al.* In vivo properties of an anti-GnRH Spiegelmer: an example of an oligonucleotide-based therapeutic substance class. *Proc Natl Acad Sci U S A* **99**, 8898-8902, doi:10.1073/pnas.132067399 (2002).
91 Huizenga, D. E. & Szostak, J. W. A DNA Aptamer That Binds Adenosine and Atp. *Biochemistry* **34**, 656-665, doi:DOI 10.1021/bi00002a033 (1995).
92 Holeman, L. A., Robinson, S. L., Szostak, J. W. & Wilson, C. Isolation and characterization of fluorophore-binding RNA aptamers. *Fold Des* **3**, 423-431, doi:10.1016/S1359-0278(98)00059-5 (1998).
93 McCombie, W. R., McPherson, J. D. & Mardis, E. R. Next-Generation Sequencing Technologies. *Cold Spring Harb Perspect Med* **9**, doi:10.1101/cshperspect.a036798 (2019).
94 Ansorge, W. J. Next-generation DNA sequencing techniques. *N Biotechnol* **25**, 195-203, doi:10.1016/j.nbt.2008.12.009 (2009).
95 Hu, T., Chitnis, N., Monos, D. & Dinh, A. Next-generation sequencing technologies: An overview. *Hum Immunol* **82**, 801-811, doi:10.1016/j.humimm.2021.02.012 (2021).
96 Beier, R., Boschke, E. & Labudde, D. New strategies for evaluation and analysis of SELEX experiments. *Biomed Res Int* **2014**, 849743, doi:10.1155/2014/849743 (2014).
97 Hunniger, T. *et al.* Food sensing: selection and characterization of DNA aptamers to Alicyclobacillus spores for trapping and detection from orange juice. *J Agric Food Chem* **63**, 2189-2197, doi:10.1021/jf505996m (2015).
98 Ruscito, A. & DeRosa, M. C. Small-Molecule Binding Aptamers: Selection Strategies, Characterization, and Applications. *Front Chem* **4**, doi:10.3389/fchem.2016.00014 (2016).
99 Cowperthwaite, M. C. & Ellington, A. D. Bioinformatic analysis of the contribution of primer sequences to aptamer structures. *J Mol Evol* **67**, 95-102, doi:10.1007/s00239-008-9130-4 (2008).
100 Gao, S., Zheng, X., Jiao, B. & Wang, L. Post-SELEX optimization of aptamers. *Anal Bioanal Chem* **408**, 4567-4573, doi:10.1007/s00216-016-9556-2 (2016).

101 Tolle, F., Brandle, G. M., Matzner, D. & Mayer, G. A Versatile Approach Towards Nucleobase-Modified Aptamers. *Angew Chem Int Ed Engl* **54**, 10971-10974, doi:10.1002/anie.201503652 (2015).
102 Knight, R. & Yarus, M. Analyzing partially randomized nucleic acid pools: straight dope on doping. *Nucleic Acids Res* **31**, e30, doi:10.1093/nar/gng030 (2003).
103 Mohammadinezhad, R., Jalali, S. A. H. & Farahmand, H. Evaluation of different direct and indirect SELEX monitoring methods and implementation of melt-curve analysis for rapid discrimination of variant aptamer sequences. *Anal Methods* **12**, 3823-3835, doi:10.1039/d0ay00491j (2020).
104 Zhao, X., Li, G. & Liang, S. Several affinity tags commonly used in chromatographic purification. *J Anal Methods Chem* **2013**, 581093, doi:10.1155/2013/581093 (2013).
105 Shamah, S. M., Healy, J. M. & Cload, S. T. Complex target SELEX. *Acc Chem Res* **41**, 130-138, doi:10.1021/ar700142z (2008).
106 Yu, F. *et al.* Screening aptamers for serine beta-lactamase-expressing bacteria with Precision-SELEX. *Talanta* **224**, 121750, doi:10.1016/j.talanta.2020.121750 (2021).
107 Alcantara-Silva, R. *et al.* PISMA: A Visual Representation of Motif Distribution in DNA Sequences. *Bioinform Biol Insights* **11**, 1177932217700907, doi:10.1177/1177932217700907 (2017).
108 Sabrowski, W. *et al.* The use of high-affinity polyhistidine binders as masking probes for the selection of an NDM-1 specific aptamer. *Sci Rep* **12**, 7936, doi:10.1038/s41598-022-12062-2 (2022).
109 Bayat, P. *et al.* SELEX methods on the road to protein targeting with nucleic acid aptamers. *Biochimie* **154**, 132-155, doi:10.1016/j.biochi.2018.09.001 (2018).
110 Zhuo, Z. *et al.* Recent Advances in SELEX Technology and Aptamer Applications in Biomedicine. *Int J Mol Sci* **18**, doi:10.3390/ijms18102142 (2017).
111 Klug, S. J. & Famulok, M. All You Wanted to Know About Selex. *Mol Biol Rep* **20**, 97-107, doi:Doi 10.1007/Bf00996358 (1994).
112 Xu, G. *et al.* Structural Insights into the Mechanism of High-Affinity Binding of Ochratoxin A by a DNA Aptamer. *J Am Chem Soc* **144**, 7731-7740, doi:10.1021/jacs.2c00478 (2022).
113 Zhang, N. *et al.* Structural Biology for the Molecular Insight between Aptamers and Target Proteins. *Int J Mol Sci* **22**, doi:10.3390/ijms22084093 (2021).
114 Tian, H., Duan, N., Wu, S. & Wang, Z. Selection and application of ssDNA aptamers against spermine based on Capture-SELEX. *Anal Chim Acta* **1081**, 168-175, doi:10.1016/j.aca.2019.07.031 (2019).
115 Ke, W., Bethel, C. R., Thomson, J. M., Bonomo, R. A. & van den Akker, F. Crystal structure of KPC-2: insights into carbapenemase activity in class A beta-lactamases. *Biochemistry* **46**, 5732-5740, doi:10.1021/bi700300u (2007).
116 Khan, S., Ali, A. & Khan, A. U. Structural and functional insight of New Delhi Metallo beta-lactamase-1 variants. *Future Med Chem* **10**, 221-229, doi:10.4155/fmc-2017-0143 (2018).
117 Civit, L. *et al.* Systematic evaluation of cell-SELEX enriched aptamers binding to breast cancer cells. *Biochimie* **145**, 53-62, doi:10.1016/j.biochi.2017.10.007 (2018).
118 Niedringhaus, T. P., Milanova, D., Kerby, M. B., Snyder, M. P. & Barron, A. E. Landscape of next-generation sequencing technologies. *Anal Chem* **83**, 4327-4341, doi:10.1021/ac2010857 (2011).
119 Shokralla, S., Spall, J. L., Gibson, J. F. & Hajibabaei, M. Next-generation sequencing technologies for environmental DNA research. *Mol Ecol* **21**, 1794-1805, doi:10.1111/j.1365-294X.2012.05538.x (2012).
120 Grohmann, C. & Blank, M. Upgrading Affinity Screening Experiments by Analysis of Next-Generation Sequencing Data. *Methods Mol Biol* **1701**, 411-424, doi:10.1007/978-1-4939-7447-4_23 (2018).
121 Katoh, K. & Toh, H. Recent developments in the MAFFT multiple sequence alignment program. *Brief Bioinform* **9**, 286-298, doi:10.1093/bib/bbn013 (2008).

122 Kupakuwana, G. V., Crill, J. E., 2nd, McPike, M. P. & Borer, P. N. Acyclic identification of aptamers for human alpha-thrombin using over-represented libraries and deep sequencing. *Plos One* **6**, e19395, doi:10.1371/journal.pone.0019395 (2011).
123 Joseph, D. F. *et al.* DNA aptamers for the recognition of HMGB1 from Plasmodium falciparum. *Plos One* **14**, e0211756, doi:10.1371/journal.pone.0211756 (2019).
124 Zhu, Z. *et al.* Single-molecule emulsion PCR in microfluidic droplets. *Anal Bioanal Chem* **403**, 2127-2143, doi:10.1007/s00216-012-5914-x (2012).
125 Wang, R. *et al.* Bismuth antimicrobial drugs serve as broad-spectrum metallo-beta-lactamase inhibitors. *Nat Commun* **9**, 439, doi:10.1038/s41467-018-02828-6 (2018).
126 Pemberton, O. A., Zhang, X. & Chen, Y. Molecular Basis of Substrate Recognition and Product Release by the Klebsiella pneumoniae Carbapenemase (KPC-2). *J Med Chem* **60**, 3525-3530, doi:10.1021/acs.jmedchem.7b00158 (2017).
127 Kufareva, I. & Abagyan, R. Methods of protein structure comparison. *Methods Mol Biol* **857**, 231-257, doi:10.1007/978-1-61779-588-6_10 (2012).
128 Wu, X. *et al.* A novel method for high-level production of TEV protease by superfolder GFP tag. *J Biomed Biotechnol* **2009**, 591923, doi:10.1155/2009/591923 (2009).
129 Raran-Kurussi, S., Cherry, S., Zhang, D. & Waugh, D. S. Removal of Affinity Tags with TEV Protease. *Methods Mol Biol* **1586**, 221-230, doi:10.1007/978-1-4939-6887-9_14 (2017).
130 Even-Desrumeaux, K. *et al.* Masked selection: a straightforward and flexible approach for the selection of binders against specific epitopes and differentially expressed proteins by phage display. *Mol Cell Proteomics* **13**, 653-665, doi:10.1074/mcp.O112.025486 (2014).
131 Kulbachinskiy, A. V. Methods for selection of aptamers to protein targets. *Biochemistry (Mosc)* **72**, 1505-1518, doi:10.1134/s000629790713007x (2007).
132 Yang, L. *et al.* Ni-Nitrilotriacetic Acid Affinity SELEX Method for Selection of DNA Aptamers Specific to the N-Cadherin Protein. *Acs Comb Sci* **22**, 867-872, doi:10.1021/acscombsci.0c00165 (2020).
133 Bridonneau, P., Chang, Y. F., Buvoli, A. V., O'Connell, D. & Parma, D. Site-directed selection of oligonucleotide antagonists by competitive elution. *Antisense Nucleic Acid Drug Dev* **9**, 1-11, doi:10.1089/oli.1.1999.9.1 (1999).
134 Tsuji, S. *et al.* RNA aptamer binding to polyhistidine-tag. *Biochem Biophys Res Commun* **386**, 227-231, doi:10.1016/j.bbrc.2009.06.014 (2009).
135 Doyle, S. A., Murphy, M. B. APTAMERS AND METHODS FOR THEIR IN VTRO SELECTION AND USES THEREOF United States patent (2005).
136 Kim, E., Kang, M. & Ban, C. Aptamer-antibody hybrid ELONA that uses hybridization chain reaction to detect a urinary biomarker EN2 for bladder and prostate cancer. *Sci Rep* **12**, 11523, doi:10.1038/s41598-022-15556-1 (2022).
137 Schilling, K. B., DeGrasse, J. & Woods, J. W. The influence of food matrices on aptamer selection by SELEX (systematic evolution of ligands by exponential enrichment) targeting the norovirus P-Domain. *Food Chem* **258**, 129-136, doi:10.1016/j.foodchem.2018.03.054 (2018).
138 Cheung, R. C., Wong, J. H. & Ng, T. B. Immobilized metal ion affinity chromatography: a review on its applications. *Appl Microbiol Biotechnol* **96**, 1411-1420, doi:10.1007/s00253-012-4507-0 (2012).
139 Yuce, M., Ullah, N. & Budak, H. Trends in aptamer selection methods and applications. *Analyst* **140**, 5379-5399, doi:10.1039/c5an00954e (2015).
140 Firer, M. A. Efficient elution of functional proteins in affinity chromatography. *J Biochem Biophys Methods* **49**, 433-442, doi:10.1016/s0165-022x(01)00211-1 (2001).
141 Zuguo, Z., Yunmei, Y., Xie, L., Guoming, L., Laxi, Z., Na, M., Shuangshang, Y., Biyu, X. New Delhi metallo-beta-lactamase-1 aptamer, its screening method and application. *China patent* (2012).
142 Zuguo, Z. A kind of aptamer that can identify NDM-1 and VIM-2 simultaneously. *China patent* (2018).

143 Hasegawa, H., Savory, N., Abe, K. & Ikebukuro, K. Methods for Improving Aptamer Binding Affinity. *Molecules* **21**, 421, doi:10.3390/molecules21040421 (2016).
144 Qi, S. *et al.* Strategies to manipulate the performance of aptamers in SELEX, post-SELEX and microenvironment. *Biotechnol Adv* **55**, 107902, doi:10.1016/j.biotechadv.2021.107902 (2022).
145 Yu, H., Alkhamis, O., Canoura, J., Liu, Y. & Xiao, Y. Advances and Challenges in Small-Molecule DNA Aptamer Isolation, Characterization, and Sensor Development. *Angew Chem Int Ed Engl* **60**, 16800-16823, doi:10.1002/anie.202008663 (2021).
146 Ahmad, K. M. *et al.* Probing the limits of aptamer affinity with a microfluidic SELEX platform. *Plos One* **6**, e27051, doi:10.1371/journal.pone.0027051 (2011).
147 Marimuthu, C., Tang, T. H., Tominaga, J., Tan, S. C. & Gopinath, S. C. Single-stranded DNA (ssDNA) production in DNA aptamer generation. *Analyst* **137**, 1307-1315, doi:10.1039/c2an15905h (2012).
148 Schutze, T. *et al.* Probing the SELEX Process with Next-Generation Sequencing. *Plos One* **6**, doi:10.1371/journal.pone.0029604 (2011).
149 Grada, A. & Weinbrecht, K. Next-generation sequencing: methodology and application. *J Invest Dermatol* **133**, e11, doi:10.1038/jid.2013.248 (2013).
150 Tan, S. Y. *et al.* SELEX Modifications and Bioanalytical Techniques for Aptamer-Target Binding Characterization. *Crit Rev Anal Chem* **46**, 521-537, doi:10.1080/10408347.2016.1157014 (2016).
151 Woodbury Jr, C. P. & Von Hippel, P. H. On the determination of deoxyribonucleic acid-protein interaction parameters using the nitrocellulose filter-binding assay. *Biochemistry* **22**, 4730-4737 (1983).
152 Hellman, L. M. & Fried, M. G. Electrophoretic mobility shift assay (EMSA) for detecting protein–nucleic acid interactions. *Nat Protoc* **2**, 1849-1861 (2007).
153 Green, L. S., Bell, C. & Janjic, N. Aptamers as reagents for high-throughput screening. *Biotechniques* **30**, 1094-1096, 1098, 1100 passim, doi:10.2144/01305dd02 (2001).
154 Wochner, A. & Glokler, J. Nonradioactive fluorescence microtiter plate assay monitoring aptamer selections. *Biotechniques* **42**, 578-+, doi:10.2144/000112472 (2007).
155 Nguyen, H. H., Park, J., Kang, S. & Kim, M. Surface plasmon resonance: a versatile technique for biosensor applications. *Sensors (Basel)* **15**, 10481-10510, doi:10.3390/s150510481 (2015).
156 Ullah, S. F., Moreira, G., Datta, S. P. A., McLamore, E. & Vanegas, D. An Experimental Framework for Developing Point-of-Need Biosensors: Connecting Bio-Layer Interferometry and Electrochemical Impedance Spectroscopy. *Biosensors (Basel)* **12**, doi:10.3390/bios12110938 (2022).
157 Ponzo, I., Moller, F. M., Daub, H. & Matscheko, N. A DNA-Based Biosensor Assay for the Kinetic Characterization of Ion-Dependent Aptamer Folding and Protein Binding. *Molecules* **24**, doi:10.3390/molecules24162877 (2019).
158 Wang, R. E., Zhang, Y., Cai, J., Cai, W. & Gao, T. Aptamer-based fluorescent biosensors. *Curr Med Chem* **18**, 4175-4184, doi:10.2174/092986711797189637 (2011).
159 Jerabek-Willemsen, M., Wienken, C. J., Braun, D., Baaske, P. & Duhr, S. Molecular Interaction Studies Using Microscale Thermophoresis. *Assay Drug Dev Techn* **9**, 342-353, doi:10.1089/adt.2011.0380 (2011).
160 Velazquez-Campoy, A., Ohtaka, H., Nezami, A., Muzammil, S. & Freire, E. Isothermal titration calorimetry. *Curr Protoc Cell Biol* **Chapter 17**, Unit 17 18, doi:10.1002/0471143030.cb1708s23 (2004).
161 Ruigrok, V. J. B. *et al.* Characterization of aptamer-protein complexes by X-ray crystallography and alternative approaches. *Int J Mol Sci* **13**, 10537-10552, doi:10.3390/ijms130810537 (2012).
162 Smyth, M. S. & Martin, J. H. x ray crystallography. *Mol Pathol* **53**, 8-14, doi:10.1136/mp.53.1.8 (2000).

163 Kypr, J., Kejnovská, I., Bednářová, K. & Vorlíčková, M. Circular dichroism spectroscopy of nucleic acids. (2012).
164 Baldock, B. L. & Hutchison, J. E. UV-Visible Spectroscopy-Based Quantification of Unlabeled DNA Bound to Gold Nanoparticles. *Anal Chem* **88**, 12072-12080, doi:10.1021/acs.analchem.6b02640 (2016).
165 Nikolaus, N. & Strehlitz, B. DNA-Aptamers Binding Aminoglycoside Antibiotics. *Sensors-Basel* **14**, 3737-3755, doi:10.3390/s140203737 (2014).
166 Hu, L. *et al.* Selection, Characterization and Interaction Studies of a DNA Aptamer for the Detection of Bifidobacterium bifidum. *Int J Mol Sci* **18**, doi:10.3390/ijms18050883 (2017).
167 McConnell, E. M., Holahan, M. R. & DeRosa, M. C. Aptamers as Promising Molecular Recognition Elements for Diagnostics and Therapeutics in the Central Nervous System. *Nucleic Acid Ther* **24**, 388-404, doi:10.1089/nat.2014.0492 (2014).
168 Houwena, F. P. & Kageb, A. Aptamers the Chemical Antibodies. *Antibodies Applications and New Developments*, 300-314 (2012).
169 Eschenfeldt, W. H. *et al.* Cleavable C-terminal His-tag vectors for structure determination. *J Struct Funct Genomics* **11**, 31-39, doi:10.1007/s10969-010-9082-y (2010).
170 Hianik, T., Ostatna, V., Sonlajtnerova, M. & Grman, I. Influence of ionic strength, pH and aptamer configuration for binding affinity to thrombin. *Bioelectrochemistry* **70**, 127-133, doi:10.1016/j.bioelechem.2006.03.012 (2007).
171 Sabrowski, W., Stocklein, W. F. M. & Menger, M. M. Immobilization-Free Determination of Dissociation Constants Independent of Ligand Size Using MicroScale Thermophoresis. *Methods Mol Biol* **2570**, 129-140, doi:10.1007/978-1-0716-2695-5_10 (2023).
172 Dreymann, N., Moller, A. & Menger, M. M. Label-Free Determination of the Kinetic Parameters of Protein-Aptamer Interaction by Surface Plasmon Resonance. *Methods Mol Biol* **2570**, 141-153, doi:10.1007/978-1-0716-2695-5_11 (2023).
173 Wienken, C. J., Baaske, P., Rothbauer, U., Braun, D. & Duhr, S. Protein-binding assays in biological liquids using microscale thermophoresis. *Nature Communications* **1**, doi:10.1038/ncomms1093 (2010).
174 Esposito, D. & Chatterjee, D. K. Enhancement of soluble protein expression through the use of fusion tags. *Curr Opin Biotechnol* **17**, 353-358, doi:10.1016/j.copbio.2006.06.003 (2006).
175 Zheng, X. *et al.* A saxitoxin-binding aptamer with higher affinity and inhibitory activity optimized by rational site-directed mutagenesis and truncation. *Toxicon* **101**, 41-47, doi:10.1016/j.toxicon.2015.04.017 (2015).
176 Miriagou, V. *et al.* Combined disc methods for the detection of KPC- and/or VIM-positive Klebsiella pneumoniae: improving reliability for the double carbapenemase producers. *Clin Microbiol Infect* **19**, E412-415, doi:10.1111/1469-0691.12238 (2013).
177 Migliavacca, R. *et al.* Simple microdilution test for detection of metallo-beta-lactamase production in Pseudomonas aeruginosa. *J Clin Microbiol* **40**, 4388-4390, doi:10.1128/JCM.40.11.4388-4390.2002 (2002).
178 Bernabeu, S., Bonnin, R. A. & Dortet, L. Comparison of three lateral flow immunochromatographic assays for the rapid detection of KPC, NDM, IMP, VIM and OXA-48 carbapenemases in Enterobacterales. *J Antimicrob Chemother* **77**, 3198-3205, doi:10.1093/jac/dkac303 (2022).
179 NGBiotech. *NG-Test CARBA 5 Rapid test for the detection of carbapenemases KPC, OXA-48-like, VIM, IMP and NDM in a bacterial colony from culture*, http://www.virotechdiagnostics.com/uploads/tx_multishop/images/cmsfiles/5b7680da5d968.pdf (2020).
180 Pei, X. *et al.* Sandwich-type immunosensors and immunoassays exploiting nanostructure labels: A review. *Anal Chim Acta* **758**, 1-18, doi:10.1016/j.aca.2012.10.060 (2013).
181 BioMérieux. *RAPIDEC® CARBA NP Test Instructions*, https://www.biomerieux-usa.com/sites/subsidiary_us/files/18_rapidec-brochure.pdf (2018).

182 Gopinath, S. C. B. Methods developed for SELEX. *Anal Bioanal Chem* **387**, 171-182, doi:10.1007/s00216-006-0826-2 (2007).
183 Otieno, B. A., Krause, C. E. & Rusling, J. F. Bioconjugation of Antibodies and Enzyme Labels onto Magnetic Beads. *Methods Enzymol* **571**, 135-150, doi:10.1016/bs.mie.2015.10.005 (2016).
184 Benelmekki, M. *et al.* Design and characterization of Ni2+ and Co2+ decorated Porous Magnetic Silica spheres synthesized by hydrothermal-assisted modified-Stober method for His-tagged proteins separation. *J Colloid Interface Sci* **365**, 156-162, doi:10.1016/j.jcis.2011.09.051 (2012).
185 Smith, P. K. *et al.* Measurement of Protein Using Bicinchoninic Acid. *Analytical Biochemistry* **150**, 76-85, doi:Doi 10.1016/0003-2697(85)90442-7 (1985).
186 Pace, C. N., Vajdos, F., Fee, L., Grimsley, G. & Gray, T. How to measure and predict the molar absorption coefficient of a protein. *Protein Sci* **4**, 2411-2423, doi:10.1002/pro.5560041120 (1995).
187 Wilkins, M. R. *et al.* Protein identification and analysis tools in the ExPASy server. *Methods Mol Biol* **112**, 531-552, doi:10.1385/1-59259-584-7:531 (1999).
188 Gan, S. D. & Patel, K. R. Enzyme immunoassay and enzyme-linked immunosorbent assay. *J Invest Dermatol* **133**, e12, doi:10.1038/jid.2013.287 (2013).
189 Volpe, G., Compagnone, D., Draisci, R. & Palleschi, G. 3,3 ',5,5 '-tetramethylbenzidine as electrochemical substrate for horseradish peroxidase based enzyme immunoassays. A comparative study. *Analyst* **123**, 1303-1307, doi:DOI 10.1039/a800255j (1998).
190 Mullis, K. *et al.* Specific enzymatic amplification of DNA in vitro: the polymerase chain reaction. *Cold Spring Harb Symp Quant Biol* **51 Pt 1**, 263-273, doi:10.1101/sqb.1986.051.01.032 (1986).
191 Saiki, R. K. *et al.* Primer-directed enzymatic amplification of DNA with a thermostable DNA polymerase. *Science* **239**, 487-491, doi:10.1126/science.2448875 (1988).
192 Stellwagen, N. C. & Stellwagen, E. Effect of the matrix on DNA electrophoretic mobility. *J Chromatogr A* **1216**, 1917-1929, doi:10.1016/j.chroma.2008.11.090 (2009).
193 Stellwagen, N. C. in *Nucleic Acid Electrophoresis* (ed Dietmar Tietz) 1-53 (Springer Berlin Heidelberg, 1998).
194 Ando, T. A nuclease specific for heat-denatured DNA in isolated from a product of Aspergillus oryzae. *Biochim Biophys Acta* **114**, 158-168, doi:10.1016/0005-2787(66)90263-2 (1966).
195 Levy, S. E. & Myers, R. M. Advancements in Next-Generation Sequencing. *Annu Rev Genomics Hum Genet* **17**, 95-115, doi:10.1146/annurev-genom-083115-022413 (2016).
196 Kircher, M., Heyn, P. & Kelso, J. Addressing challenges in the production and analysis of illumina sequencing data. *Bmc Genomics* **12**, 382, doi:10.1186/1471-2164-12-382 (2011).
197 Shen, J., Li, Y., Gu, H., Xia, F. & Zuo, X. Recent development of sandwich assay based on the nanobiotechnologies for proteins, nucleic acids, small molecules, and ions. *Chem Rev* **114**, 7631-7677, doi:10.1021/cr300248x (2014).
198 Deka, J. *et al.* Surface passivation improves the synthesis of highly stable and specific DNA-functionalized gold nanoparticles with variable DNA density. *ACS Appl Mater Interfaces* **7**, 7033-7040, doi:10.1021/acsami.5b01191 (2015).

10. Curriculum Vitae

Working experience

Since 07/2022	Project lead – Project Veggie Mom (funded by Fraunhofer Zentrum für digitale Diagnostik)
Since 02/2019	Research associate at Fraunhofer IZI-BB in the group functional nucleic acids / aptamers
10/2010 - 09/2013	6 internships in different departments of Mercedes-Benz Sales Germany and Mercedes-Benz USA LLC.,

Studies

10/2016 - 01/2019	Master program biochemistry Freie Universität Berlin Master thesis: Generation and characterization of DNA aptamers against small molecules using Capture-SELEX
10/2013 - 09/2016	Bachelor program biochemistry Freie Universität Berlin Bachelor thesis: “Generation and first characterization of LRRC8 knock-in cell lines to determine the subunit composition of the volume-regulated anion channel”
10/2010 - 09/2013	Cooperate studies of business administration at Daimler AG / Mercedes-Benz Sales Germany and Berlin school of economics and law

Awards, scholarships, and trainings

04/2022	Online participation in the conference „Aptamers 2022 Oxford“
06/2021	Training: „Prägnante Performance: Souverän und überzeugend im Job (TALENTA start und speed up)“
02/2019 - 02/2021	Fraunhofer internal scholarship TALENTA start
10/2020	Participation in the conference „Doktorandenseminar der deutschen Nucleinsäurechemiegesellschaft e.V.“
09/2019	Poster award (first price) and participation in the conference „New and emerging technologies“ hosted by glyconet Berlin Brandenburg
06/2019	Training: §15 GenTSV hosted by BioMedConcept GmbH
04/2019	Poster award and participation in the conference „Aptamers 2019 Oxford“ hosted by the International Society On Aptamers
10/2018	Participation in the conference RNA Biochemistry 2018 & Workshop „Synthetic RNA Biology" hosted by GBM
09/2018	Workshop on Biomolecular Interaction Analytics employing MicroScale Thermophoresis
06/2018	Illumina MiniSeq Instrument Training

Trainings throughout the cooperate studies

Project management, Moderation and presentation, Communication and cooperation

11. List of Publications

11.1. Original Articles

Wiebke Sabrowski, Nico Dreymann, Anja Möller, Denise Czepluch, Patricia P. Albani, Dimitrios Theodoridis & Marcus M. Menger. *The use of high-affinity polyhistidine binders as masking probes for the selection of an NDM-1 specific aptamer.* Sci Rep 12, 7936 (2022).

Nico Dreymann, **Wiebke Sabrowski**, Jennifer Danso, Marcus M. Menger. *Aptamer-based Sandwich Assay Formats for Detection and Discrimination of Human High- and Low-Molecular-Weight uPA for Cancer Prognosis and Diagnosis.* Cancers, 14, 5222 (2022).

Nico Dreymann, Julia Wuensche, **Wiebke Sabrowski**, Anja Moeller, Denise Czepluch, Dana Vu Van, Susanne Fuessel and Marcus M. Menger. *Inhibition of Human Urokinase-Type Plasminogen Activator (uPA) Enzyme Activity and Receptor Binding by DNA Aptamers as Potential Therapeutics through Binding to the Different Forms of uPA*, Int. J. Mol. Sci. 23(9), 4890 (2022).

Ana D. Mandić, Anni Woting, Tina Jaenicke, Anika Sander, **Wiebke Sabrowski**, Ulrike Rolle-Kampcyk, Martin von Bergen & Michael Blaut. *Clostridium ramosum regulates enterochromaffin cell development and serotonin release.* Sci Rep 9, 1177 (2019).

11.2. Book Chapter

Wiebke Sabrowski, Walter F. M. Stöcklein & Marcus M. Menger. *Immobilization-Free Determination of Dissociation Constants Independent of Ligand Size Using MicroScale Thermophoresis.* In: Mayer, G., Menger, M.M. (eds) Nucleic Acid Aptamers. Methods in Molecular Biology, vol 2570 (2022).

12. List of Abbreviations

Table 35: List of Abbreviations.

Abbreviation	Meaning of the abbreviation
Aptamer-F	Aptamer shortened by the forward primer region
Aptamer-FR	Aptamer shortened by both primer regions
Aptamer-R	Aptamer shortened by the reverse primer binding region
APS	Ammonium persulfate
Au-NP	Gold nanoparticles
bp	Base pairs
BSA	Bovine serum albumin
CD	Circular dichroism
CFHR1	Complement Factor H-related 1
Cp	Carbapenemase producing
CRE	Carbapenem-resistant *Enterobacteriaceae*
Cy5	Cyanine 5
DANA	Diversity assay for nucleic acids
ddH_2O	Double-distilled water
dNTP	Deoxynucleotide triphosphates
DNA	Deoxyribonucleic acid
dsDNA	Double stranded deoxyribonucleic acid
DSR	Selection round of doped SELEX
EDC	1-ethyl-3-(3-dimethylaminopropyl) carbodiimide
EDTA	Ethylenediaminetetraacetic acid
EMSA	Electrophoretic Mobility Shift Assay
ESBL	Extended-spectrum β-lactamases
EtOH	Ethanol
FLAA	Fluorescent-dye linked aptamer assay
His	Multiple histidines (mostly hexa histidine) as a purification tag
His-Protein	Protein with N-terminal His-tag
HRP	Horseradish peroxidase
IMP	Carbapenemases active against impenem
ITC	Isothermal titration calorimetry
k_a	Association rate
k_d	Dissociation rate
K_D	Dissociation constant
KPC-2	Klebsiella pneumoniae Carbapenemase-2
LFD	Lateral flow device

MALDI-TOF	Matrix-assisted laser desorption - ionisation-time of flight
MIC	Minimum inhibitory concentrations
mPD1	Mouse programmed cell death protein 1-His
MST	Microscale thermophoresis
MTP	Micro titer plate
NDM-1	New Delhi metallo-beta-lactamase 1
NGS	Next generation sequencing
NHS	N-hydroxysuccinimide
Nt	Nucleotide
NTA	Nitrilotriacetic acid
NTC	No template control
OXA-23	Oxacillinase 23
PAA	Polyacrylamide
PAG	Phosphoprotein membrane anchor with glycosphingolipid microdomains
PAGE	Polyacrylamide gel electrophoresis
PCR	Polymerase chain reaction
PGN	Peptidoglycans
Protein-His	Protein with C-terminal His-tag
RNA	Ribonucleic acid
Rpm	Rounds per minute
RU	Response units
SA	Streptavidin
SBS	Sequencing by synthesis
SELEX	Systematic evolution of ligands by exponential enrichment
SDS	Sodium dodecyl sulfate
SPR	Surface plasmon resonance spectroscopy
SR	Selection round
ssDNA	Single stranded deoxyribonucleic acid
TEMED	Tetramethylethylenediamine
TEV	Tobacco etch virus
Tosyl	P-toluene-sulfonyl
UDP	Uridine diphosphate
VIM	Verona integron-encoded metallo-β-Lactamase

13. Lists of Figures and Tables

13.1. List of Figures

13.2. List of Tables

14. Appendix

14.1. Appendix Figures

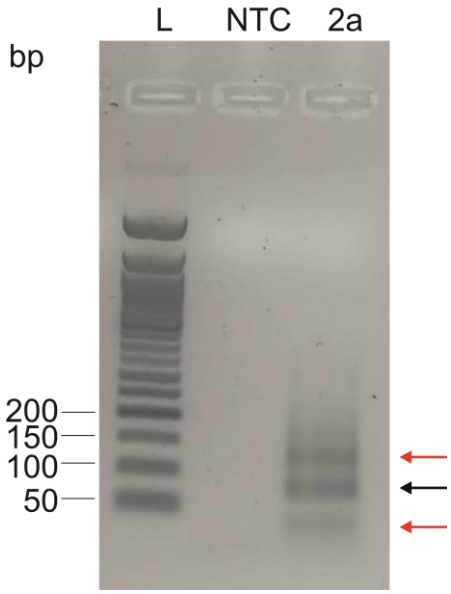

Appendix Figure 1: Byproduct formation visualized by UV radiation after gel electrophoresis of the PCR product after PCR2a of SR8.1, selected against His-NDM-1 (2a). The black arrow indicates the PCR product at the expected length of 80 bp. The red arrows indicate byproducts at approximately 130 bp and below 50 bp. NTC = no template control, L = 50 bp DNA ladder.

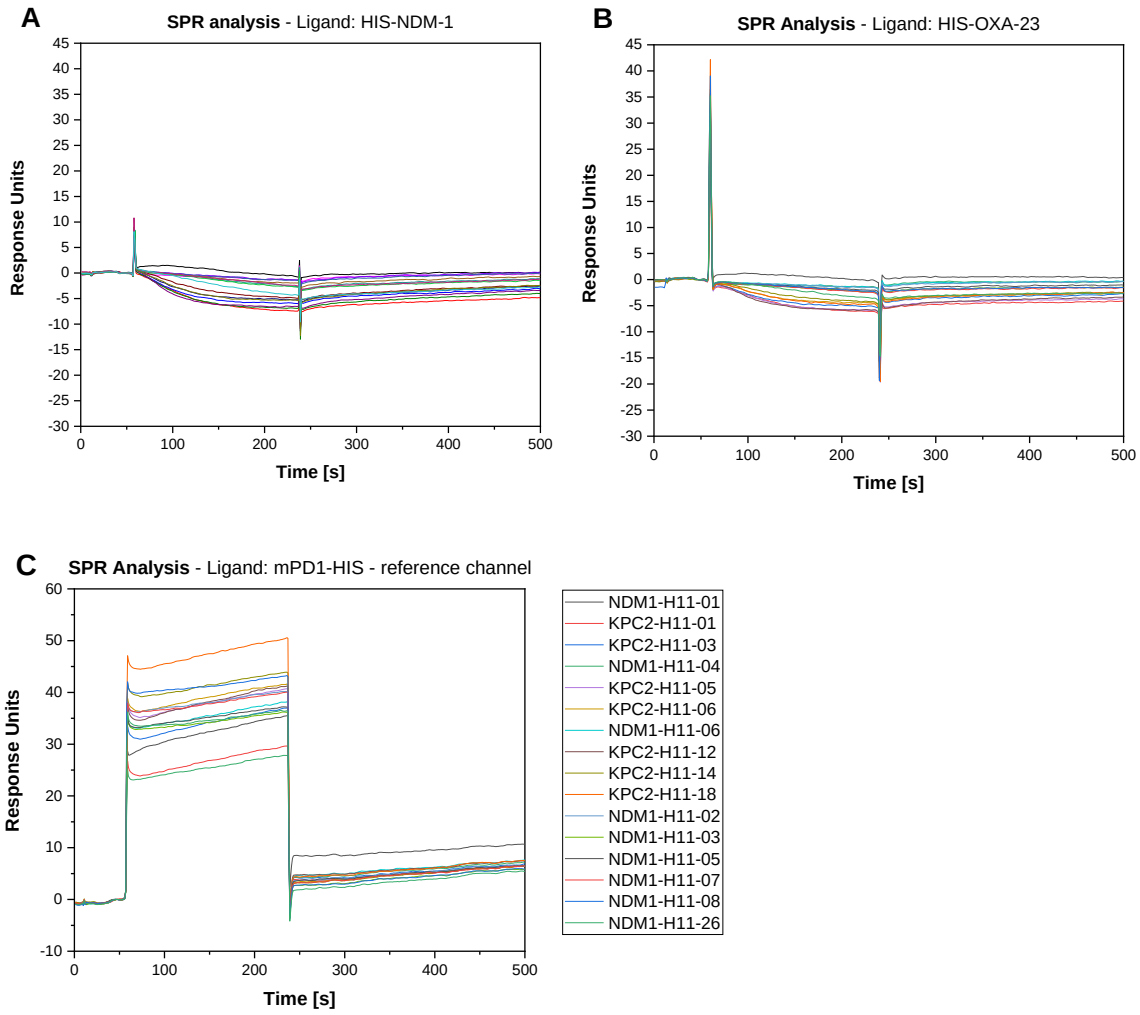

Appendix Figure 2: Characterization of aptamer candidates selected against His-KPC-2 and His-NDM-1 after SR11.1 by SPR. Response units over the course of 500 s are shown. Injection of aptamer candidates did not result in binding signals derived from the His-NDM-1 (A) and the His-OXA-23 (B) channels. (C) Binding to the reference channel with immobilized mPD1-His was also not observed.

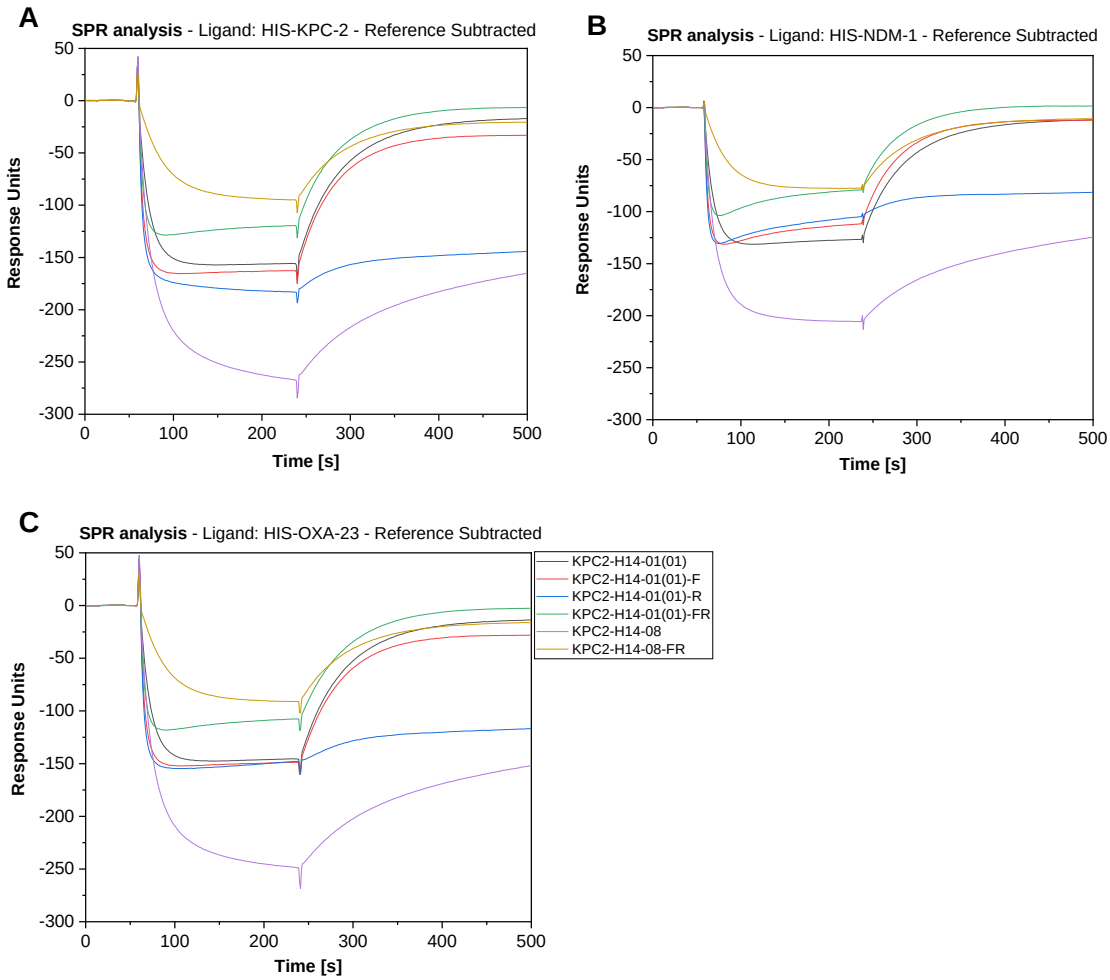

Appendix Figure 3: SPR analysis of aptamers KPC2-H14-01(01), KPC2-H14-01(01)-R, KPC2-H14-01(01)-F and KPC2-H14-01(01)-FR as well as KPC2-H14-08 and KPC2-H14-08-FR binding to immobilized carbapenemases (A) His-KPC-2, (B) His-NDM-1, (C) His-OXA-23. Response units over the course of 500 s are shown. Unrelated protein mPD1-His was immobilized on the reference channel. The reference signal was subtracted. Negative binding curves indicate the strongest binding signal for mPD1-His.

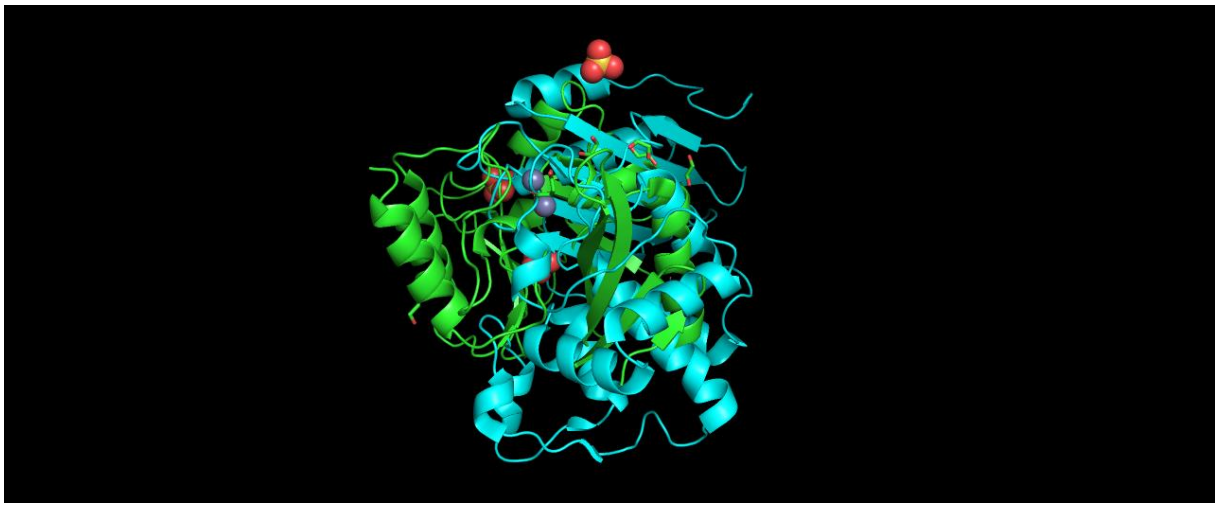

Appendix Figure 4: Structural alignment of NDM-1 and KPC-2. Crystal structures of NDM-1 (green) [125] with ligands succinic acid ($C_4H_6O_4$, depicted in green and red), Zn^{2+} (purple), 1,2-ethanediol ($C_2H_6O_2$, depicted in green and red) and OH^- (red) and KPC-2 (cyan) [126] with ligand SO_4^{2-} (depicted in yellow and red) were aligned by PyMOL.

14.2. Appendix Tables

Appendix Table 1: Concentration of immobilized His-KPC-2, coupling efficiency and use as target and negative selection target (selection against His-NDM-1).

Concentration [pmol/µl beads]	Coupling efficiency [%]	Used as the targets for SRs	Used as negative selection target for SRs
9.9	82	1.1 - 2.1	-
9.0	72	1.2 - 5.1	5.1 - 6.1
6.7	97	6.1 - 8.1	7.1 - 7.2
3.7	98	8.1	8.1
4.6	75	9.1 - 10.1	9.1 - 10.1
14.2	92	11.1	11.1
10.8	100	12.1	-
9.8	86	13.1 - 14.1	
7.8	100	12.2_Comp - 14.2_Comp	
		11.2_Mask - 12.3_Mask	
5.3	100	13.3_Mask	
20	93	12.2_Co^{2+}-NTA - 14.2_Co^{2+}-NTA	

Appendix Table 2: Concentration of immobilized His-NDM-1, coupling efficiency and use as target and negative selection target (selection against His-KPC-2).

Concentration [pmol/µl beads]	Coupling efficiency [%]	Used as the targets for SRs	Used as negative selection target for SRs
3.4	32	- (Pretests)	-
7.6	94	1.1 - 4.1	-
10.5	86	5.1 - 7.1	5.1 - 6.1
7.9	78	6.2 - 8.1	7.1 - 10.1
11.8	98	9.1, 11.1	-
4.7	61	10.1	11.1
10.6	78	12.1	-
7.5	87	13.1 - 14.1	
10	100	11.2_Mask - 14.2_Mask	
5	96	DSR1.1 -3.1	
18	69	DSR4.1	

Appendix Table 3: Concentration of immobilized His-OXA-23, coupling efficiency and use as negative selection target.

Concentration [pmol/µl beads]	Coupling efficiency [%]	Negative selection target (His-KPC-2 selection) SRs	Negative selection target (His-NDM-1 selection) SRs
8.4	93	8.1 - 10.1	8.1 - 9.1
3.4	28		10.1
2.2	25	11.1	11.1

Appendix Table 4: Concentration of immobilized mPD1-His, coupling efficiency and use as negative selection target.

Concentration [pmol/µl beads]	Coupling efficiency [%]	Negative selection target (His-KPC-2 selection) SRs	Negative selection target (His-NDM-1 selection) SRs
6.5	33	12.2 - 13.2 (_Mask, _Comp, _Co^{2+}-NTA)	
8.4	59	14.2 (_Comp, _Co^{2+}-NTA) + 11.2_Mask - 13.3_Mask	
6.7	46		11.2_Mask - 12.2_Mask
9.1	60		13.3_Mask - 14.2_Mask
15.5	65		DSR1.1 - DSR4.1

Appendix Table 5: Concentration of immobilized CFHR1-His, coupling efficiency and use as negative selection target.

Concentration [pmol/µl beads]	Coupling efficiency [%]	Negative selection target (His-KPC-2 selection) SRs	Negative selection target (His-NDM-1 selection) SRs
12.5	82	-	13.3_Mask - 14.2_Mask

Appendix Table 6: Identified sequence motifs after analysis of NGS data.

Selection Round	Analyzed sequences	Identified Motif	Number of sequences
NDM1-H11	50	CGGCGATAACAAAAAAAAA	5
KPC2-H11	50	CGGCGATAACAAAAAAAAA	4
NDM1-H14	50	CATAGACGACGAAGAACA*	20
		TGTATCTGGTGGTCTATG	9
		GGGGGACTGCTCGGGATTG	4
		TTCTTCT	3
KPC2-H14	50	CATAGACGACGAAGAACA*	16
		TGTATCTGGTGGTCTATG	8
		GGCGGGGGG-6-20(N)-GGGGGGATGG	6
		GGGGGACTGCTCGGGATTGC	4
		TTATTTT	4
		TTCTTCT	3
KPC2-H13.3_ Mask	300	GGACATTTTTGGTTTTTGGGTACTCCTCC	17
		CGGCGATAACAAAAAAAA	16
		AGGAG-0-3(N)-ATTA	8
		AGATCACCAGATACCCAGATACG	7
		TTGCTCGTTTAAAAAAA	6
		ATAAACAGGGGGA	4
		GTTACATCTCGTT	4
		CTTCCTT-0-7(N)-CTTTT	4
		GTGTTC-10-11(N)-TTCAA	4
		GCCG3-6(A)T-2-9(N)-CTCTT	3
		CTAACACGTTTTTTTACCTTATACTTGCGG	3
NDM1-H14.2_ Mask	100	CTTTT-3-20(N)-TCC	15
		CGGAGGTCTAAAAAAAAAAAA	7
		AAAAAAAAAA-0-4(N)-CAAA	6
		CCG-5-10(N)TC-6-19(N)-TTTTCTT	5
		GGG-3-14(N)-TGGGG	5
NDM1-DSR4	50	CGCAGTGTTCGATGAGAGTCATTCAAAGCAT	18
		CACACGCTAAAAGGAAATTAGAAGTCGTCTT	9
		AGGACATTTTTGGTTTTTGGGTACTCCTCC	8
		CGAGAAAAGTTCTGTCGTCTAAAAAGTTCTT	4
		AGCCGCAAAAAATAAAAGCCTAACGAGG	4
		TCTTTTCTTT	3